Universität Hamburg
Department Biologie

Erg K^+ current in immature Purkinje neurons of the mouse (*Mus musculus* (Linnaeus, 1758))

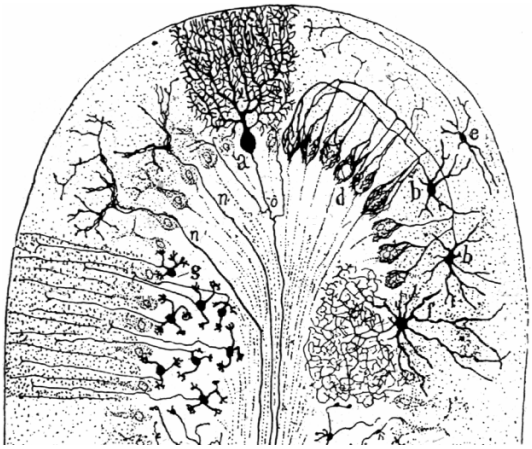

Dissertation

zur Erlangung des Doktorgrades
- Dr. rer. nat. -
am Fachbereich Biologie
der Fakultät für Mathematik, Informatik und Naturwissenschaften
an der Universität Hamburg

vorgelegt von

Dragoş Niculescu

Bukarest, Rumänien

Hamburg, 2010

Cover picture: Ramón y Cajal, S.
Histologie du système nerveux de l'homme et vertébrés
Paris, 1911

Genehmigt vom Fachbereich Biologie
der Fakultät für Mathematik, Informatik und Naturwissenschaften
an der Universität Hamburg
auf Antrag von Prof. Dr. J. R. SCHWARZ
Weitere Gutachterin der Dissertation:
Frau Priv.-Doz. Dr. S. LÜTHJE
Tag der Disputation: 29. Oktober 2010

Hamburg, den 14. Oktober 2010

A. Temming

Professor Dr. Axel Temming
Leiter des Fachbereichs Biologie

UNIVERSITY OF CALIFORNIA, SAN FRANCISCO

BERKELEY • DAVIS • IRVINE • LOS ANGELES • RIVERSIDE • SAN DIEGO • SAN FRANCISCO | SANTA BARBARA • SANTA CRUZ

Collin Spencer
UCSF Department of Neurology
513 Parnassus Avenue, Room S-268
San Francisco, CA 94143
Phone: (415) 476-2013
FAX: (415) 502-8512
E-Mail: cspencer@ucsf.neuroimmunol.org

September 15, 2010

Doctoral thesis for Dragos Niculescu, University of Hamburg

To whom it may concern:

I, Collin Spencer, the undersigned, certify that I am a native English speaker. I have read Dragos Niculescu's doctoral thesis draft and have provided the relevant advice in relation to English grammar and composition that should be incorporated into the final thesis. I affirm the thesis general language, grammar and spelling and should be readily understood by any native English speaker.

Sincerely,

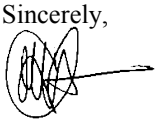

Collin Spencer

Content

1. Introduction

1.1 The Cerebellum

The cerebellum is a distinct component of the brain in almost all vertebrates. Only lampreys among vertebrates lack such a structure. In fish, amphibians and reptiles the organization of cerebellum differs in some respects from that of birds and mammals, but the characteristic big cells that receive the sensory input and that project to a group of cells that provide the output from cerebellum, are invariantly present (Sultan & Glickstein, 2007). It has been known for a long time that the cerebellum is involved in motor coordination, although some studies suggest its involvement in certain cognitive processes too (Schmahmann, 1997).

1.1.1 The Organization of cerebellum

The cerebellum consists of a cortical sheet which covers a white matter core. Buried within the white matter are the cerebellar nuclei which receive their gross input from the cerebellar cortex. Neurons in the cerebellar nuclei, in turn, constitute the output from the cerebellum, and connect to structures in the thalamus and brainstem. The mammalian cerebellum consists of three lobes: anterior, posterior and flocculo-nodular lobes (Sultan & Glickstein, 2007).

The cerebellar cortex is organized in three layers and contains five major types of cells (Figure 1). The layer closest to the white matter is the granule cell layer, made mostly of small neurons (granule cells) that receive the vast majority of the inputs to the cerebellum and send their projections into the outermost layer forming the parallel fibers. Mossy fiber afferents target granule cells, and excite the Purkinje neurons indirectly; the parallel fiber pathway causes the Purkinje neurons to discharge “simple spikes” (conventional action potentials). The mossy fibers are actually the axons of neurons located in the spinal cord, brainstem (especially the pons) and the cerebellum itself (Apps & Garwicz, 2005). Among the granule cells, the Golgi cells can be found, which also extend their dendrites into the outer, molecular layer. The intermediate layer is made of one row of cells, the Purkinje neurons, the most important cell type within the cerebellum. They got their name from the 19th century Czech physiologist and anatomist who first described them (Jan Evangelista Purkinje).

Purkinje neurons provide the only output from the cerebellar cortex. They have a massively branched dendritic tree which extends to the surface of the cerebellar cortex in a single plane, transverse to the orientation of the cerebellar folia.

The external layer, called the molecular layer because of the numerous neural processes present here, contains two major types of neurons as part of an inhibitory system that regulates the firing of Purkinje neurons: the basket and the stellate cells. In the molecular layer the axons of the granule cells branch in a characteristic T-fashion and extend parallel to the cerebellar folia (hence their name, parallel fibers) to contact the dendrites of the Purkinje neurons. Since the dendritic arbor of Purkinje neurons is perpendicular to the course of the folia, the parallel fibers contact Purkinje neuron dendrites at right angles. The other main class of excitatory fiber making synapse of Purkinje neurons are the climbing fibers coming from the inferior olive, a complex of sub-nuclei in the ventral part of the caudal brainstem. In contrast to parallel fibers where many of them contact the dendritic tree of the same Purkinje cell, only one climbing fiber sends input to a given Purkinje neuron. But the contact is so

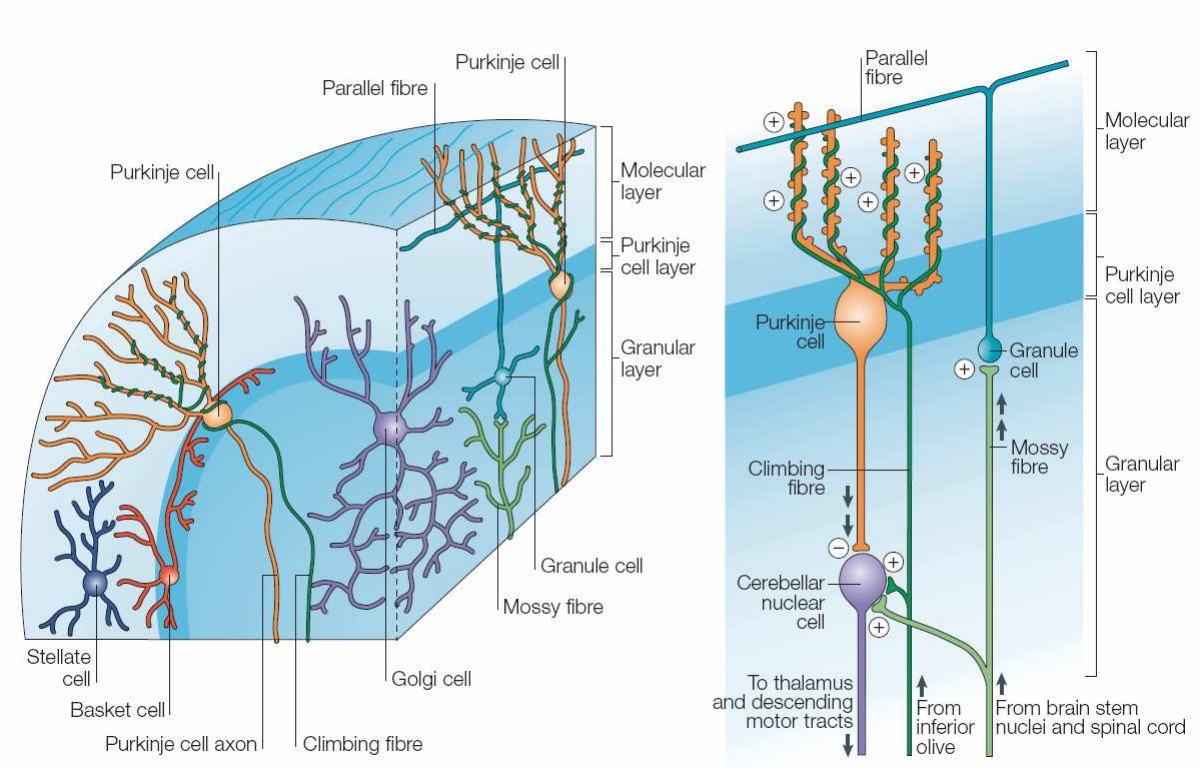

Figure 1. Basic structure of the cerebellar cortex. There are two main afferents to the cerebellar cortex: climbing fibers, which make extensive excitatory contact with Purkinje neuron dendrites, and parallel fibers, which make discrete contacts to Purkinje neuron dendrites. The parallel fibers are the axons of granule cells that receive excitatory inputs from mossy fibers. Golgi cells also receive synaptic inputs from mossy fibers. In some cases, the stem axons of climbing and mossy fibers also provide collaterals to the cerebellar nuclei. The ascending axons of granule cells branch in a T-shaped manner to form the parallel fibers. With the exception of granule cells, all cerebellar cortical neurons, including the Purkinje neurons, make inhibitory connections with their target neurons. [from Apps & Garwicz, 2005]

extensive along the whole length of the dendritic tree, that climbing fibers generate a large depolarizing event with the shape of a characteristic burst of spikes known as a complex spike (Apps & Garwicz, 2005). Another characteristic type of synaptic input is the one basket cells give to Purkinje neurons. The axons of basket cells branch and form a cup-like structure around the soma of Purkinje neurons.

The cerebellum receives input from many sources. In all mammals the flocculus receives its major input from those sense organs that signal the body's position in space. In mammals the great majority of the input to the cerebellum comes not from the vestibular system or spinal cord (as it happens in other vertebrates) but from the cerebral cortex through the pontine nuclei. Especially the motor areas send a massive input to the pons, providing information about all the motor commands given by the cortex. The major output from the cerebellum is to those structures controlling the movement of the eyes, the limbs and the body as a whole. Lesions of the cerebellum produce deficit in gait, fine tuning of limb movements and the smooth pursuit eye movements are lost (Sultan & Glickstein, 2007).

1.1.2 mGluRI activation effects on Purkinje neurons

Cerebellum has a very organized structure, all the major cell types being present in various compartments despite their different functional assignment. Purkinje neurons have a central function in information processing, and two excitatory synapses play a major role in delivering information to them: climbing and parallel fibers. Two concepts have remained central concerning the involvement of the climbing fiber signals in the motor control. First, that climbing fibers mediate motor error signals and, second, that climbing fiber activity is instrumental in the induction of synaptic plasticity underlying motor adaptation and motor learning. The importance of the cerebellum in the motor commands depends on the capacity to constantly modify the input-output transformations. This includes synaptic plasticity influencing transmission from parallel fibers to Purkinje neurons and cortical interneurons. An important factor regulating synaptic plasticity seem to be the interactions between climbing fiber and parallel fiber inputs (Apps & Garwicz, 2005).

The climbing fiber and parallel fiber synapses are glutamatergic synapses involving two main classes of receptors: ionotropic (iGluRs) and metabotropic (mGluRs). Both types of fibers

activate, at synapses on Purkinje neurons, iGluRs of the AMPA type (Llano *et al.*, 1991), but the role of mGluRs at these synapses is much less known, although they are considered to be involved in the generation of a slow postsynaptic potential, in intradendritic Ca^{2+} signaling and in long-term depression (LTD; Konnerth *et al.*, 1992).

Initially it was thought that the postsynaptic depolarization (EPSP, excitatory postsynaptic potential) due to mGluR activation can be seen only at the parallel fiber-Purkinje neuron synapses by repetitive parallel fiber stimulation. At these synapses the most abundantly expressed mGluR is the mGluR1, and the elicited depolarization is thought to be due to the release of Ca^{2+} from the internal stores. The postsynaptic currents that generate the depolarization have a smaller amplitude and a slower time course than those carried through AMPARs (Tempia *et al.*, 1998). Besides from being functionally confined to PFs (parallel fibers), the mGluRs have also been shown to be present at CF synapses on PNs (Dzubay & Otis, 2002; Figure 2).

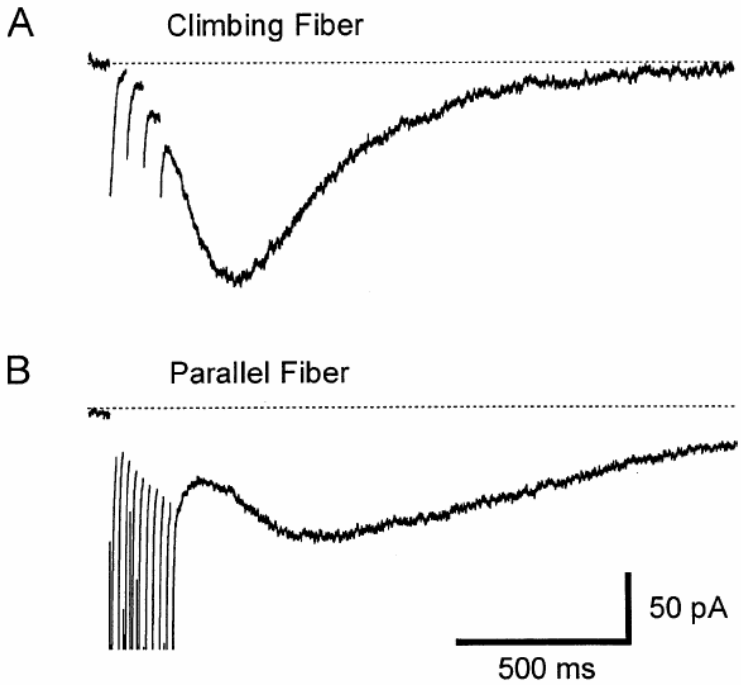

Figure 2. EPSCs in Purkinje neurons induced by stimulating climbing and parallel fibers. (**A**) mGluR1 EPSC in response to a short train of CF inputs (four stimuli at 20 Hz) in the presence of TBOA (glutamate transporter antagonist) at 34 °C. (**B**) Response, recorded from a nearby Purkinje neuron under the same conditions, elicited by a train of 10 stimuli (100 Hz) delivered to the PFs. The two responses have comparable amplitudes, but different time courses. [adapted after Dzubay & Otis, 2002]

Although the mechanisms underlying the release of Ca^{2+} from the internal stores after activation of mGluRs are well established, the mechanisms generating the slow EPSC are only poorly understood. In 2004 Canepari *et al.* have shown that the mGluR1-EPSCs are attributable to small-conductance, low-open probability Ca^{2+}-permeable cation channels. From studies on KO mice it has been revealed that the absence of TRPC3 channels makes impossible the generation of an EPSC by the application of DHPG, while the Ca^{2+} release from the intracellular stores remained unaffected (Hartmann *et al.*, 2008). More recently it has also been shown that there is a functional coupling between the mGluR1 and the $Ca_v3.1$ T-type Ca^{2+} channels present in Purkinje cell dendritic spines (Hildebrand *et al.*, 2009). Another interesting observation is that mGluR1 activation leads to a local increase in intradendritic $[Na^+]_i$ that could be explained either by a Na^+ flow into the dendrites through unspecific cation channels, or by a Na^+/Ca^{2+} exchange (Knopfel *et al.*, 2000). Apart from influencing the synaptic transmission at excitatory synapses, mGluR1 is also regulating GABAergic inhibitory synapses. Inhibition of mGluR1 prevented the long-term potentiation of $GABA_AR$ responsiveness (termed rebound potentiation; RP), whereas its activation rescues the RP induction from suppression by $GABA_BR$ (Sugiyama *et al.*, 2008).

1.2 Function of ion channels in Purkinje neurons

Many different ion channels have been characterized in PNs, amongst the voltage-dependent and calcium-dependent potassium channels, calcium channels, sodium channels and unspecific cation channels.

One important feature of the neurons involved in motor coordination is that they are spontaneously active. It has been suggested that an intrinsically active neuron can encode information in its pacemaking. Information about movement, which is relayed by both excitatory and inhibitory synapses, is encoded by Purkinje neurons as rapid and transient changes in their rate of spontaneous activity. And the increase or decrease in individual interspike durations from that of the intrinsic PN pacemaker would give information, to the deep cerebellar nuclear (DCN) neurons, relevant to motor coordination (Eccles, 1973). There are many types of ion channels in neurons, regulating the duration of APs and interspikes; and compensatory mechanisms could be imagined if one type of ion channel would be blocked, so that the firing rate wouldn't be much affected. However, the blockage of erg channels in

medial vestibular nucleus neurons (MVNn; Pessia *et al.*, 2008) or of P/Q-type Ca^{2+} channels in PNs (Walter *et al.*, 2006), disturbs the regularity of AP firing. It is therefore relevant to further consider the ion channels involved in generating APs, shaping them, generating and terminating the bursts, and the propagation along the axon of only the relevant information to the DCN neurons.

Swensen and Bean (2003) have shown that the post-spike inward currents driving sustained firing in Purkinje neurons are carried primarily by TTX-sensitive Na^+ channels and T-type Ca^{2+} channels. The inward currents are opposed by large Ca^{2+}-activated and purely voltage-activated K^+ currents. The small net inward current has an amplitude of many times less than that of each of the contributing currents; therefore a discrete change in the amplitude of any of them could affect the timing of the action potentials. If a Purkinje neuron fires short burst, the major difference between currents after the first spike and those after the second spike is a significant reduction in the Na^+ current. Longer bursts appear when the SK channels are blocked by apamin or when Ca^{2+} is replaced by Mg^{2+}. It seems that even if the Na^+ currents decline after the first interspike, they remain large enough to drive subsequent spikes at least in the absence of BK and SK channels.

In Purkinje neurons it has been shown that some Na^+ channels have an unusual behavior: after strong depolarizations, returning the membrane to voltages in the range of -60 to -20 mV elicits a resurgent Na^+ current. The channels underlying the resurgent Na^+ current are TTX-sensitive and produce a transient current on a simple depolarization from rest. At a mechanistic level, the resurgent current may represent recovery from inactivation proceeding through open states of the channel. These unusual properties are closely related to the distinctive firing behavior of Purkinje neurons, especially the ability to fire multipeaked APs. The sodium current that flows after one spike is enough to contribute significantly to the afterdepolarization leading up to the second spike (Raman & Bean, 1997).

In mammalian neurons Ca^{2+} currents are mediated via several voltage-gated calcium channels, which include five high-threshold (L, N, P, Q and R) and low-threshold (T) types (Catterall, 2000). The P/Q-type Ca^{2+} channels mediate the predominant fraction of high voltage-activated Ca^{2+} current in Purkinje neurons (Mintz *et al.*, 1992). Mostly dendritic (Rancz & Hausser, 2006), the P-type current is responsible for the generation of Ca^{2+} spikes, driving Na^+-Ca^{2+} burst firing in Purkinje neurons (Mori *et al.*, 2000). It also mediates Ca^{2+} influx

during somatic Na^+ action potentials, activating big- (BK) and small- (SK) conductance Ca^{2+}-activated K^+ currents which drive afterhyperpolarizing potentials (AHPs; Edgerton & Reinhart, 2003). The Purkinje neurons which had a mutation in the α_{1A} pore-forming subunit of P/Q-type Ca^{2+} channels exhibited a smaller dendritic tree than normal, indicative of developmental retardation in these cells caused by P/Q-type Ca^{2+} channel malfunction (Ovsepian & Friel, 2008). Pouille *et al.* (2000) proposed that the P/Q-type Ca^{2+} channels are important for eliciting repetitive firing. Their activation is able to increase the axonal $[Ca^{2+}]_i$ close to the site for fast AP initiation and where Ca^{2+}-dependent K^+ channels might be activated (Callewaert *et al.*, 1996). Interestingly, during P/Q-type Ca^{2+} channel blockade, membrane oscillations were induced or amplified, allowing Purkinje neurons to fire in bursts. This phenomenon could be determined by the suppression of a P/Q-type Ca^{2+} channel-mediated shunt of conduction that would prevent the propagation of low-threshold Ca^{2+} spikes between dendrites and soma (Pouille *et al.*, 2000).

In the dendrites of rat Purkinje neurons predominantly Kv3 subfamily K^+ channels (Kv3.3 and Kv3.4) are present at a high density. Kv3 currents have rapid activation and deactivation kinetics and inactivate partially. They require large depolarizations to be activated, making them suitable for shaping large depolarizing events while not disrupting smaller excitatory postsynaptic potentials (Martina et al., 2003). It is known that action potentials in Purkinje neurons repolarize rapidly (Martina *et al.*, 2003), but have no prominent afterhyperpolarizations, consistent with large K^+ currents with a rapid deactivation. It has been shown that the predominant K^+ current decays with a time constant < 1 ms (Raman & Bean, 1999).

The Kv3.3 channels are important for regulating the synaptically evoked Purkinje neuron complex spike, the massive postsynaptic response to the activation of climbing fiber afferent. Spikelet expression is regulated by somatic and not by dendritic Kv3.3 channel activity, the spikelets of a complex spike being generated in the axosomatic membranes (Davie *et al.*, 2008; Zagha *et al.*, 2008). Climbing fiber activation seems then to trigger the initiation of the complex spike at the axosomatic membrane, but it also triggers the prominent dendritic spikes, which were believed for a long time to be responsible for generating the complex spikes. In turn it proves that the dendritic spikes regulate the pause in axonal output after the complex spike, a well known feature of the climbing fiber response *in vivo* (Davie *et al.*, 2008).

The hyperpolarization-activated cation current (I_h) is known to be involved in synaptic integration shortening the width of postsynaptic potentials and dampening the summation of trains of inputs (Berger *et al.*, 2001). In the dendrites of Purkinje neurons, I_h exhibits a uniform distribution in striking contrast to the principal neurons of the cortex and hippocampus (Berger *et al.*, 2001; Angelo *et al.*, 2007). I_h shortens the time course of EPSPs, reducing their half-width through a two-step process: first, the effect of static "resting" conductance of I_h shortens the membrane time constant; and second, the depolarization deactivates I_h which in turn hyperpolarizes the membrane accelerating the decaying phase of the EPSP (Angelo *et al.*, 2007).

In intact Purkinje neurons from mature mice, burst firing occurs spontaneously as part of a cycle of tonic, bursting and silent periods (Womack & Khodakhah, 2002). Pouille *et al.* (2000) proposed a model for switching between these three modalities. The firing mode would be determined by the balance between depolarizing conductances and Ca^{2+}-dependent hyperpolarizing conductances activated by Ca^{2+} entry through voltage-gated Ca^{2+} channels. During a current injection a sustained Na^+ conductance is activated allowing the membrane to reach the threshold for the activation of fast-inactivating Na^+ conductance initiating fast APs. In the absence of external Ca^{2+} the membrane potential rapidly reached the potential for Na^+ channel inactivation; therefore only a short burst can be initiated, followed by a plateau. In the presence of external Ca^{2+}, Ca^{2+} entry during the APs is thought to activate Ca^{2+}-dependent hyperpolarizing conductances which maintain the membrane potential between the activation and inactivation threshold for the fast Na^+ currents; and subsequent spikes can be initiated and a sustained firing occurs. If these hyperpolarizing conductances activate transiently to a greater extent and bring the membrane potential below the threshold value for Na^+ channels, then a bursting behavior is elicited (Pouille *et al.*, 2000).

Contrary to what is generally accepted as a general mechanism for burst termination, another mechanism was suggested, in which the SK and BK channels are not important in burst termination (Womack & Khodakhah, 2004). It was concluded that the most important for generation and termination are the P/Q-type Ca^{2+} channels. The T-type Ca^{2+} channel and the hyperpolarization-activated channels are also not essential. The bursts appear to result from the interplay between a progressively depolarizing membrane potential, on which somatic Na^+-dependent APs ride, and the dendritic Ca^{2+} spikes that terminate the bursts. Two mechanisms could explain the generation and termination of the bursts: a "somatic" and a

"dendritic" mechanism. The first proposes that bursts are initiated by somatic conductances and terminated by dendritic Ca^{2+} spikes; the second is that bursts are both initiated and terminated by the dendritic Ca^{2+} spikes. In the "somatic" mechanism the Ca^{2+} spike activates when the progressive depolarization of the somatic membrane propagates and reaches the threshold for its generation. In the scenario that bursts are controlled entirely by the dendritic Ca^{2+} spikes, it is possible that the foot of the Ca^{2+} spikes causes the progressive depolarization of the somatic membrane. One observation supports the "dendritic" mechanism: there is a cyclical generation of dendritic Ca^{2+} spikes associated with bursting that remains after elimination of somatic Na^{+}-dependent APs (Womack & Khodakhah, 2004). It is possible that burst termination takes place when the Ca^{2+} spike inactivates such a large fraction of the Na^{+} channels that the cell is incapable of generating further APs. Alternatively, it may be that the large influx of Ca^{2+} mediated by the Ca^{2+} spike activates a substantial K^{+} conductance that abruptly terminates the somatic bursts. Womack and Khodakhah (2004) favor the former possibility because although Ca^{2+}-activated K^{+} channels contribute to the interburst interval, regular spontaneous bursting is not disturbed when both SK and BK channels are blocked. As for the T-type Ca^{2+} current they propose that it contributes to depolarizing the membrane toward threshold and initiation of the next burst.

As for the transmission of simple, complex spikes and bursts to the Purkinje neuron axons and further, it seems that there is not a one to one relation between somatic and axonal spikes (Khaliq & Raman, 2005; Monsivais *et al.*, 2005). Simultaneous somatic and axonal recordings revealed that simple spikes propagate faithfully at physiological frequencies, whereas calcium spikes do not. Individual spikelets in the complex spike do not propagate faithfully, with only approximately half of the spikelets propagating as axonal APs. One explanation has been proposed for the existence of a complex spike at the somatic level that actually doesn't propagate faithfully along the axon. On one hand the large synaptic and intrinsic conductances underlying the complex spike can provide a much more effective reset of synaptic integration than a simple spike which could be relatively ineffective (Hausser *et al.*, 2001); and on the other hand, the axonal doublet evoked by the complex spike in the axon is associated with an interspike far shorter than in simple spike trains, therefore constituting a distinct signal to the downstream synapses and being at the same time energy efficient (Monsivais *et al.*, 2005).

1.3 The Erg K^+ channels

In humans, the K^+ channel group consists of 78 members that can be divided into four structural types according to their mode of activation and number of transmembrane segments (Harmar *et al.*, 2009): voltage-gated K^+ channels (K_v) with six transmembrane segments, Ca^{2+}-activated K^+ channels (K_{Ca}) with six or seven transmembrane segments, 2-pore K^+ channels (K_{2P}) with four transmembrane segments and inwardly rectifying K^+ channels (K_{ir}) with two transmembrane segments (Figure 3). Rodent homologues for almost all K^+ channel members have been identified.

Ether-à-go-go-related gene (erg) K^+ channels (K_v11) belong to the voltage-gated K^+ channel family which is the largest in this group comprising 40 members in humans, classified into 12 subfamilies (K_v1 to K_v12). The first K_v channel was cloned in *Drosophila* and named *Shaker* after the phenotype of the mutant flies. Similar to it, all mammalian K_v channels consist of four α-subunits, each containing six transmembrane α-helical segments (S1-S6) and a P-loop (entering the pore), which are arranged to form a central pore. Within a subfamily, different types of α-subunits can constitute a given channel; therefore K^+ channels can be either homotetramers or heterotetramers. Each ion conduction pore is lined by four S5-P-S6 segments. The four S1-S4 segments act as voltage sensors, each of them having four positively charged arginine residues in the S4 helix. The voltage sensor responds to changes in the voltage across the membrane and functions as a "gate" through the S4-S5 linker (Wulff *et al.*, 2009).

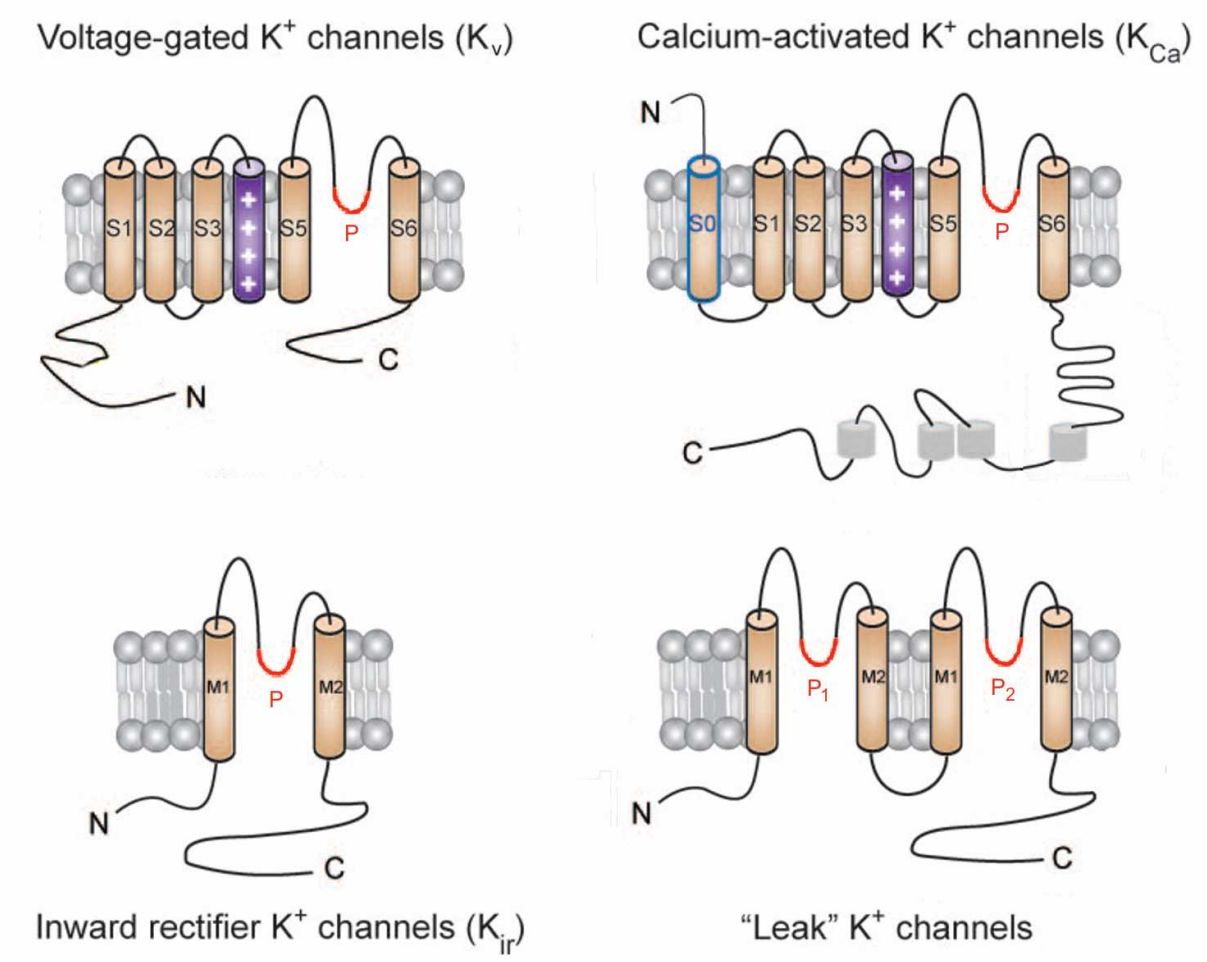

Figure 3. Structural types of α subunits within the K^+ channel group. The voltage-gated K^+ channels (Kv) and some Ca^{2+}-activated K^+ channels (K_{Ca}) have 6 transmembrane segments (S), whereas other K_{Ca} have an additional S domain. The inward rectifier K^+ channels (K_{ir}) have 2 transmembrane domains (M1 and M2) and a pore (P) loop. The "leak" K^+ channels have 4 transmembrane domains (M1 to M4) and two P loops (K_{2P}). [adapted after Benarroch, 2009]

Erg K^+ channels constitute a subfamily of the *ether-à-go-go* gene (EAG) voltage-gated K^+ channel family that comprises also the eag (K_v10) and elk (eag-like, K_v12) channels (Figure 4). Mutants of these channels have been studied for the first time in *Drosophila melanogaster*. Here, a rhythmic leg-shaking phenotype during ether anesthesia has been described in mutants of the *eag* locus. In the larvae of these mutants a high frequency of action potential firing, in motor nerve fibers, was found. This increased excitability suggested that the *eag* locus encodes a K^+ channel (Warmke *et al.*, 1991). A low-stringency screen of a *Drosophila* head cDNA with an *eag* cDNA probe identified a cDNA with an incomplete open reading frame (ORF), related to the eag protein, and therefore designated *elk* (Warmke & Ganetzky, 1994). In addition to the *eag* and *elk* loci, a member of the *erg* subfamily has been identified as the seizure locus (*sei*) in *Drosophila*; mutations of this locus induce a temperature-sensitive

paralysis combined with hyperactivity in the flight motor pathway (Titus *et al.*, 1997). These members in *Drosophila* have homologues in mammals which were identified for the first time in 1994 (Warmke & Ganetzky, 1994).

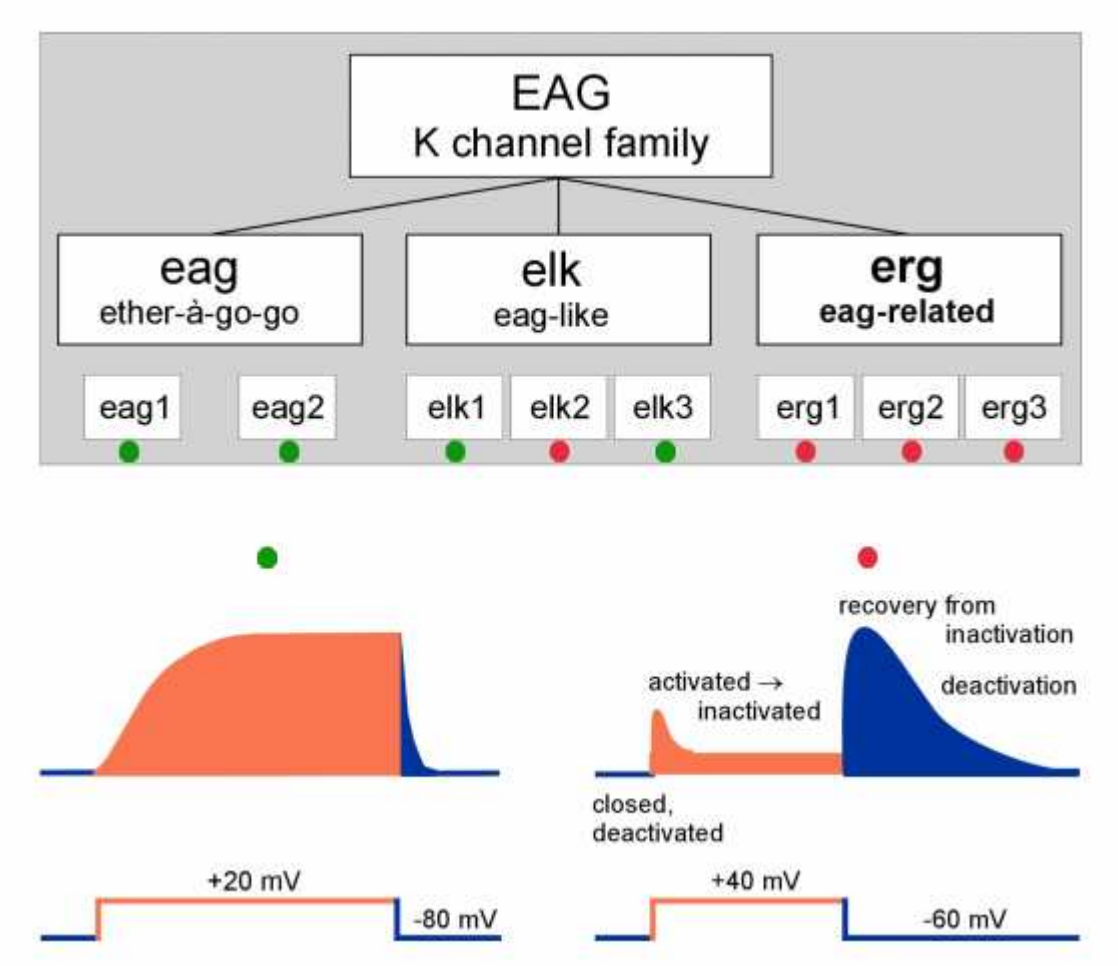

Figure 4. The *ether-à-go-go* gene (EAG) K^+ channel family. This family consists of three subfamilies: eag (*ether-à-go-go* gene), elk (eag-like gene), and erg (eag-related gene). Each of these subfamilies has 2 or 3 members. The schematic drawing on the left shows an eag-, elk1- or elk3-mediated current (green circles) which does not inactivate upon depolarization and upon repolarization has a tail current typical for delayed rectifiers. The schematic drawing on the right of an erg- or elk2-mediated K^+ current (red circles) illustrates that a depolarization elicits a small transient current followed by a small steady-state current. Upon repolarization the typical tail current occurs. [adapted after Schwarz & Bauer, 2004]

The erg K^+ channel subfamily is made of mainly three protein subunits: erg1 (Kv11.1), erg2 (Kv11.2) and erg3 (Kv11.3) coded by three different genes (Kcnh2, Kcnh6 and Kcnh7). By alternative splicing different protein isoforms can occur for each of the genes (Figure 5), e.g. Kcnh2 can be translated into functional erg1a and erg1b channel proteins, but also into erg1a-uso and erg1b-uso subunits that do not form functional channels (Guasti *et al.*, 2008), but when combined with the others modulate the biophysical properties of the current (Aydar & Palmer, 2006).

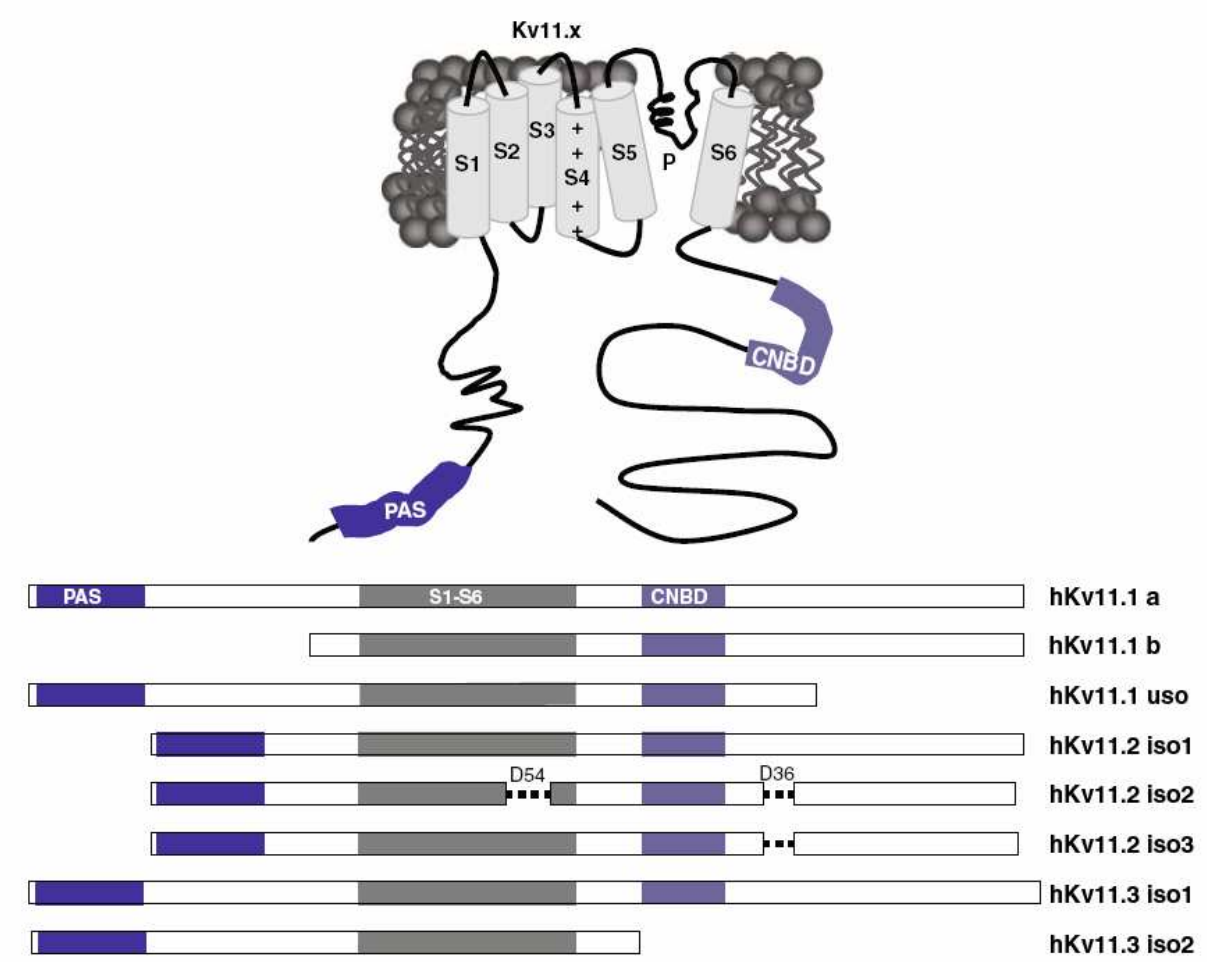

Figure 5. Human hKv11 channels. Schematic diagram of a Kv11 α subunit containing 6 transmembrane segments S1-S6 and a P loop; the N-terminal PAS domain and the C-terminal cyclic nucleotide binding domain (CNBD) are also highlighted. The bar diagrams depict the known isoforms in humans of the three channel subtypes. [adapted after Einarsen *et al.*, 2009]

The properties of the functional subunits have been studied by expression in cell lines or *Xenopus* oocytes. Erg2 proved to be the strongest inward rectifier since it activates at the most positive potential, whereas erg3 is the weakest, activating at more negative potentials (and also has a faster activation and deactivation and slower inactivation kinetics (Wimmers *et al.*, 2002). In contrast to other K_v channels, erg K^+ channels are characterized by a peculiar inward rectification mechanism caused by the two voltage-dependent activation and inactivation gates (Figure 4 bottom, Figure 6). The dependence of erg current amplitude on the $[K^+]_o$ has also been documented, a paradoxical increase in current amplitude despite decreased electrical driving force being observed in elevated $[K^+]_o$ for all three subunits (Shibasaki, 1987; Sturm *et al.*, 2005). Moreover, at higher temperatures the erg current amplitude increases considerably (Vandenberg *et al.*, 2006).

Upon depolarization the time course of erg current activation is slow reaching a steady-state only after a few seconds. Stronger depolarizations elicit smaller outward currents because of inactivation which is due to the C-type (close to the C-terminus) inactivation gate resulting in inward rectification. Upon repolarization typical transient, hook-shaped tail currents occur due to the fast recovery from inactivation and slow deactivation (Schwarz & Bauer, 1999).

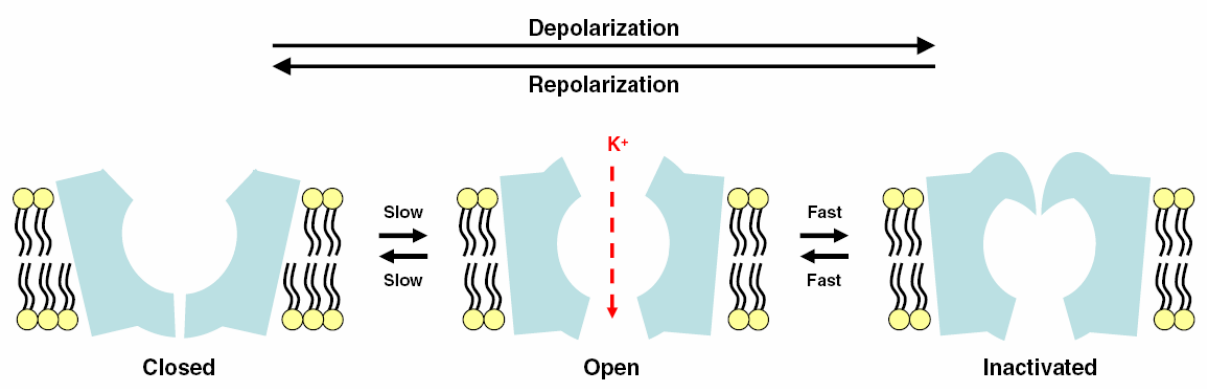

Figure 6. Gating scheme of erg K^+ channels. The three main states that erg K^+ channels occupy are illustrated (closed, open or inactivated) and the transitions between them. At membrane potentials below -60 mV, most erg K^+ channels reside in the closed state. Upon depolarization, the channels move to the open state (activation) at a low rate, followed by a collapse of the outer mouth (inactivation) at a high rate. Upon repolarization, the pore regains its structure and the channels reopen (recovery from inactivation) before moving back to the closed state (deactivation) [adapted after Larsen, 2010]

The history of erg K^+ channel discovery starts in 1990 when Sanguinetti and Jurkiewicz showed that the delayed rectifier K^+ current of guinea pig ventricular myocytes is made of two components. One of the components (I_{Kr}) exhibits prominent inward rectification and activates very rapidly when compared to the other (I_{Ks}). Moreover, the fast component is blocked by the methanesulfonanilide class III antiarrhythmic agent, E-4031. Therefore it was possible to isolate the effects of the fast component on the duration of an action potential (AP), which increases when I_{Kr} is blocked.

With the discovery of the human erg gene (back then named *HERG*, now KCNH2) as a member of the EAG K^+ channel family (Warmke & Ganetzky, 1994) a further step was made towards the identification of the molecular basis for some human heart diseases. It has been proven that the I_{Kr} component of the cardiac delayed rectifier K^+ current was mediated by HERG ($hK_v11.1$) channels (Sanguinetti *et al.*, 1995; Trudeau *et al.*, 1995). Mutations in the KCNH2 gene were found to be the physical basis for some forms of inherited long QT interval (LQT) syndrome (Curran *et al.*, 1995). Two years later (1997), London *et al.* cloned

the mouse equivalent of KCNH2, back then named *Merg1* (now Kcnh2), coding for its protein isoform Merg1a (K_v11.1a), but also coding for two other N-terminal truncated isoforms: Merg1a' (K_v11.1a'), which lacks the first 59 amino acids and is not expressed abundantly, and Merg1b (K_v11.1b), which has a markedly shorter N-terminal domain starting with 36 unique amino acids (for the human homologues see Figure 3). Merg1a and Merg1b subunits coassemble to form heteromultimeric channels with deactivation kinetics that are faster than those of Merg1a or HERG currents and slower than those of Merg1b currents, but nearly identical to what has been observed for I_{Kr}.

Additional to the Kcnh2 gene coding for the erg1 K^+ channel two other members of the erg subfamily have been identified in rat in 1997, Kcnh6 and Kcnh7, back then named *erg2* and *erg3*. These two genes are predominantly expressed in the nervous system, in contrast to Kcnh2 which is widely expressed in both neural and non-neural tissues (Shi *et al.*, 1997).

Since the discovery of erg K^+ channels and their different subunit composition, many tissues and cell types from various species have been characterized with respect to the biophysical properties of the erg currents, their involvement in physiology, distribution in the plasma membrane and subunit expression. In the cardiac tissue in the sinoatrial node cells, the erg current with its slow time course of deactivation contributes to the ionic mechanisms underlying pacemaking (Zaza *et al.*, 1997), whereas in the atrial and ventricular myocytes the I_{Kr} plays an important function in plateau formation and repolarization of the action potential (Hancox *et al.*, 1998).

Erg currents have also been detected in smooth muscle cells of esophagus, stomach, colon and gallbladder (Akbarali *et al.*, 1999; Ohya *et al.*, 2002; Shoeb *et al.*, 2003; Parr *et al.*, 2003, respectively). It is assumed that the erg currents contribute to the maintenance of the resting potential of these cells. In esophageal smooth muscle cells blockade of erg K^+ channels induces spontaneous contractions, presumably due to an increase in $[Ca^{2+}]_i$ following the opening of voltage-gated Ca^{2+} channels.

Glomus cells of the rabbit carotid body have an erg current which is also believed to contribute to the maintenance of the resting potential. After the blockage of the current, the cell depolarizes, the $[Ca^{2+}]_i$ increases and the afferent nerve fibers fire action potentials at a higher frequency, mimicking the effects induced by hypoxia on the action potential frequency

(Overholt *et al.*, 2000). Reactive oxygen species have been shown to increase the HERG currents (Taglialatela *et al.*, 1997). Presumably, the EAG domain of the erg protein which is known to be O_2-sensitive in other proteins is responsible for the sensitivity of the ion channel (Pellequer *et al.*, 1999).

In various pituitary cells or pituitary-derived tumor cell lines hormone secretion is regulated by changes in their excitability. In lactotropes, TRH stimulates prolactin secretion by a membrane depolarization accompanied by an increase in the rate of Ca^{2+} action potential firing leading to an increase in $[Ca^{2+}]_i$ (Corrette *et al.*, 1995). In native lactotropes and in clonal rat somatomammotropes (GH3/B6; Bauer *et al.*, 1990) the erg current is modulated by TRH (Corrette *et al.*, 1996; Schafer *et al.*, 1999). The erg current reduction is mainly due to a shift in the erg current activation curve to more positive membrane potentials and a decrease in the maximal amplitude of the current (Schledermann *et al.*, 2001). In mouse gonadotropes the erg current can be partially blocked by GnRH through the same mechanisms. The complete blockage of the erg current by application of E-4031 depolarizes the cells and the $[Ca^{2+}]_i$ increases, theoretically contributing to the LH secretion process (Hirdes *et al.*, 2010). The hormone-induced effects on the erg currents is thought to be mediated by a G protein-coupled intracellular signal cascade involving an as yet unknown intracellular messenger. Although it is very likely that ion channel phosphorylation is involved in the TRH-induced signal cascade, activation of protein kinases C and A do not mediate this effect (Schledermann *et al.*, 2001).

Endogenous erg currents have been also studied in neuroblastoma cells, which exhibit a high variability in erg current amplitude. This variability was due to different stages of the cell cycle. After synchronization the erg current amplitudes were more homogeneous (Arcangeli *et al.*, 1995). Neuritogenesis was accompanied by a hyperpolarization of the resting potential by 10-20 mV due to an increase in erg current amplitude; both were abolished by pertussis toxin (PTX), demonstrating that the effect of the cell adhesion molecules on the erg K^+ channels are mediated by G proteins (Arcangeli *et al.*, 1993). Moreover, the action potential frequency accommodation seen in these cells is due to the erg K^+ channels (Chiesa *et al.*, 1997).

The erg K^+ channels have been also found to be expressed during the early stages of neuronal differentiation. In embryonic neuronal cells originating from quail neural crest cells the erg

K^+ channels are replaced at later stages by classical inward-rectifying K^+ channels which make the resting membrane potential more negative than at immature stages (Arcangeli *et al.*, 1997).

A growing interest in the function of erg K^+ channels in neurons developed after it has been shown that all three subunits are expressed in the brain. Using specific antibodies Guasti *et al.* (2005) have shown that erg1a, erg1b and erg3 proteins are highly expressed in mice olfactory bulb, paleocortex, hippocampus, neocortex, thalamus, hypothalamus, midbrain, cerebellum and spinal cord. In contrast, erg2 has a much lower protein expression, with the highest levels in the red nucleus and Purkinje neurons. Previous NR-ISH (nonradioactive in situ hybridization) studies in rat brain have shown that the erg K^+ channel mRNAs are present in most neuronal cell types (Saganich *et al.*, 2001; Papa *et al.*, 2003).

In several of these neuronal cell types the erg currents have been biophysically characterized and their involvement in excitability has been assessed. In rat embryonic serotonergic neurons a fast erg current has been characterized with activation and deactivation kinetics closer to erg1b and erg3 currents respectively (Hirdes *et al.*, 2005). In the neurons of the medial vestibular nucleus the blockage of the erg current increased the spontaneous action potential frequency and in some cells induced a more irregular firing pattern. The threshold, amplitude and overall shape of the action potentials were not modified upon application of erg channel blocker, whereas it increased the steepness of the interspike slopes (Pessia *et al.*, 2008). In mice deprived of pheromonal stimulation the reduction of erg current density in basal vomeronasal neurons current injection leads to an irregular firing pattern due to Na^+ channel inactivation upon depolarization (Hagendorf *et al.*, 2009). Erg currents in mitral/tufted neurons from the mouse olfactory bulb are modulated by the metabotropic receptor for glutamate, mGluR type I. The mGluRI agonist DHPG reduces the maximal erg current amplitude to approximately 75% and shifts the activation curve to more positive potentials by around 4 mV resulting in an erg current reduction near the resting potential contributing to the depolarization caused by mGluRI stimulation. Specific block of the erg current depolarizes the membrane potential and the action potential frequency increases, especially in a more elevated K^+ solution (5 mM; Hirdes *et al.*, 2009). In the neurons of the mouse medial nucleus of the trapezoid body (MNTB), application of E-4031 depolarizes the membrane potential, reduces AP threshold and accommodation and increases AP frequency (Hardman & Forsythe, 2009).

Previously, part of the biophysical properties of erg currents in cerebellar Purkinje neurons from immature, postnatal day 5 to 9 (P5 to P9), and young adult (P22 to P42) mice have been characterized (Sacco *et al.*, 2003). However, effects of the erg current on the action potential pattern were only assessed in the P22 to P42 mice, in which action potential accommodation disappeared in half of the neurons when an erg channel specific blocker was applied. Upon stimulation of climbing fibers, complex spikes could be recorded from Purkinje neurons as a first big spike and additional spikelets (around 4). After blockage of the erg current there was a small increase in the number of spikelets (0.6; Sacco *et al.*, 2003).

In recent years some connections between the HERG genes and brain related pathologies were indicated. A primate-specific isoform of the more common subunit (KCNH2-1A), KCNH2-3.1, was identified which is upregulated in patients with schizophrenia (Huffaker *et al.*, 2009). In contrast to the firing pattern in control rat primary cortical neurons, when the KCNH2-3.1 subunit is overexpressed, trains of APs no longer accommodate due to fast deactivation of the isoform-carried current. Since the KCNH2-3.1 subunit is expressed only in primates it is tempting to suggest that it may be involved in cognitive processes. The change in the firing pattern could affect higher-order cognition possibly leading to some of the symptoms seen in patients with schizophrenia. In another study (Johnson *et al.*, 2009), it was found that within the group of patients with the LQT2 syndrome caused by mutations in the KCNH2 gene there is a higher percentage of persons that have the positive “seizure phenotype”, personal history of seizures or a history of antiepileptic drug therapy than within any other LQT syndrome subtype group. Therefore, the patients with a KCNH2 mutation could also be susceptible for epilepsy rather than simply a ventricular arrhythmia with subsequent collapse and seizure activity.

2. Materials and Methods

2.1 Acute slice preparation

Cerebellar slices were prepared from 5-10- and 22-42- day-old male C57BL/6 mice. In accordance with institutional guidelines, the very young animals were decapitated in a single step while the older ones were anesthetized with isoflurane (Abbot, Mumbai, India) and subsequently decapitated. The brain was quickly (1-2 min) removed and immersed in ice-cold carbogenated (95% O_2, 5% CO_2, 30 min) artificial cerebro-spinal fluid (ACSF) solution (see in Solutions and chemicals) containing (in mM): 125 NaCl, 2.5 KCl, 3 $MgCl_2$, 1.25 NaH_2PO_4, 26 $NaHCO_3$, 20 glucose, pH 7.4. The brain was cut on the mid-sagittal plane with a scalpel and the two halves were glued with cyanoacrylate on the cutting plate of a Vibratome (Leica VT1200S). Parasagittal slices of 200 µm were cut and subsequently incubated in a recovery ACSF (2 mM $MgCl_2$ from the above mentioned ACSF were replaced with 2 mM $CaCl_2$) and incubated at 35° C for 1 hour. The recordings were made within 8 hours after incubation.

2.2 Heterologous expression

2.2.1 Transformation and plasmid purification

The cDNAs for rat *erg* channel subunits, r-*erg1a*, r-*erg1b*, r-*erg2* and r-*erg3* (kindly provided by Prof. Dr. Christiane K. Bauer, Institute for Vegetative Physiology and Pathophyisiology, UKE, University of Hamburg), have been placed into pcDNA3 vectors (Invitrogen, Carlsbad, USA) and amplified by transformation of competent bacteria. 100 µl of competent *Escherichia coli* cells were placed in pre-cooled tubes together with 2 µl of cooled β-mercaptoethanol (1:10 dilution) and left on ice for 10 minutes. Then, 0.5 µl of the vector (DNA 1 µg/µl) was added and left for 30 minutes on ice with the bacteria. After a heat shock to 42 °C for 40 s to transform the bacteria, the mix was allowed to cool down for 2 minutes on ice. 900 µl of preheated Super Optimal broth - Catabolite repression (SOC) medium was added to each tube and incubated afterwards at 37 °C on a shaker with 225 rpm for 60 minutes. After incubation, 50 µl of the mix were placed on Lysogeny broth (LB)-agar plates

with 100 µg/ml ampicillin and spread out on the whole surface. The plates were then kept at 37 °C overnight.

The next day the plates were checked for grown colonies, and only one colony was picked up with a sterile tip and placed in Erlenmeyer beakers with 50 ml of LB medium and 50 µl of ampicillin; the beakers were incubated overnight at 37 °C on a shaker with 125 rpm.

The bacteria-containing LB-medium was collected in 50 ml tubes and centrifuged at 5000 x g for 15 min at 4 °C. The supernatant was discarded and in order to proceed to cell lysis the pellet of bacterial cells was resuspended in 4 ml of precooled Buffer S1 + RNase A (NucleoBond plasmid purification kit, Macherey-Nagel, Düren, Germany). 4 ml of Buffer S2 was added to the suspension and the tubes were gently inverted 6-8 times for mixing. The mixture was incubated at room temperature (20-25 °C) for 3 min. Precooled Buffer S3 (4 ml) was added to the suspension and the lysate was gently mixed until a homogeneous suspension containing an off-white flocculate was formed. The suspension was incubated for 5 min on ice. For a Midi-preparation a NucleoBond AX 100 Column was used and equilibrated with 2.5 ml of Buffer N2. The column was allowed to empty by gravity flow. In order to filter the suspension a NucleoBond Folded Filter was placed in a small funnel and pre-wet with a few drops of deionized H_2O; then the bacterial lysate was loaded onto the wet filter and the flow-through collected. The cleared lysate was then loaded onto the column which was allowed to empty by gravity flow (binding step). The column was then washed with 10 ml of Buffer N3; the flow-through was discarded. The plasmid DNA was afterwards eluted with 5 ml of Buffer N5. The precipitation of the eluted plasmid DNA was achieved with 3.5 ml room-temperature isopropanol. After careful mixing the precipitated DNA was centrifuged at 15,000 x g for 30 min. at 4 °C. The supernatant was carefully discarded. The DNA pellet was washed with 2 ml of room-temperature 70% ethanol, vortexed briefly and centrifuged at 15,000 x g for 10 min at room temperature. The ethanol was removed with a pipette tip. The pellet was allowed to dry at room temperature for around 10 min. The DNA pellet was then re-dissolved in 50 µl of Tris-HCl (10 mM). By using a GeneQuant spectrophotometer (Pharmacia Biotech, Piscataway, USA) the absorbance at 260 nm was determined for a 1:100 dilution of the samples; and by multiplying with 5 the amount of DNA (in µg) in the initial 50 µl of Tris-HCl was calculated. Subsequently, the adequate volume of Tris-HCl was added in order to reach a concentration of 1 µg/µl of DNA. Plasmid integrity and the way the insert was oriented were determined by agarose gel (1.5%) electrophoresis. The following restriction enzymes were

used: for pcDNA3/rerg1a – Nhe I (1 site), Bgl II (2 sites), Sma I (3 sites); for pcDNA3/rerg1b – Hind III (1 site), Sma I (2 sites); for pcDNA3/rerg2 – Srf I (1 site), Hind III & Eco81 I (each 1 site); for pcDNA3/rerg3 - Eco81 I (2 sites). Each digestion mix had a final volume of 30 µl, of which 1 µl was the plasmid DNA and 3 µl the buffer (Fermentas, St. Leon-Rot, Germany: Tango buffer for NheI, Sma I, Eco81 I; Orange buffer for BglII; Red buffer for Hind III; Universal buffer – Stratagene, Amsterdam, The Netherlands for Srf I). In the digestion mix containing both Hind III and Eco81 I, the Tango buffer was used; since the efficiency of Hind III in this buffer is 50% the amount of enzyme was doubled (1 µl). From all the other enzymes 0.5 µl were added to the mix. Autoclaved H_2O was added to get the final volume of 30 µl. All mixes were incubated for 20-30 min at 37 °C, except for the mix containing Sma I which was incubated at 30 °C. After incubation, 10 µl of migration buffer was added to each mix and 10 µl were subsequently pipetted in each slot of the agarose gel; 4 µl of HyperLadder I (Bioline, Taunton, USA) were pipetted in the first slot. After 30-45 min at 120 V the gel was visualized under UV light.

2.2.2 Transfection

The *human* embryonic kidney (HEK)293 cell line was used as the overexpression system. The cells were cultivated in 25 cm^3 tissue flasks (Sarstedt, Newton, USA) in DMEM / Ham's F12 medium supplemented with 10% FBS (PAA Laboratories, Pasching, Austria) and with 1% Pen/Strep, 1% L-Glutamine (Gibco Invitrogen Co., Auckland, NZ) at 37 °C and 5% CO_2. Medium was replaced every 2 days. In 3-4 days the cells divide and cover almost the entire surface to which they had attached. When this stage was reached, the medium was removed, 2 ml of 0.05% Trypsin-EDTA (Invitrogen, Carlsbad, USA) was added and the flasks were put back into the incubator for 2 min. Subsequently, 2 ml of culture medium was added and cell density was determined in a Neubauer chamber. Each time a new culture flask was prepared, the cells were added at a density of 10^6 cells per 7 ml of medium. For transfection, the cells were placed on poly-L-lysine (PLL) coated glass coverslips in 35-mm cell-culture dishes (Nunc, Roskilde, Denmark) at a density of 10^5 cells per 2 ml and used within four days. The sterile glass coverslips were previously incubated with a solution of poly-L-lysine (PLL, Sigma-Aldrich, St. Louis, USA) for 1 hour and washed with autoclaved H_2O in order to remove the unbound PLL.

Before the transfection procedure the cells were allowed to stay in culture for at least one day following the enzymatic digestion. The transfection mix was prepared by diluting 5 µl of Lipofectamine (Invitrogen, Carlsbad, USA) and 1 µl of the plasmid of interest (1 µg/µl) with 1.5 µl of the "marker" plasmid pcDNA3/mCherry (0.4 µg/µl, kindly provided by Dr Ulrich Boehm, ZMNH, Germany) in 250 µl of Optimem (Invitrogen, Carlsbad, USA) each. In the case of the subunits that had a lower expression, such as r-erg1b and r-erg2, 1.5 µl of cDNA solution was added. After 5 min at room temperature the two dilutions were combined and incubated at room temperature for 20 min. After the cells were washed with 1 ml of Optimem, the 500 µl transfection mix was added and the culture dishes were incubated for 4 hours. After the transfection step ended the mix was replaced by 2 ml of culture medium. The next day the cells were ready for electrophysiological recordings. Transfected cells were visible by red fluorescence when stimulated at 540 nm.

2.3 Electrophysiology

2.3.1 The Patch-clamp technique

Given that an intact cell has a membrane potential, a membrane resistance and a capacitance, one could construct an electronic model of a cell:

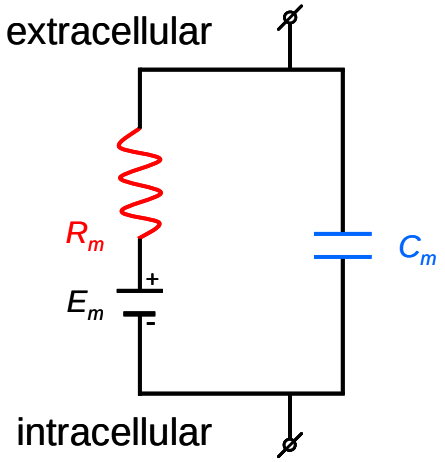

Figure 7. The equivalent electrical circuit for the plasma membrane. The plasma membrane separates two environments: the extracellular and intracellular compartments. Since both these compartments contain electrically charged compounds (especially ions) and the plasma membrane is a lipid bilayer, the latter creates a barrier blocking the free circulation of the electrolytes (and this is equivalent to a resistance from an electrical circuit, R_m). Acting like an insulator, having electrical charges on both sides, the plasma membrane constitutes also a capacitor (C_m). The difference in charge between these two environments creates a driving force for the charged particles (E_m). [adapted after Hille, 2001]

Electrophysiological techniques can be divided into indirect methods that employ extracellular electrodes, and direct methods that utilize micropipettes to make contact to the cell of interest. The latter include intracellular recording techniques, in which the pipette penetrates the cell, and patch clamp, where the pipette makes only contact to the cell. The equivalent circuits of electrophysiological experimental situations contain mainly resistors and capacitors. A cell-pipette system contains a set of such resistors and capacitors as follows:

- membrane resistance: represents the opposing force to ionic transfer across the plasma membrane;
- membrane capacitance: appearing due to the fact that the plasma membrane is an insulator separating two environments, the extracellular and intracellular spaces;
- pipette resistance: represents the resistance of the narrow column of fluid that is contained in the pipette;
- pipette capacitance: created because of the pipette glass walls that separate the bath solution from the pipette solution;
- leak resistance: represents the resistance of the connection between the pipette and the cell membrane to ionic conductance between the cytosol and the bath.

One of the features of patch clamp that makes the method so powerful is that it can be used in different ways so that the experimenter can study ion channels at different levels (the whole population of ion channels or individual ion channels) and manipulate easily the fluid on the extracellular or intracellular side of the membrane during a recording (Molleman, 2003). The various patch-clamp configurations in the order of their possible formation are (see Figure 8):

- Cell-attached patch mode: the pipette is positioned against the plasma membrane where the glass makes a very strong connection to the membrane lipids; the cell remains intact but in this configuration no manipulation of the media on the intracellular side of the membrane or of the potential over the patch is possible.
- Whole-cell mode: the membrane under the pipette tip in cell-attached mode is ruptured and the pipette solution and the electrode make direct electrical contact with the cytoplasm; since the patch electrode is on one side of the plasma membrane and the ground electrode is on the other, the membrane potential can be directly recorded.
    - The volume of the cytoplasm is negligible compared with that of the pipette and many intracellular factors relevant to the subject of study can be washed out in the

pipette solution; to avoid this, in many cases it is possible to perform perforated-patch clamp, where the electrical contact with the cytosol is established through pores in the plasma membrane, formed by a membrane perforating agent added to the pipette solution (nystatin or amphotericin B).

  - Sometimes it is needed to isolate the somatic membrane of neurons from the dendritic or axonal membrane; a variant of the whole-cell configuration is the one in which the nucleus is taken away from the rest of the cell together with some of the somatic membrane, while the pipette remains connected to the membrane and communicates with the cytoplasm surrounding the nucleus (nucleated patch mode).

- Outside-out mode: which is obtained by pulling away the patch pipette from a cell in the whole-cell configuration; the membrane will eventually break and owing to the properties of the phospholipids, fold back on itself into a patch covering the pipette. This configuration can be used to study the effects of extracellular factors on single ion channels, because the bath composition can be altered easily during recording.
- Inside-out excised patch: is obtained from a cell-attached patch configuration, where the pipette is pulled away. As the pipette is pulled away the membrane elongates and breaks at some point, forming a vesicle attached to the pipette tip; the vesicle can be destroyed by a short exposure to air, and this leaves a patch with the cytosolic side facing the bath. Inside-out patches are ideal for studying the effects of cytosolic factors on channels.

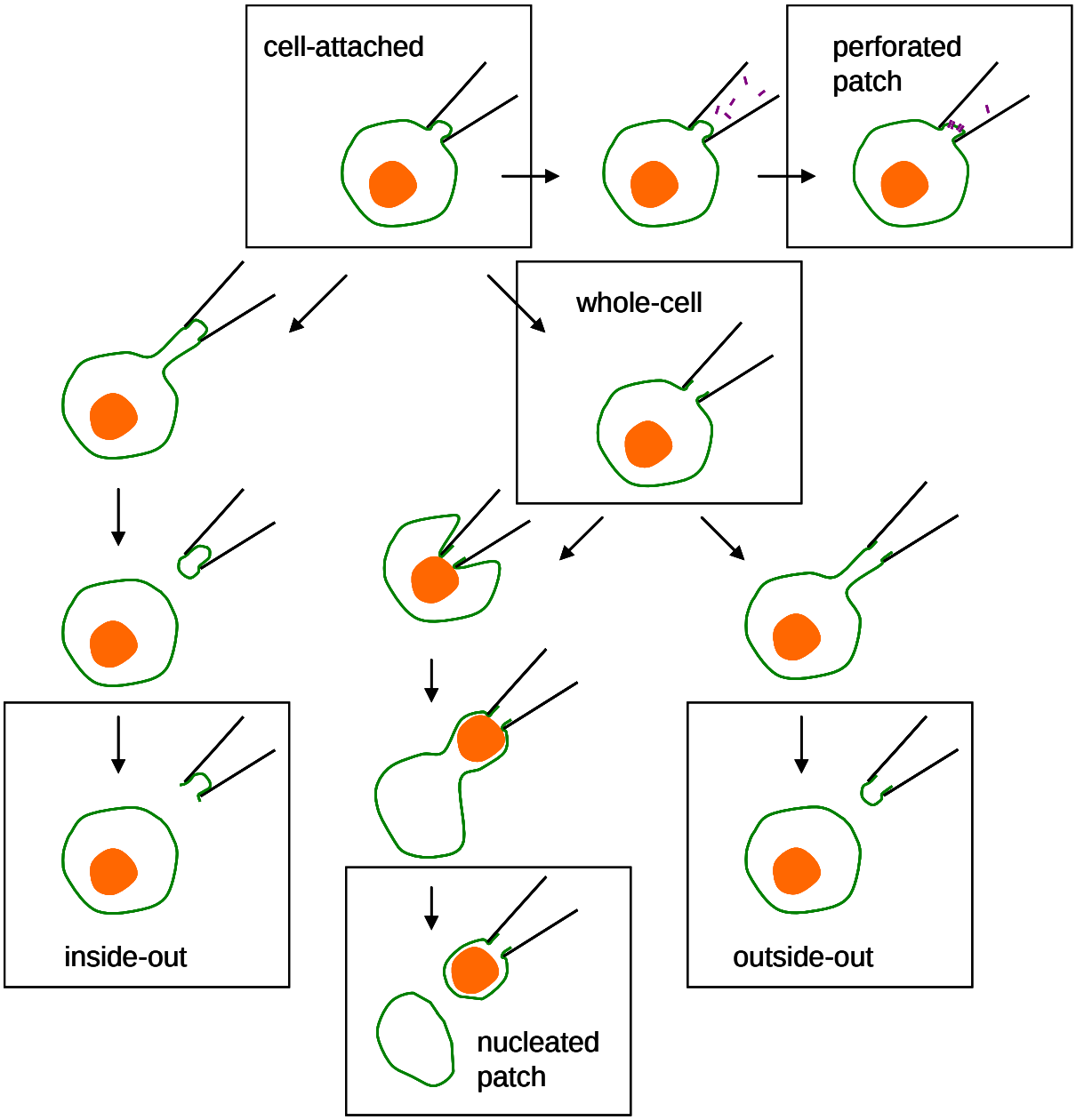

Figure 8. Patch-clamp configurations. The cell-attached configuration is the first that can be obtained when the pipette forms a strong connection to the cell membrane. If in the pipette solution some perforating agent is incorporated (in violet), the perforated patch configuration is obtained. If instead, the membrane under the patch is disrupted a whole-cell configuration is formed. From this configuration two others can be obtained: the nucleated patch, by taking away the nucleus with the surrounding plasma membrane, and the outside-out by taking away only the plasma membrane which breaks off and reseals. Starting from the cell-attached configuration a vesicle is formed in the tip of the pipette by pulling the pipette away; the vesicle can be broken by shortly taking the pipette out of solution, forming the inside-out configuration.

Since in the present work only the cell-attached and whole-cell configurations have been used, only the two of them will be further considered for the description of their equivalent circuits (Figure 9). It is known that the highest resistance in a series circuit determines the current flow. Therefore if the current flow is intended to be monitored through a certain compartment,

then the resistance of that compartment should be the highest in comparison to the other resistors in the circuit.

In the case of the cell-attached configuration there are several resistors in the series circuit, namely the resistance of the pipette ($R_{pipette}$), patch resistance (R_{patch}) and membrane resistance (R_m). As the patch resistance is the highest, the entire circuit monitors the current flow through the patch and any ion channels in it. The quality of this monitoring activity depends also on another resistor placed in parallel with the others: the leak resistance (R_{leak}). The leak resistance represents the quality of the seal between the glass of the micropipette and the membrane; and if the seal is good, then the R_{leak} is very high and no significant current will leak away. The relevant capacitances in the circuit are the pipette capacitance ($C_{pipette}$) and the capacitance of the patch of membrane. The latter is very small and can be ignored. The whole-cell capacitance (C_m) is not important in this configuration, because the membrane resistance (R_m) is so much smaller than R_{patch} that it actually short-circuits C_m. $C_{pipette}$, although small must be well compensated in order to avoid the eventual artifacts.

In the whole-cell configuration the patch of membrane under the pipette is disrupted; in electronic terms this implies that the R_{patch} becomes very low, and the access resistance (R_{access}) remains. The membrane potential (E_m) is disrupted as the integrity of the plasma membrane is lost and the pipette electrode has direct electrical contact with the cytoplasm. In this configuration the whole-cell membrane resistance becomes the largest current-limiting resistor, and thus the circuit monitors the current flow through the membrane of the entire cell. The membrane capacitance plays an important role in whole-cell recording, mainly because it affects the voltage clamp time characteristics. Any change in holding potential will be delayed because R_{access} and $R_{pipette}$ in series with C_m form a significant RC circuit. The sum of R_{access} and $R_{pipette}$ is sometimes referred to as series resistance (Molleman, 2003).

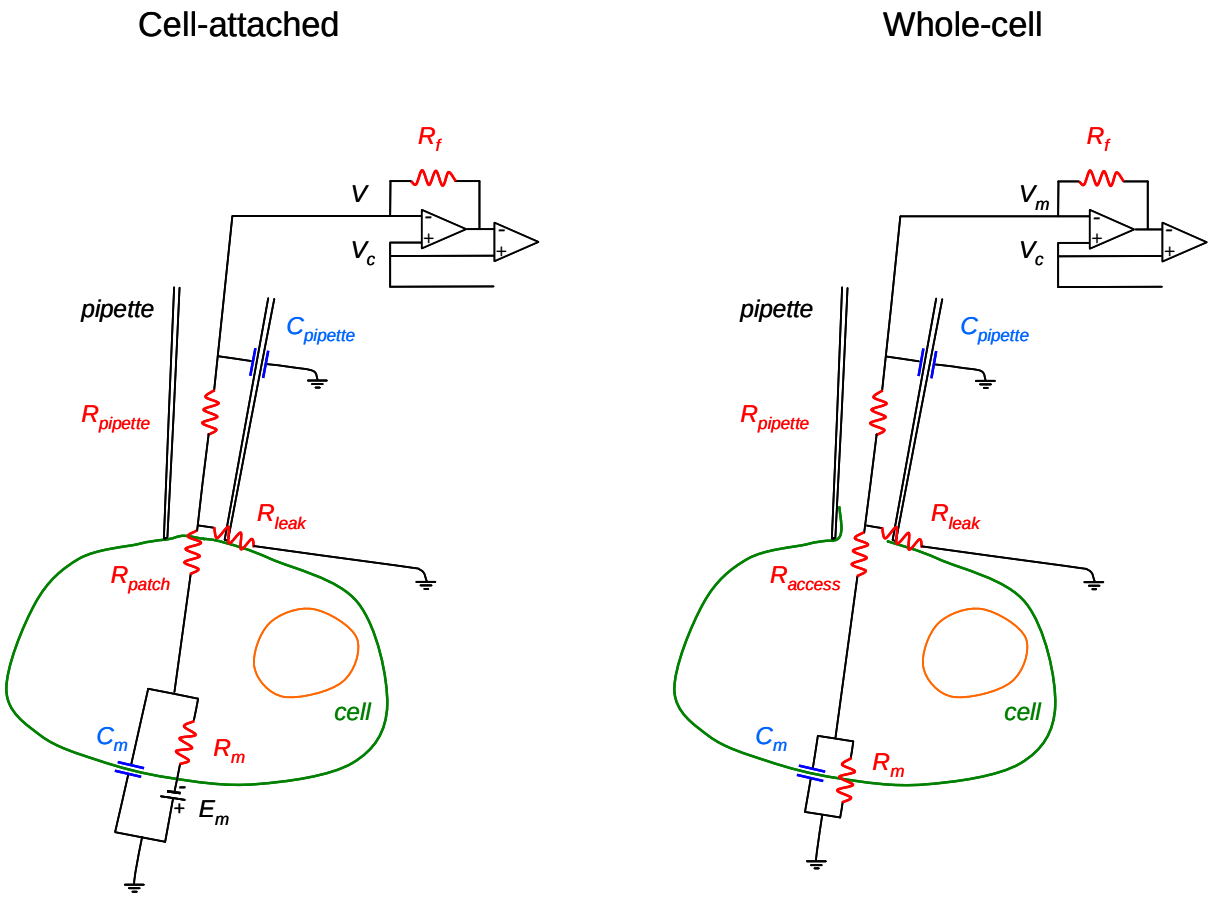

Figure 9. The pipette-cell system. The pipette-cell system presents electronic properties in which the circuits are made mainly of resistors and capacitors. In both types of configurations discussed here a membrane (C_m) and a pipette capacitance ($C_{pipette}$) occur, since the plasma membrane and the pipette walls are separating two charged environments. The narrow column of solution in the pipette poses resistance ($R_{pipette}$) to the ionic flow, as well as the membrane under the patch (R_{patch}) in the cell-attached configuration, or the small connection to the interior of the cell (R_{access}) in the whole-cell configuration. The pipette connection to the plasma membrane has a resistance to leakage (R_{leak}). The membrane of the cell has its own resistance (R_m) to ionic currents. In the case of cell-attached mode the intrinsic membrane potential of the cell is not disturbed (E_m). The membrane voltage at a certain moment (V_m) is measured and compared with the voltage command (V_c) by the differential amplifier. In the case of the cell-attached mode the measured voltage (V) is only the difference in charge between the pipette and the extracellular solutions. R_f is the feedback resistance of the electronic setup. [adapted after Molleman, 2003]

2.3.2 Solutions and chemicals

The composition of extracellular and intracellular solutions is described in Table 1. The stock extracellular solutions in the form of ACSF (artificial cerebro-spinal fluid) were kept as follows: the bathing 2.5 mM K^+ ACSF was prepared as a 10x solution lacking $NaHCO_3$ (in order not to have precipitates with the divalent cations) and at the final dilution containing only 1 mM $MgCl_2$. The $NaHCO_3$ solution was also prepared as a 10x stock and mixed with the 2.5 mM K^+ ACSF on the day of the experiment. In order to get to a final concentration of 3 mM divalent cations either in the form of 3 mM $MgCl_2$, 2 mM $MgCl_2$ and 1 mM $CaCl_2$ or

1 mM $MgCl_2$ and 2 mM $CaCl_2$, according volumes were added from $MgCl_2$ (250 mM) and $CaCl_2$ (1 M) stock solutions. For cutting the cerebellar slices 350 ml of 2.5 mM K^+, 3 mM Mg^{2+} ACSF were prepared, whereas for recovery 100 ml of 2.5 mM K^+, 1 mM Mg^{2+}, 2 mM Ca^{2+} ACSF were used (adapted from Sacco *et al.*, 2003). Usually, for bathing the slices during the experiment a 2.5 K^+ or 5 K^+ ACSF were used (adapted to the experiment concerning the divalent ion concentrations).

ACSF solutions other than 2.5 mM K^+ and the Ringer solution used for patch-clamp recordings of cultured cells were prepared at final concentrations according to Table 1.

The intracellular solutions (Table 2) were prepared by adding the energy storing compounds in the end in order to avoid their decay. The final solutions were aliquoted in volumes of 1 ml and stored at -20° C. On the day of experiment one aliquot was left to thaw on ice and then kept on ice in a syringe with filter; the thawed solution was used only on that respective day. Two such intracellular solutions were used: one in which KCl was replaced with K-methanesulfonate (Jackson & Bean, 2007), and a second solution in which KCl was replaced with K-gluconate (Sacco *et al.*, 2003). For the majority of experiments the K-methanesulfonate-based solution was used as it offered a longer survival time of the cell in the whole-cell configuration. The K-gluconate-based solution was used only for the on-cell experiments because it offered a better seal formation. Liquid junction potentials were not corrected.

For the isolation of the erg current the application of the antiarrhythmic drug E-4031 (1 µM, Eisai, Tokyo, Japan) was sufficient to achieve a fast and complete block. In order to eliminate the influence of other neuronal cell types that feed on Purkinje neurons synaptic blockers were added to the ACSF (AP-5, 50 µM (Ascent Scientific, Princeton, USA); CNQX, 10 µM (Ascent Scientific, Princeton, USA); bicuculline 20 µM (Ascent Scientific, Princeton, USA) to block NMDA, AMPA and $GABA_A$ receptors, respectively (Sacco *et al.*, 2003; Rossi *et al.*, 2008)). To see the rapid effect of erg channel blockage on the firing activity of the cell, a slightly increased concentration of E-4031 was used (5 µM). In order to test the modulatory effect of mGluRI receptors on erg channels, (S)-3,5-DHPG (50 µM, Ascent Scientific, Princeton, USA) was applied to the bath (Yuan et al., 2007). All experiments were done at room temperature (22-25 °C).

Table 1. Extracellular solutions

Substance	Concentrations (mM)											
	2.5 K^+ ACSF			5/8 K^+ ACSF				40 K^+ ACSF		5 K^+ Ringer		
NaCl	125			122.5/119.5				87.5		135		
KCl	2.5			5/8				40		5		
$CaCl_2$	2			2	1					1		
$MgCl_2$	1	3		1	2	3/3		3		2		
NaH_2PO_4	1.25			1.25/1.25				1.25				
$NaHCO_3$	26			26/26				26				
HEPES										10		
Glucose	20			20/20				20		5		
pH	7.4 (carbogen)			7.4 (carbogen)				7.4 (carbogen)		7.4 (NaOH)		

Table 2. Intracellular solutions

Substance	Concentrations (mM)	
	K^+-methanesulfonate	K^+-gluconate
K^+-methanesulfonate	123	
K^+-gluconate		140
NaCl	9	
$MgCl_2$	1.8	4
EGTA	0.9	0.5
HEPES	9	10
Na_2-Phosphocreatine	14	
MgATP	4	
Na_2ATP		4
Na_3GTP	0.3	0.4
pH	7.3 (KOH)	7.3 (KOH)

2.3.3 Experimental procedure

Slices were bathed in a continuous flow of carbogenated ACSF containing either 3 mM Mg^{2+} or 1 mM Ca^{2+} and 2 mM Mg^{2+} as divalent cations for voltage-clamp experiments, or 2 mM Ca^{2+} and 1 mM Mg^{2+} for current-clamp experiments. Purkinje cells were visualized with a Zeiss Axioskop 2 FS Plus with a 40x objective. Cells were chosen for recordings only if their dendritic initial segment was visible under infrared differential interference contrast optics. Capillaries made of borosilicate glass (GC150F-10, Harvard Apparatus, Edenbridge, UK) were pulled with an electrode puller (Flaming/Brown micropipette puller, Model P-97, Sutter Instrument, Novato, USA). Somatic, whole-cell recordings were made with patch pipettes of 3-5 MΩ resistance when filled with any of the two internal solutions. The erg current and the action potentials were recorded using a HEKA EPC9 amplifier (HEKA Elektronik, Lambrecht, Germany). High positive pressure was applied to the pipette solution in order to remove the debris and access the membrane of Purkinje neurons. Upon pushing against the membrane the pressure was released and negative pressure was applied together with a hyperpolarization to -60 mV until a seal of 2-4 GΩ resistance was formed. For the on-cell configuration having a good seal was enough to see the pairs of inward and outward currents caused by nearby action potentials. The whole-cell configuration was obtained by applying short pulses of negative pressure to the membrane patch until its rupture. The recordings were taken into consideration only if access resistance was below 30 MΩ. In current-clamp recordings no current was injected so that the spontaneous membrane potential was monitored.

For the nucleated-patch configuration, after getting the whole-cell configuration, the pipette was placed close to the nucleus and then the pipette was pulled away while applying strong negative pressure. The connection between the nucleated patch and the rest of the cell, consisting of plasma membrane and a thin thread of cytoplasm, became thinner and thinner as the pipette was lifted away until its rupture. The seal resistance usually remained very stable. But since a strong negative pressure was applied on the nucleus while getting the nucleated patch, the access resistance increased above the accepted limit. Therefore, positive pressure was again applied through the pipette in order to push back the nucleus from the cytoplasmic layer until the access resistance decreased again. Since the expected currents were in the range of a few tens of pA, only patches that had an access resistance below 15 MΩ were further considered.

The slices were perfused continuously with carbogenated ACSF at a speed of approximately 1 ml/min, and only when a good patch-clamp configuration was obtained the speed was increased to approximately 1.5 ml/min in order to assure a rapid exchange of solutions and achieve a rapid block of the erg current or activation of the mGluR1 receptor.

The glass coverslips with HEK293 cells were placed under the microscope in the recording chamber filled with 5 mM K^+ Ringer solution. In order to identify cells with a good transfection rate, the cells were stimulated at 540 nm and the ones with a medium to high red fluorescence were chosen. The cells with a very high fluorescence were usually damaged and the erg currents actually smaller than in the cells with medium fluorescence. Only cells with smooth surface without debris and a cytoplasm without vacuoles were patch clamped. The patching procedure was similar to the one used for Purkinje neurons; the only difference concerned the positive pressure applied to the intracellular solution, which in the case of HEK cells was lower since there were no additional tissue surrounding the cells to be pushed away.

2.3.4 Data analysis

The data were analyzed using PulseFit (HEKA Elektronik, Lambrecht, Germany), Igor Pro 6.03 (Wavemetrics, Lake Oswego, USA) and Excel (Microsoft, Redmond, USA) software packages. When averages were calculated, the values were given as mean ± standard error of the mean.

The voltage dependence of activation and current availability were obtained from the amplitudes of the tail currents at -100 mV. Since the tail currents elicited by different test pulses were measured at the same potential, thus the driving force did not change, there was no need to normalize to the conductance, hence the peak amplitudes of the erg current were used to determine the voltage dependence. The mean values for each potential were fitted by a Boltzmann function:

$$\frac{I}{I_{\max}} = \frac{1}{1 + e^{\frac{V_{1/2} - V_m}{k}}}$$

where I is the tail current recorded at -100 mV, I_{max} is the maximum current generated by the best sigmoid fit to the data, $V_{1/2}$ is the membrane potential at which I is 50% of I_{max}, and k is the slope factor of the fit and describes the membrane potential difference from 1/e (≈37%) to 1-1/e (≈63%) of the normalized tail current.

The membrane current density was calculated by dividing the amplitude of the current by the capacitance of the membrane (either the membrane of the whole cell or of the nucleated patch) and expressed as pA/pF.

Whole-cell conductance G can be determined from the peak current at -100 mV and the potential difference between membrane potential Vm and the equilibrium potential for K^+, E_K. G represents the inverse of membrane resistance R and equals the quotient of membrane current I and the driving force. The driving force for an ion through the plasma membrane is the difference between the membrane potential V_m and the equilibrium potential for that ion E (in this case E_K). E_K can be obtained from Nernst's equation:

$$G = \frac{I}{V_m - E_K} \qquad E_K = -\frac{RT}{zF} * \ln \frac{[K^+]_i}{[K^+]_o}$$

where R is the universal gas constant which equals 8.31 J K^{-1} mol^{-1}, T is the absolute temperature in Kelvin, z is the valence of the K^+ ions (+1), F is the Faraday constant (F = 9.65×10^4 C mol^{-1}), and $[K^+]_i$ and $[K^+]_o$ are the intracellular and extracellular potassium concentrations, respectively.

Steady-state inactivation was determined as the fraction of the steady-state current amplitude from the peak current amplitude. At the most negative potentials, depending on the channel subunit, the values were not evaluated because of increasing interference of deactivation, which apparently slows the time course of current decay.

The activation time constant was calculated from the tail currents at -100 mV, after the cell was taken previously to +20 mV by pulses of exponentially increasing durations. The average

peak current at each potential was calculated, and then the means were fitted with a single exponential function.

For estimating the recovery from inactivation and deactivation time constants, current traces were elicited by pulses at different potentials after the erg current was previously fully activated by a pulse at +20 mV. The current traces had different shapes and presented different recovery from inactivation and deactivation kinetics depending on each membrane potential. Since erg current deactivation was shown to have two components, a slow and a fast component, two exponential functions were used for some potentials to fit the deactivating part of the current trace (at potentials between -120 and -100 mV the slow component has a larger amplitude than at more depolarized potentials). Recovery from inactivation was fitted for all potentials with one exponential function.

Activation: $$I(t) = I_{\min} + I_{\max} * \left(1 - e^{\frac{-t}{\tau_{act}}}\right)$$

Recovery from inactivation: $$I(t) = I_{\min} + I_{\max} * \left(1 - e^{\frac{-t}{\tau_{rec}}}\right)$$

Deactivation (-90 to -60 mV): $$I(t) = I_{\min} + I_{\max} * e^{\frac{-t}{\tau_{deac}}}$$

Deactivation (-120 to -100 mV): $$I(t) = I_{\min} + I_{\max F} * e^{\frac{-t}{\tau_{deacF}}} + I_{\max S} * e^{\frac{-t}{\tau_{deacS}}}$$

where I_{min} and I_{max} describe the minimum and maximum of the voltage activated, recovered from inactivation or deactivating current of the exponential fit. τ_{act} and τ_{rec} describe the time course of activation and recovery, respectively, and represent the time courses for the current to reach 1-1/e (≈63%) of I_{max}. τ_{deact} describes the time course of deactivation (τ_{deactF} represents the fast component and τ_{deactS} the slow component) representing the time needed for the current to reach 1/e (≈37%) of I_{max}.

3. Results

The erg current was present in almost all Purkinje neurons that were investigated. In a physiological solution (2.5 – 5 mM K^+), the erg current amplitude was relatively small (usually below 100 pA), whereas other K^+ channels gave very large currents (reaching even 10 nA in the case of the A-type and delayed-rectifier currents combined). Since it was known that the erg current amplitude increases with increasing extracellular K^+ concentration (Sturm *et al.*, 2005), a 40 mM K^+ solution was used to evaluate the biophysical parameters in PNs. For the functional experiments a physiological K^+ concentration was used.

3.1 Biophysical characterization of the erg current in Purkinje neurons

The 40 mM K^+ ACSF, used for all biophysical experiments had the Ca^{2+} ions from the physiological ACSF replaced with Mg^{2+} in order to eliminate the presence of Ca^{2+} currents and Ca^{2+} dependent K^+ currents.

The voltage dependence of erg current activation was investigated by maintaining the cells at a holding potential of -80 mV in order to recover from inactivation and deactivate all the erg channels. The voltage protocol began with a step at -80 mV for 4 s followed by depolarizing test pulses of 5 s duration starting from a holding potential of -80 mV up to 40, in 10 mV increments. All these steps were followed by a negative one to -100 mV for 500 ms upon which the erg current was revealed as a transient inward current. The amplitude of this tail current is a measure of the erg current activation at the end of the preceding steps (Figure 10A). Application of the erg channel blocker E-4031 (5 µM) had almost no effect on the outward currents elicited during the depolarizing test pulses, but clearly reduced the transient current recorded at -100 mV (Figure 10B). The erg currents were isolated as E-4031-sensitive currents by subtracting the two sets of traces before and after application of E-4031 (Figure 10Ca-b). The difference currents displayed the hook-like appearance due to fast recovery from inactivation and slow deactivation. The reason why there was almost no erg current upon the depolarizing test pulses was that activation of erg channels was slow whereas inactivation was fast. As the maximal activated current at each potential a mean value was taken from the hook-like region of the tail currents at -100 mV (in order to reduce the

contribution of noise to the total amplitude). The average values for each test potential were fitted with a Boltzmann function; the $V_{1/2}$ equaled -44.28 ± 0.4 mV and the slope (k) was 4.94 ± 0.6 mV (n = 7; Figure 10D).

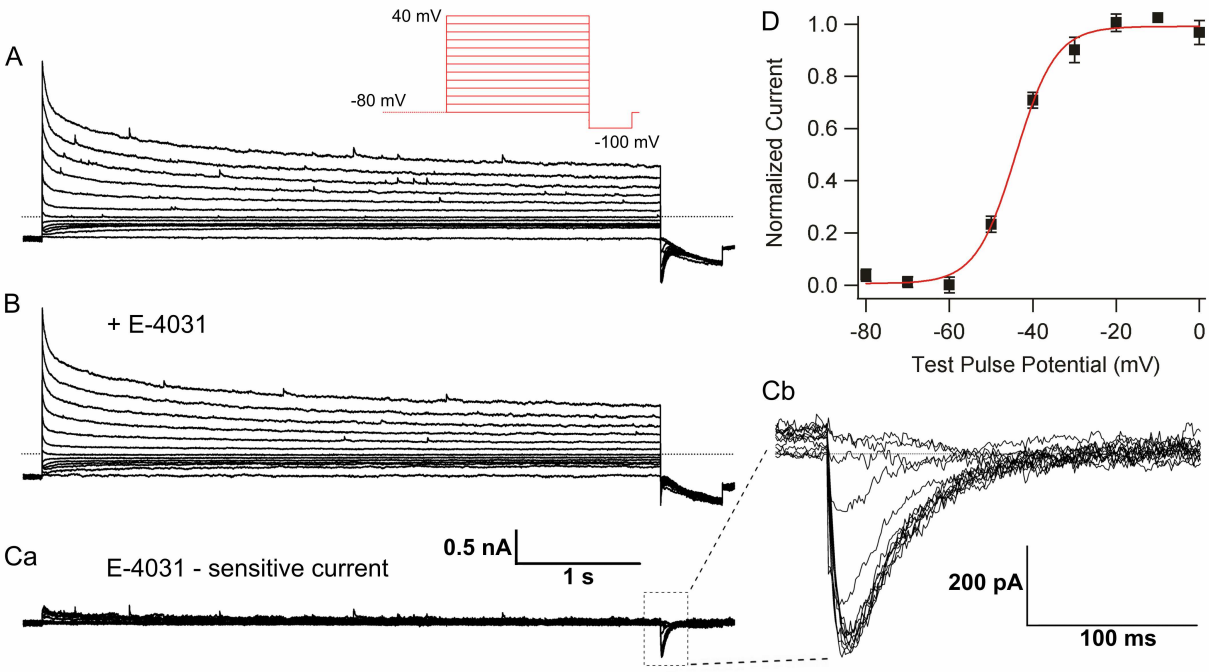

Figure 10. Voltage dependence of erg current activation in Purkinje neurons. Representative traces of currents measured in a 40 mM K^+, Mg^{2+}-based ACSF are illustrated as the total current (**A**), the E-4031 resistant current (**B**) and as the E-4031-sensitive current (**Ca**). The protocol for activation is depicted in the inset. (**Cb**) Enlarged erg tail current traces measured at -100 mV. (**D**) The means of the peak currents are plotted against the test pulse potentials, and fitted with a Boltzmann function yielding a $V_{1/2}$ of -44.1 mV and a slope factor (k) of 4.8 mV (n=7) [P5-P10]

The time course of erg current activation was determined by an envelope-of-tail protocol at one membrane potential (+20 mV; Figure 11, inset). Since at depolarized potentials the erg currents inactivate very fast, it is impossible to study the activation time course directly. Therefore, by exponentially increasing the duration of the test pulse at the potential of interest (in the present case +20 mV), the fractions of activated erg current can be obtained as tail currents at -100 mV. From a holding potential of -80 mV (4 s), a depolarizing pulse was applied to +20 mV to activate the erg current. Gradual prolongation of the initial 1-ms pulse (with a Δt factor of 2 and Δt increase of 5 ms) to +20 mV resulted in increasing activation of the erg channels and therefore increasing the amplitudes of the erg current measured upon a hyperpolarizing step to -100 mV (250 ms; Figure 11Aa-b). The time-dependent increase of

the tail current amplitudes was fitted with a single exponential function, yielding the time course of activation at +20 mV (53.66 ± 9.5 ms, n = 5; Figure 11B).

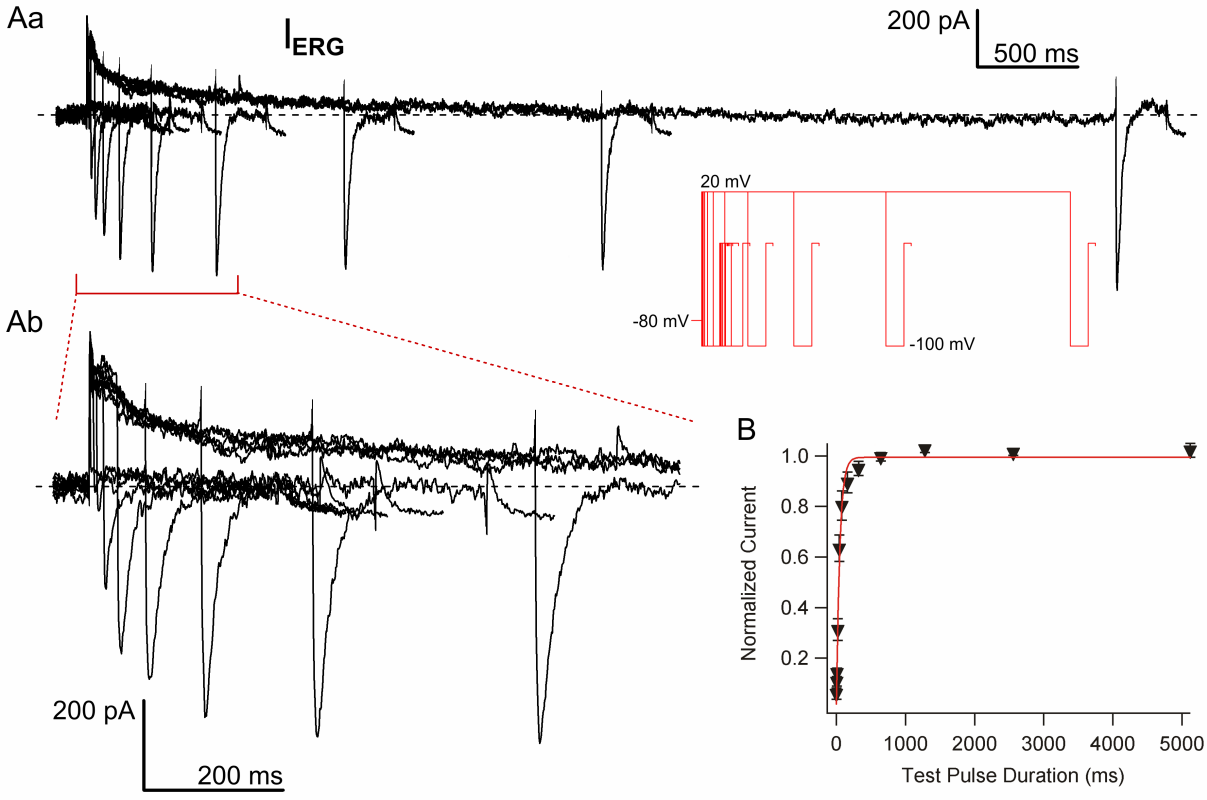

Figure 11. Time course of erg current activation in Purkinje neurons. Traces of E-4031 sensitive current are illustrated (**Aa**) together with the "envelope-of-tail" protocol (inset) obtained using the 40 mM K^+, 3 mM Mg^{2+} ACSF. The hook-like erg currents were measured at -100 mV after being activated at +20 mV for exponentially increasing durations. (**Ab**) In the magnification, the first peak currents are shown for a better view of the increase in amplitude. (**B**) The mean values of peak current amplitudes were plotted against the duration of the pulse at +20 mV, and fitted with a single exponential function, yielding the activation time constant of 49.2 ms (n = 5) [P5-P10]

Erg current availability, recovery from inactivation and deactivation were investigated using a complex pulse protocol. The holding potential was set to -20 mV so that the erg channels became activated. Each 1 s test pulse ranging from 40 to -120 mV in 10 mV increments was preceded by a 2-s pulse to 20 mV to ensure a full activation. As the test pulses became more negative the elicited erg current displayed a faster recovery from inactivation as well as a faster deactivation (Figure 12C). This shows the voltage dependence of the properties of the erg current. For potentials between -60 and -90 mV the erg currents were fitted by the sum of two exponential functions in order to obtain the recovery from inactivation (τ_{rec}, Figure 13A) and deactivation (τ_{deac}) time constants. For potentials between -100 and -120 mV the deactivating part of the erg current was fitted with two exponentials revealing a fast and a

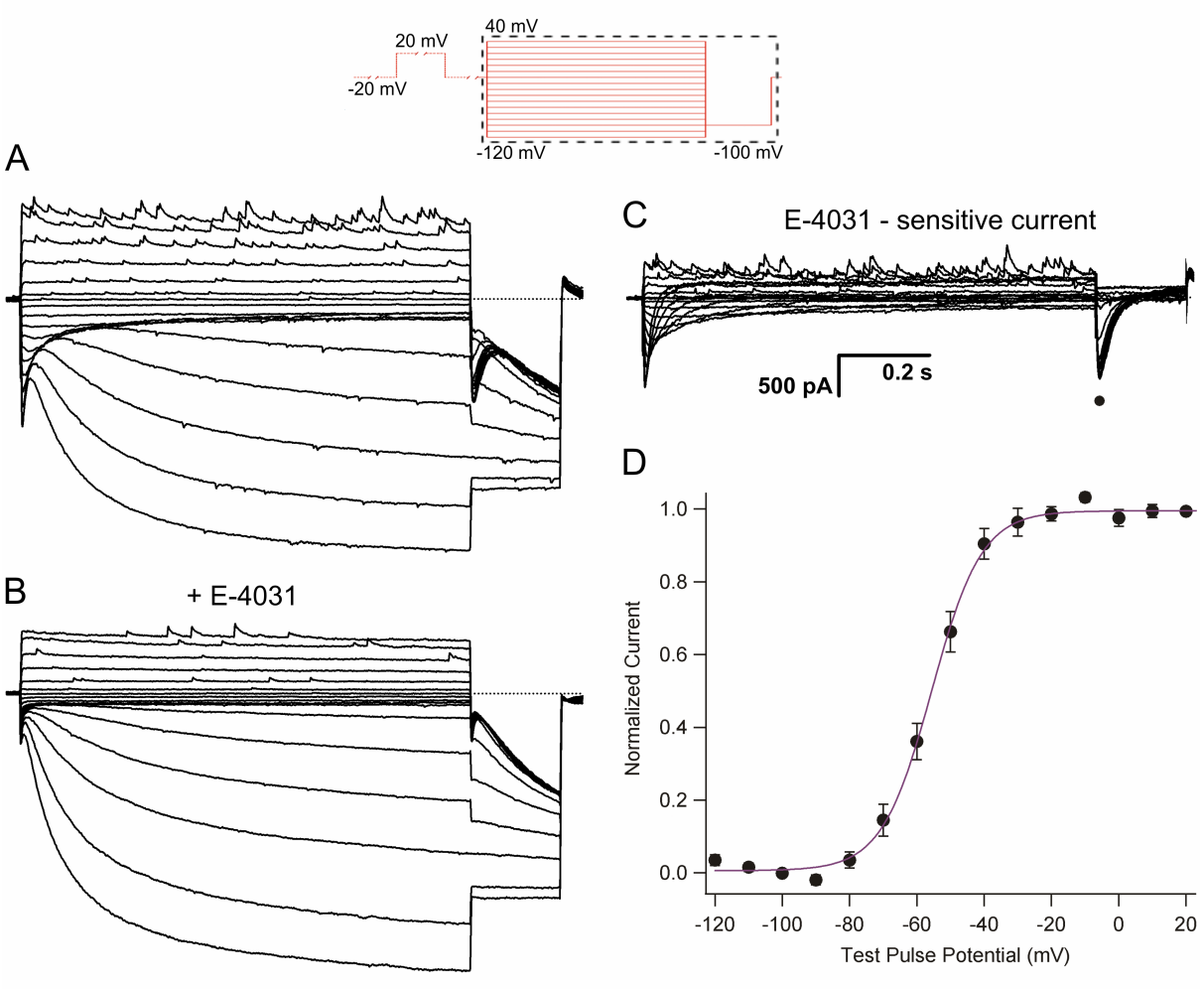

Figure 12. Voltage dependence of erg current availability in Purkinje neurons. Representative current traces are illustrated that have been obtained with the availability pulse protocol, depicted in red at the top, either in control 40 mM K^+ ACSF (**A**) or in the presence of E-4031 (**B**). (**C**) The E-4031-sensitive current, obtained as difference current. (**D**) The mean tail peak current amplitudes at -100 mV (●) are plotted against voltage and fitted with a Boltzmann function ($V_{1/2}$ = -55.6 mV, k = 7.4 mV, n = 8) [P5-P10]

slow component (Figure 13B). All test pulses were followed by a 200 ms pulse to -100 mV to elicit tail currents of the erg channels that did not deactivate during the preceding step. Tail currents decreased with more negative test potentials. This indicates that at the end of the more negative test pulses the deactivation of the erg current was more complete. Therefore the amplitude of the tail currents mirrors the erg channels "available" for mediating current. Erg tail current amplitudes were plotted against the voltage of the test pulses, fitted with a Bolzmann function and then normalized to the amplitude of the Bolzmann function. For this "availability" curve the $V_{1/2}$ was -55.6 ± 1.9 mV whereas the slope factor, k = 7.49 ± 0.6 mV (n = 8; Figure 12D).

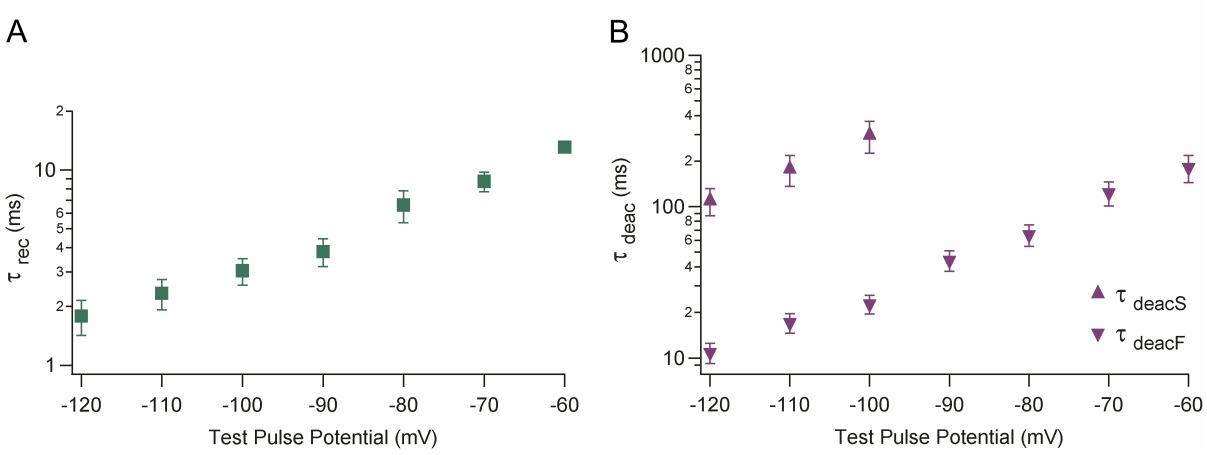

Figure 13. Time courses of erg current recovery from inactivation and deactivation in Purkinje neurons. The erg current traces elicited by the various test pulses with the availability protocol (illustrated in Figure 12) were fitted with the sum of two or three exponential functions in order to obtain the time constants of recovery from inactivation (τ_{rec}, **A**) and fast (τ_{deacF}) and slow (τ_{deacS}) time constants of deactivation (**B**). [P5-P10]

3.2 Distribution of erg channels in Purkinje neurons

Since it is well-known that Na^+ and Ca^{2+} channels in PNs are distributed predominantly to specific compartments, like soma or dendritic tree (Stuart & Hausser, 1994; Rancz & Hausser, 2006), respectively, the question arose whether erg channels were also confined to a special compartment, distributed along a gradient or present at the same density throughout the entire plasma membrane. An electrophysiological approach was used in order to address the question concerning erg channel functional distribution. The estimation of erg channel distribution was done by calculating the current density for two patch clamp configurations: whole-cell (Figure 14Aa) and nucleated patch (Figure 14Ba). Therefore, for each cell the current density was calculated (in 40 mM K^+ ACSF) dividing the recorded erg current (Figure 14Ab) by the given cell capacitance. After the erg current was recorded, the pipette was easily pulled away from the slice until the nucleated patch was obtained. When a good access of below 15 MΩ was reached, the remaining erg current was recorded (Figure 14Bb). Not for all (only for approximately 50 %) nucleated patches it was possible to identify an erg current, maybe due to small total current density or to an unstable cell. But in the nucleated-patches in which such a current could be identified it had an amplitude very similar to what could be calculated from the current density of the intact cell and the capacity of the nucleated patch. This actually means that the erg current densities for the intact cells and for the nucleated patches were almost identical (11.1 ± 1.56 pA/pF for whole-cell, and -10.92 ± 1.2 pA/pF for nucleated patch configurations; n.s., paired two-tailed t-test, n = 5, Figure 14C). This indicates that in the plasma membrane there are present functional erg channels and that the channels do not seem to be confined to one region of the cell membrane or another.

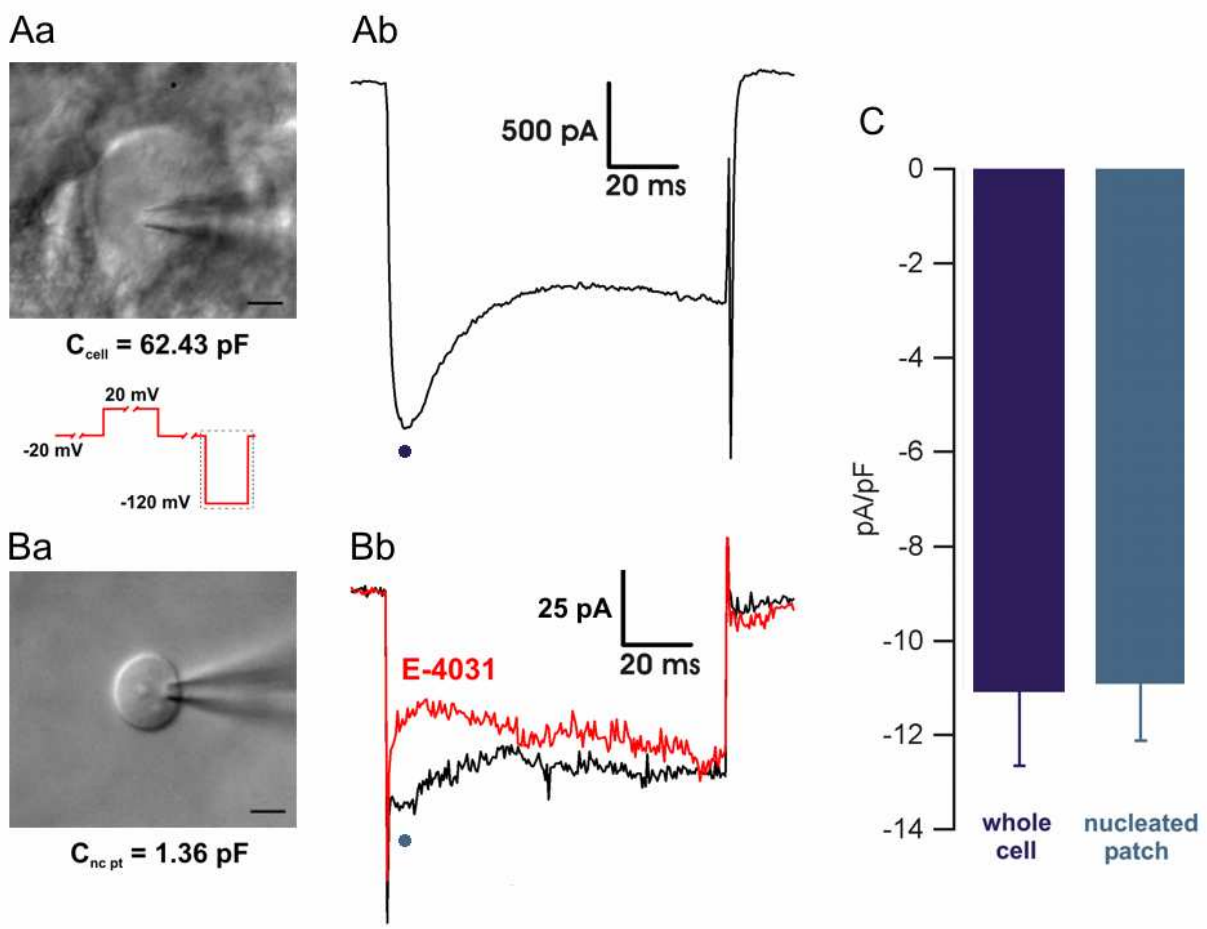

Figure 14. The apparent homogeneous distribution of the erg channels in Purkinje neurons. (**Aa**) View of an intact PN in the whole-cell configuration (C_{cell} represents the whole-cell capacitance). The peak erg tail currents were measured at -120 mV after full activation (pulse protocol in inset). The paired measurements were done first in the whole-cell configuration (**Ab**) and subsequently in the nucleated patch configuration (**Ba**, $C_{nc\ pt}$ represents the capacitance of the nucleated patch) to compare the current density in the membrane of the whole cell (erg current amplitude was calculated as the difference from peak to steady-state deactivation) to the current density in the somatic membrane (as E-4031-sensitive current, **Bb**), respectively. (**C**) Averages for current densities in both configurations showed no difference (-11.1 ± 1.56 pA/pF for whole-cell, and -10.92 ± 1.2 pA/pF for nucleated patch configurations; n.s., paired two-tailed t-test, n = 5). The scale bar equals 5 µm. [P5-P10]

3.3 Physiological role of the erg current in Purkinje neurons

As described in paragraph 3.1, erg currents in PNs are half maximally activated at -44 mV in a 40 mM K^+ solution, so it is likely, that it is partially activated at the normal resting membrane potential of PNs (-56.6 ± 2.61 mV, n=8). In order to investigate the effect of erg channel blockage by E-4031 on the spontaneous firing behavior of the Purkinje neurons, action potential associated currents were measured by on-cell patch-clamp recordings. To make the cells more excitable than in the commonly used 2.5 mM K^+, a 5 K^+ ACSF with 2 mM Ca^{2+} was used. After forming a gigaseal, the action potentials were recorded as pairs of inward and outward currents (Figure 15A-B). In the P5-P10 mouse group a good connection to the cell proved to be very important due to the weaker APs and smaller currents. In the P22-P42 group the action currents were larger. To preserve only the intrinsic firing pattern of the cells, synaptic blockers were applied to the bath (bicuculline (20 µM), AP-5 (50 µM) and CNQX (10 µM)). In the neonatal/infant mice (P5 to P10), the spontaneous activity consisted of regular single action potentials. Out of ten spontaneously firing Purkinje neurons four reacted to E-4031 application by increasing the firing frequency. The mean firing frequency of the four reactive cells was 6.84 ± 1.07 Hz in control conditions, whereas after blockage of

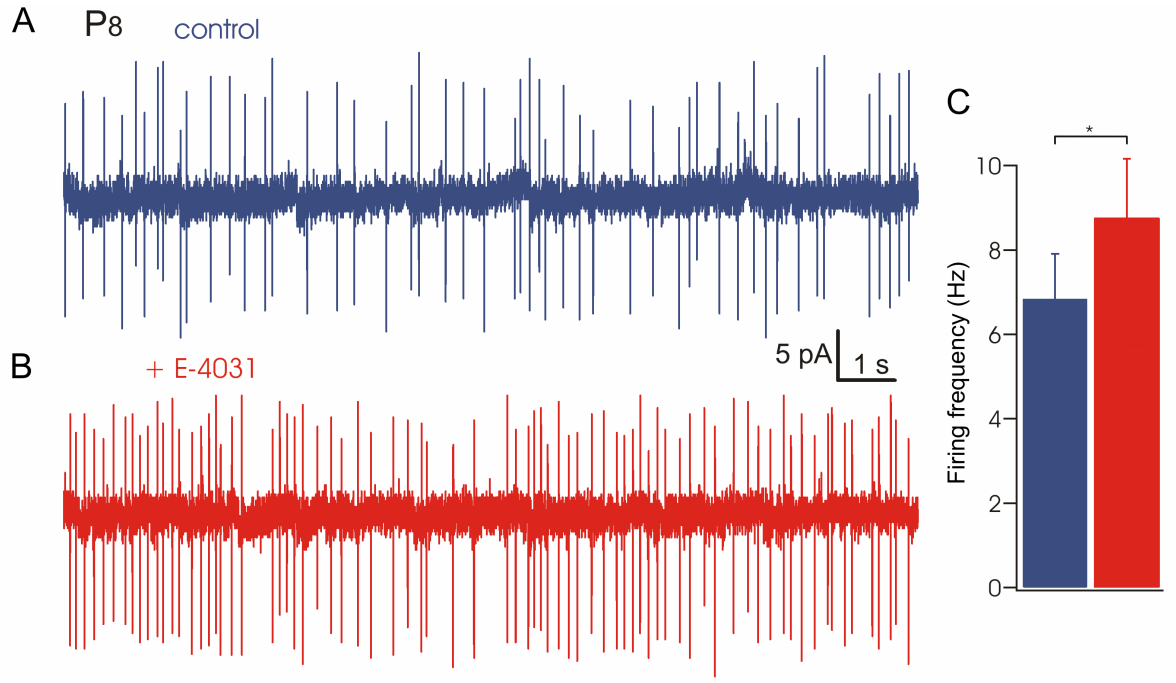

Figure 15. Increase of spontaneous action current frequency in Purkinje neurons of immature mice after blocking erg channels. On-cell recordings in control 5 mM K^+ ACSF (**A**) of a PN (P8) exhibiting spontaneous firing at a low frequency. The action current frequency increase after application of E-4031 (5 µM; **B**) was representative for 40% of neurons. (**C**) In this subgroup of the P5-P10 mice, the change in action current frequency from 6.8 ± 1.1 Hz to 8.7 ± 1.4 Hz was significant (* $p < 0.05$, paired two-tailed t-test; n = 4)

erg currents it increased significantly to 8.74 ± 1.42 Hz ($p < 0.05$, paired two-tailed t-test; Figure 15C).

In the young adult mouse group (P22-P42) 40% of cells reacted to the application of E-4031 (4 out of 10; Figure 16A-B). Ten cells were studied in which action currents occurred not regular, as in the infant animals, but mostly in bursts, although some had single action currents. After application of E-4031, the reactive bursting cells had an increased burst duration, and the interburst interval and the intraburst frequency decreased. In control solution the average duration of a burst, in the reactive subgroup, was 199 ± 43 ms (n = 110) whereas after blockage of the erg current it increased to 712.7 ± 115.4 ms (n = 76; $p < 0.001$, unpaired two-tailed t-test; Figure 16C). The interburst duration decreased from 714.6 ± 52 ms (n = 141) in control, to 465.6 ± 30.1 ms (n = 155) with E-4031 (in the reactive subgroup; $p < 0.001$, upaired two-tailed t-test). The intraburst frequency decreased from 111.3 ± 2.3 Hz (n = 109) to 58 ± 4.3 Hz (n = 76; $p < 0.001$, unpaired two-tailed t-test), whereas the overall firing frequency increased but not significantly.

In order to be sure that the observed effects were due to erg current blockage by E-4031 and not to cell deterioration over time, control experiments were performed on another set of ten Purkinje neurons for each study group. The neurons were kept for the same amount of time only in the control ACSF and no change in their firing pattern was observed.

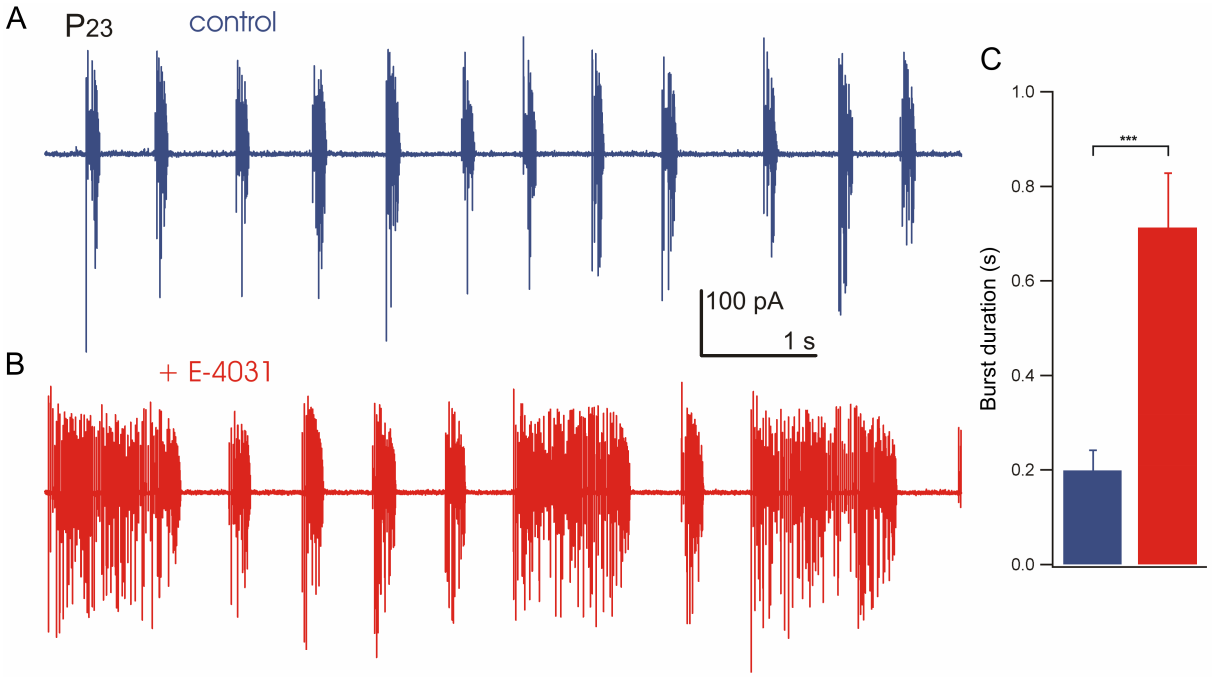

Figure 16. Increase of spontaneous burst duration in Purkinje neurons of young adult mice after blocking erg channels. On-cell recordings from a PN of a P23 mouse firing action potential bursts in 5 mM K^+ ACSF (**A**). After the blockage of the erg channels by E-4031 the cell (**B**), representative for 40% of the PNs, responded with a prolongation of burst duration. (**C**) The burst duration in this subgroup increased from an average of 199 ± 43 ms in control solution, to 713 ± 115 ms after application of E-4031 (*** $p<0.001$, unpaired two-tailed t test, $n_{control} = 110$, $n_{E-4031} = 76$)

While the on-cell patch-clamp configuration was suitable to observe the firing pattern of the neurons, the shape and threshold of action potentials, and the membrane potential and resistance could not be determined. Therefore, further experiments using the whole-cell configuration were performed with PNs from immature mice mice using 5 mM K^+, 2 Ca^{2+} ACSF and for recording the spontaneous membrane potential in the current-clamp configuration no current was injected. Most of the cells were spontaneously active comparable to the on-cell configuration. The firing behavior of Purkinje neurons at different depolarization steps was examined by injecting current adequate to first hyperpolarize the cells to -60 mV and then depolarize with six rectangular 500 ms current pulses starting from 50 pA up to 300 pA in 50 pA increments. Some neurons, when only 50 pA of current were injected, did not depolarize enough to reach the threshold for action potential firing; but after E-4031 application a single AP occurred (Figure 17).

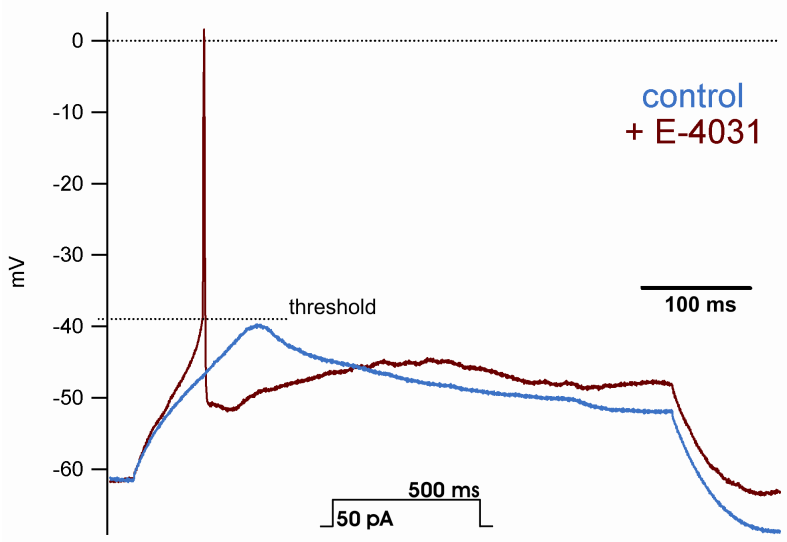

Figure 17. Erg current inhibition increased excitability of Purkinje neurons. Representative voltage traces evoked by a 50 pA pulse of depolarizing current, showing that in the presence of erg currents the cell was unable to fire an AP; whereas after application of E-4031 the membrane potential reached the threshold for firing one AP. [P5-P10]

At larger depolarizations trains of action potentials occurred in all the studied cells. At very large depolarizations the AP firing frequency saturated or, in some cells failures in AP firing, presumably due to Na^+ channel inactivation, appeared. For both these reasons it was chosen to further analyze the firing pattern occurring at the lowest amount of injected current (100 pA) that generated a sustained firing in all cells. Spike-frequency adaptation was almost complete within three spikes (Figure 18Aa-b). In control ACSF, the average AP threshold was -37.74 ± 0.7 mV; after blockage of erg channels the average threshold decreased to -39.73 ± 0.7 mV ($p < 0.001$, paired two-tailed t-test, Figure 18Ac, B). This resulted in a shortening of the delay from the start of the depolarizing current pulse to the initiation of the first AP (from 24.65 ± 1.3 ms in control, to 21.37 ± 1.3 ms with E-4031, $p < 0.001$, $n = 24$). The instantaneous firing frequency (IFF, reciprocal of the interspike interval) significantly increased from 32.09 ± 2.6 Hz (control) to 39.32 ± 3.7 Hz after application of E-4031 (paired two-tailed t-test, $p < 0.001$, $n = 24$) for the first AP (Figure 18B). When comparing the neurons with trains of at least 11 APs, a significant increase in IFF occurred for all APs after erg current blockage ($n = 12$, Figure 19B).

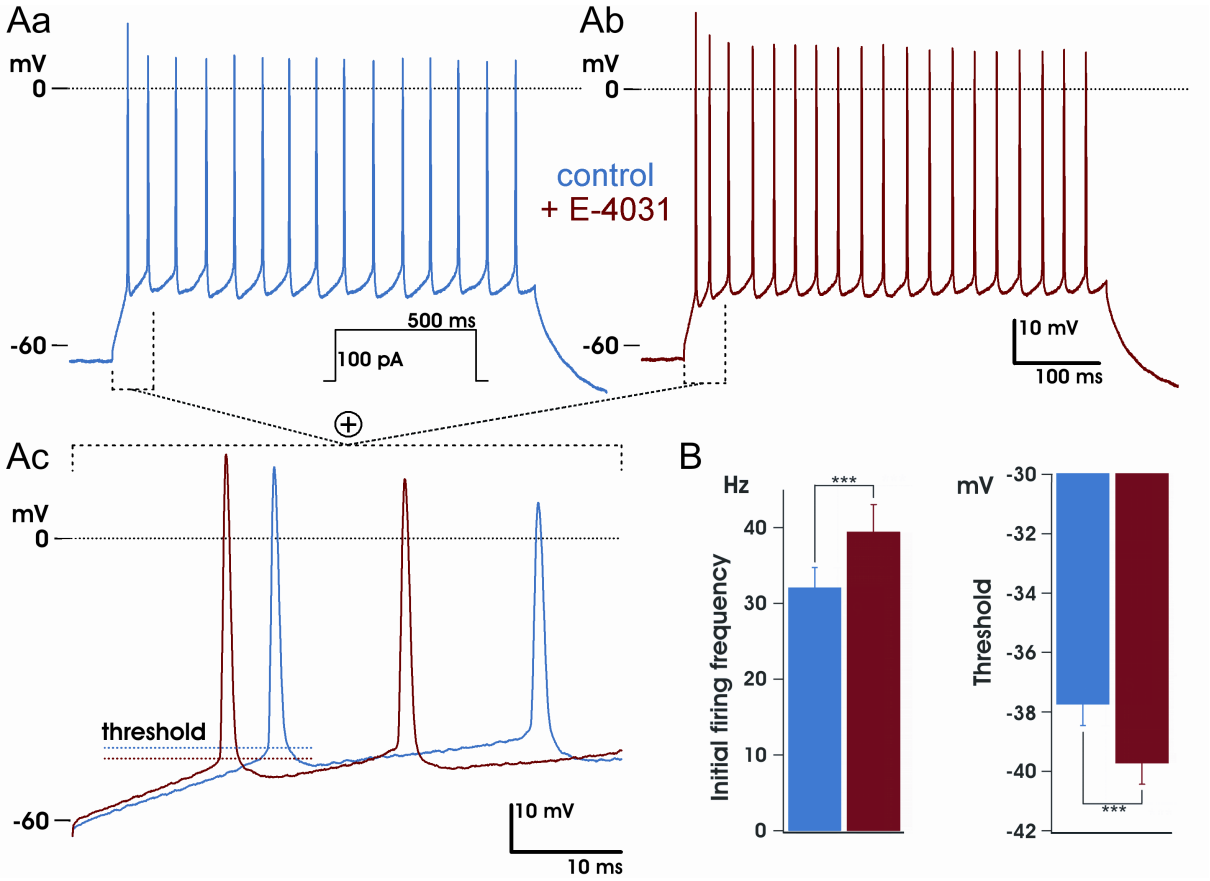

Figure 18. Blockage of erg currents increased excitability of Purkinje neurons. (**Aa**) Sustained firing upon injection of 100 pA of depolarizing current for 500 ms. Upon erg current blockage (**Ab**), the AP threshold of the first AP decreased (**Ac, B**), and the initial firing frequency increased (**B**). (*** $p < 0.001$, paired, two-tailed t-test, n = 24) [P5-P10]

The IFF average values for the fourth to the eleventh AP did not show a big variation from each other (before or after application of E-4031), but only a linear decrease (Figure 19B); however, some neurons (25%) exhibited, after erg channel blockage, a great variation in IFF (Figure 19A). In order to evaluate this variation, the average IFF values were calculated from the fourth to the eleventh AP, for both conditions, and each IFF value was normalized to the average. The differences to mean of normalized values, were tested for significance, proving that after the erg current was abolished the irregularity in the firing pattern increased ($p < 0.001$, unpaired two-tailed t-test, n = 38 before and n = 50 after application of E-4031).

The mean firing frequency of all APs during the depolarizing 500 ms pulse at different amounts of injected current was also evaluated (Figure 19C). At low amounts of injected current (50, 100, 150 pA) a significant difference could be seen between control and in the presence of E-4031 ($p < 0.001$, $p < 0.001$ and $p < 0.01$, respectively, n = 24). At 100 pA the

difference in the mean firing frequency was the highest, increasing from 25.42 ± 1 Hz in control to 29.42 ± 1.71 Hz in the presence of E-4031 (n = 24).

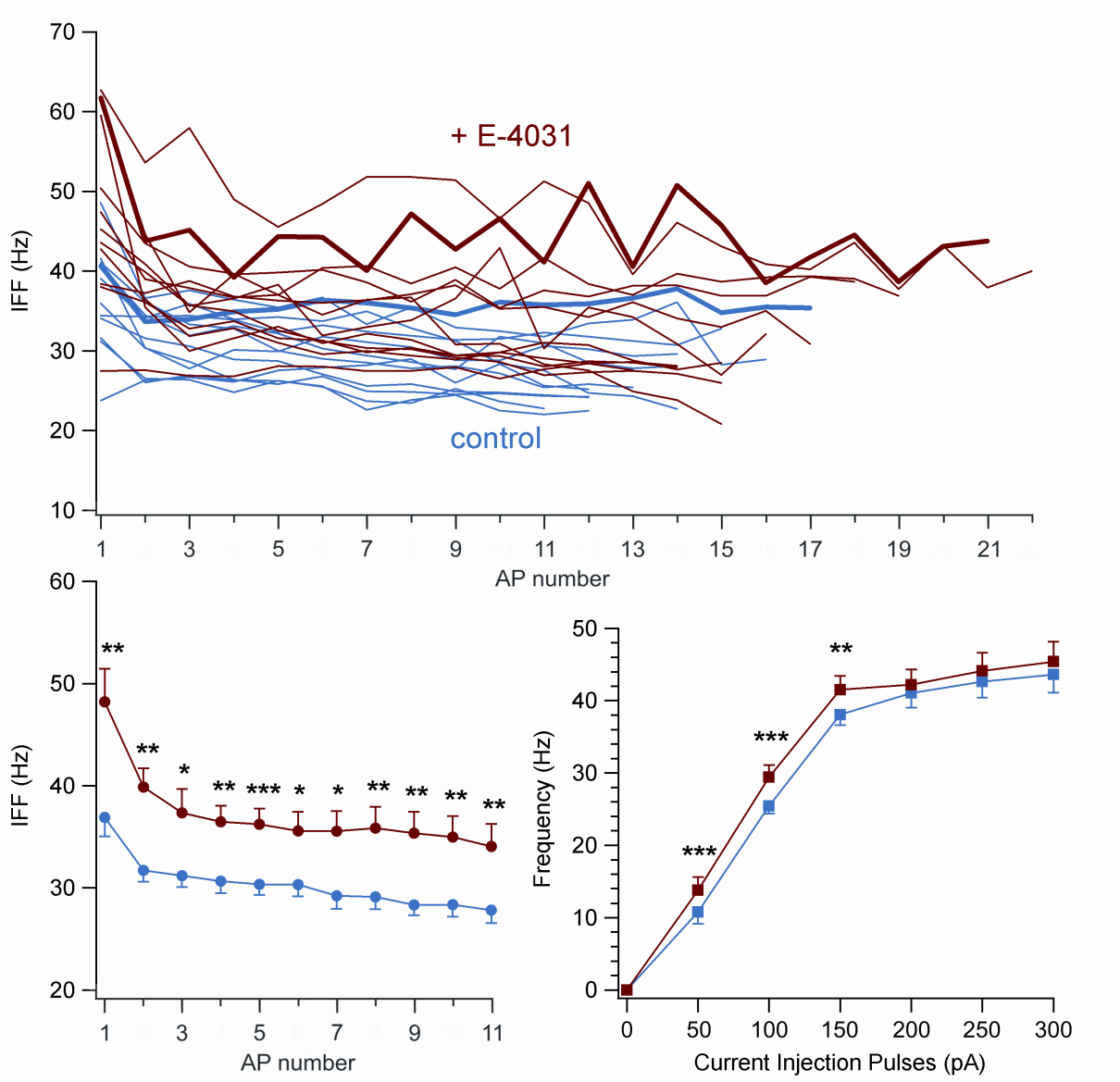

Figure 19. Erg channel blockage increased the instantaneous and the mean firing frequency in Purkinje neurons. (**A**) Instantaneous firing frequency (IFF) for individual neurons (having at least 11 APs) before (blue) and after E-4031 (red); a more irregular firing pattern occurred in some neurons after erg channel blockage. (**B**) Average IFF values for the first 11 APs (n = 12), which all increased by approximately 10 Hz after the blockage of erg channels, while spike-frequency adaptation remained similar. (**C**) Increased mean firing frequencies for different amounts of injected current after E-4031 application (* $p < 0.05$, ** $p < 0.01$, *** $p<0.001$, paired, two-tailed t-test, n = 24) [P5-P10]

The influence of the erg currents on the excitability of the cells was studied also by applying ramps of depolarizing current (5 mM K^+, 2 mM Ca^{2+} ACSF). After spontaneous action potential firing was suppressed by injecting a hyperpolarizing current, 0 to 200 pA of depolarizing current were injected during a 1-s ramp and then 200 pA were injected for 200 ms (Figure 20A). In the presence of E-4031 the membrane depolarized faster, reaching the firing threshold earlier (Figure 20B), which was also lower, comparable to the effect seen with rectangular current injection (see Figure 18Ac). Moreover, in the presence of E-4031, the cell was unable to fire APs as the depolarization persisted and reached a higher value.

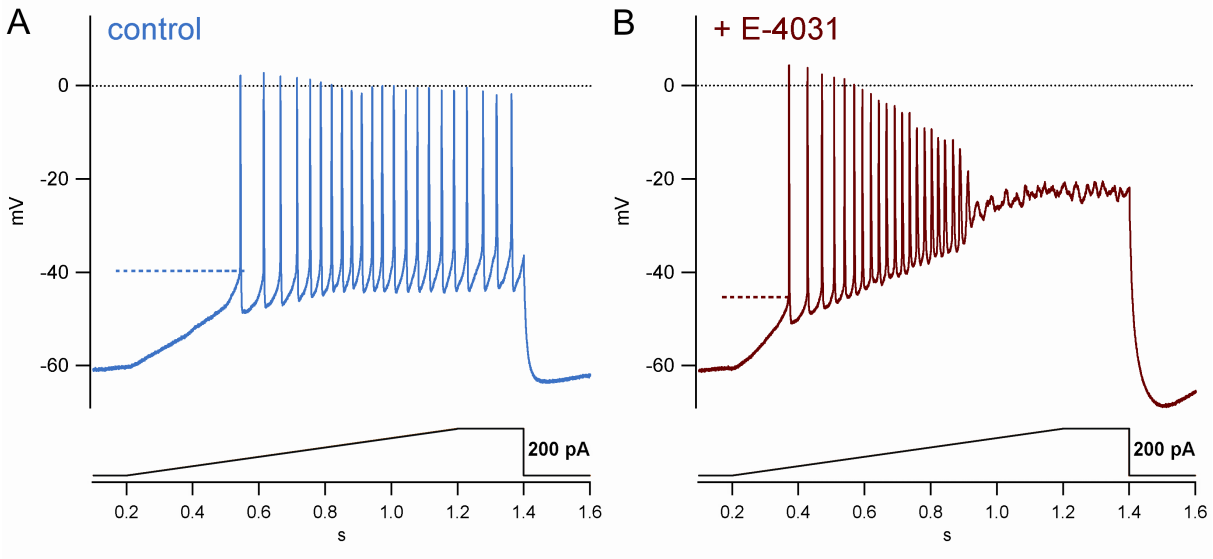

Figure 20. Blocking erg currents changed the firing pattern of a Purkinje neuron. The PN was depolarized by injecting 0 to 200 pA (ramp protocol, see inset). (**A**) While the amount of injected current increased, the membrane potential depolarized until the threshold for AP firing was reached. Also the interspike interval decreased; then, it increased again due to spike-frequency adaptation. (**B**) Upon blockage of the erg channels a decrease in firing threshold could be observed (dotted line), interspike intervals decreased compared to control and a depolarization block of action potential firing occurred when the amplitude of the injected current further increased. [P5-P10]

3.4 Erg currents in Purkinje neurons elicited by action potential clamp

To assess the amount of erg current that is activated during action potential firing of Purkinje neurons, a membrane potential trace that was previously recorded in a current-clamp experiment (Figure 20, control) was used as a potential template for voltage-clamp. Using this "ramp firing" protocol (Figure 21A), whole-cell currents were measured before and during application of E-4031. During each ramp protocol, transient inward and outward currents were activated, presumably corresponding to Na^+ and K^+ conductances (Figure 21B). For an optimal isolation of the E-4031 sensitive current, a Ca^{2+} free ACSF was used. In approximately 40% of neurons (3 out of 7), an accumulating outward current was activated, which was blocked in the presence of E-4031. The difference maximal current (evaluated as current density equaled 0.52 ± 0.03 pA/pF, n = 3; Figure 21C, 22A) presumably corresponds to erg currents that activate slowly during the ramp-induced depolarization and the train of APs. The reason why this difference current cannot be seen in all cases (although the presence of the erg current was proven in over 95% of cells) could be the variable current densities of

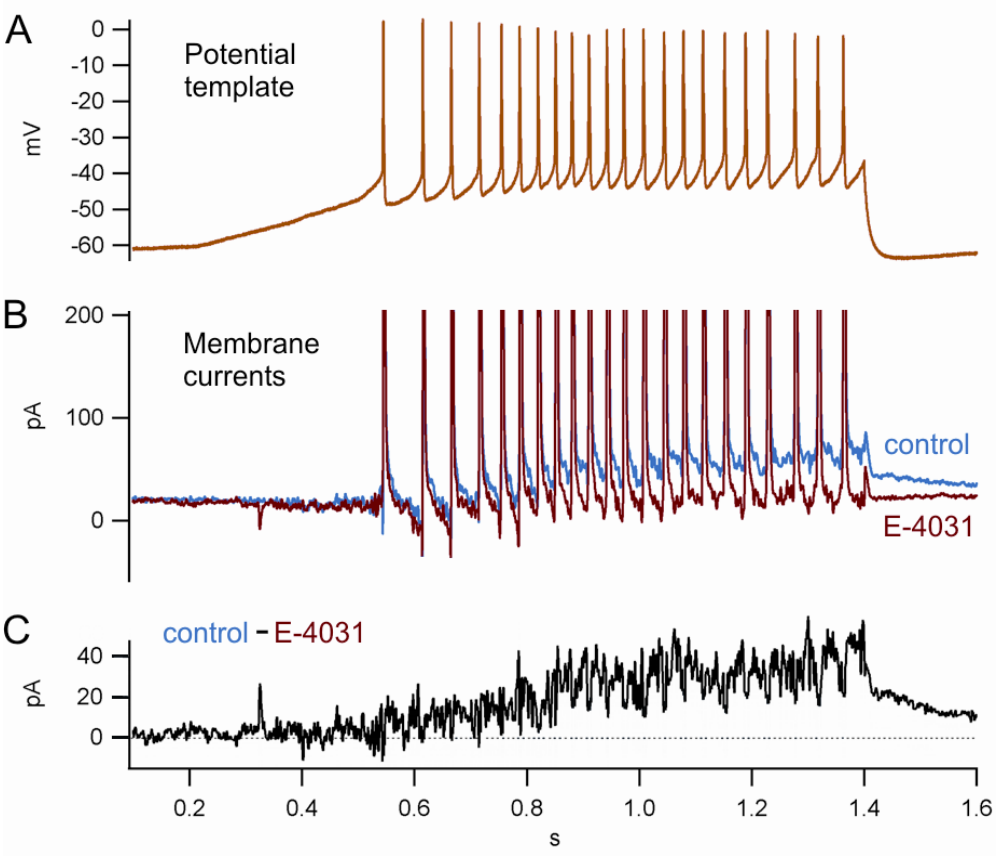

Figure 21. Voltage clamp with a sustained firing trace. (**A**) The response in control 5 mM K^+ ACSF solution to the ramp protocol illustrated in Figure 20 was then used as a template ("ramp firing") for voltage command. The Purkinje neurons exhibited currents in response to the voltage template (**B**), and by subtraction the E-4031 sensitive current was obtained (**C**). [P5-P10]

the erg current among PNs.

In order to isolate the erg current in more physiological conditions, ACSFs with different Ca^{2+} concentrations (1 and 2 mM) were also used. The accumulating currents had similar amplitudes as with 0 mM Ca^{2+} (0.43 ± 0.06 pA/pF, n = 5 (Figure 22B); 0.56 ± 0.14 pA/pF, n = 3 (Figure 22C), for 1 and 2 mM Ca^{2+}, respectively). No significant differences were found between the current densities in these conditions (unpaired two-tailed t-test). The fraction of cells that presented such currents remained around 40%.

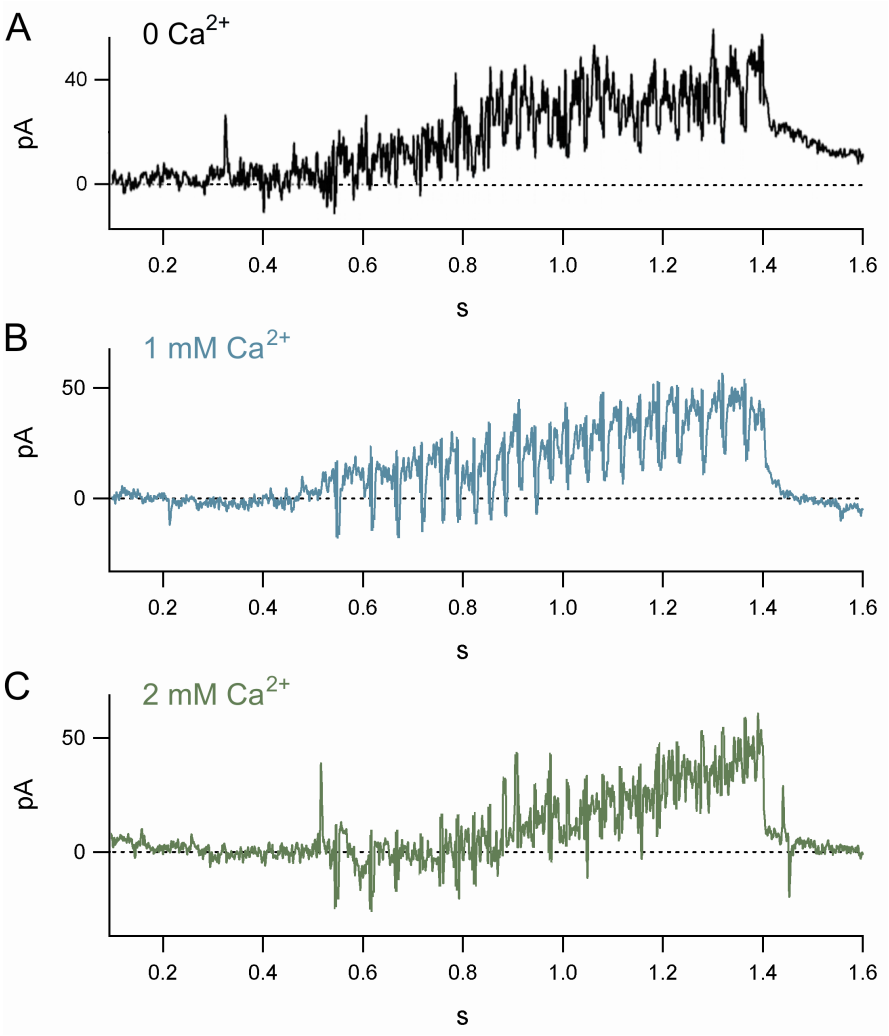

Figure 22. Erg currents in Purkinje neurons elicited with a "ramp firing" protocol in different Ca^{2+} concentrations. For all three Ca^{2+} concentrations the amplitudes of the E-4031-sensitive currents expressed as current densities were approximately the same (0.52 ± 0.03 pA/pF, n = 3 (**A**); 0.43 ± 0.06 pA/pF, n = 5 (**B**); 0.56 ± 0.14, n = 3 (**C**), for 0, 1 and 2 mM Ca^{2+}, respectively); no significant differences were found (unpaired two-tailed t-test). [P5-P10]

3.5 Properties of erg channel subunits expressed in HEK293 cells

For a better understanding of the erg current expressed by Purkinje neurons, in terms of biophysical properties and functional implications, a more detailed characterization was necessary of each of the participating subunits to the constitution of the erg channels in these neurons. Therefore the cDNAs for r-erg1a, r-erg1b, r-erg2 or r-erg3, each known to be present in Purkinje neurons (Guasti *et al.*, 2005), were expressed in HEK293 cells together with the cDNA for a fluorescent marker (mCherry). First, the voltage dependence of steady-state activation and inactivation, of all subunits, was studied, to determine the "window" current, which is the steady-state current occurring in a certain voltage range. The K^+ concentration (5 mM) of the Ringer solution and the composition of the pipette solution was identical to the one in which the physiological effects of erg channel blockage in Purkinje neurons were measured. Moreover, 1 mM Ca^{2+} was added so that the voltage dependence was closer to the physiological conditions. The protocol used to study the voltage dependence of activation was identical to the one used in Purkinje neurons (see Figure 10), with the only difference of an additional step to 50 mV when r-erg2 was recorded from transfected cells (as the activation curve of this subunit had a known shift to the right; Hirdes *et al.*, 2005). The peak tail currents elicited by the step to -100 mV were normalized to the maximal current, plotted versus the test-pulse potential and fitted with a sigmoid function. The following $V_{1/2}$ were obtained for the four subunits: -30.15 ± 1.62 mV for r-erg3 (n = 6), -13.34 ± 1.57 mV for r-erg1a (n = 6), -2.61 ± 1.69 mV for r-erg1b (n = 5) and 10.24 ± 2.33 mV for r-erg2 (n = 4; Figure 23). The r-erg3 channels activated at the most negative potentials among all subunits. In contrast, r-erg2 channels activated at more depolarized potentials, the first indication of current appearing at potentials of -10 to 0 mV, where the r-erg3 current was maximally activated. In between these extremes, the other two subunits resided.

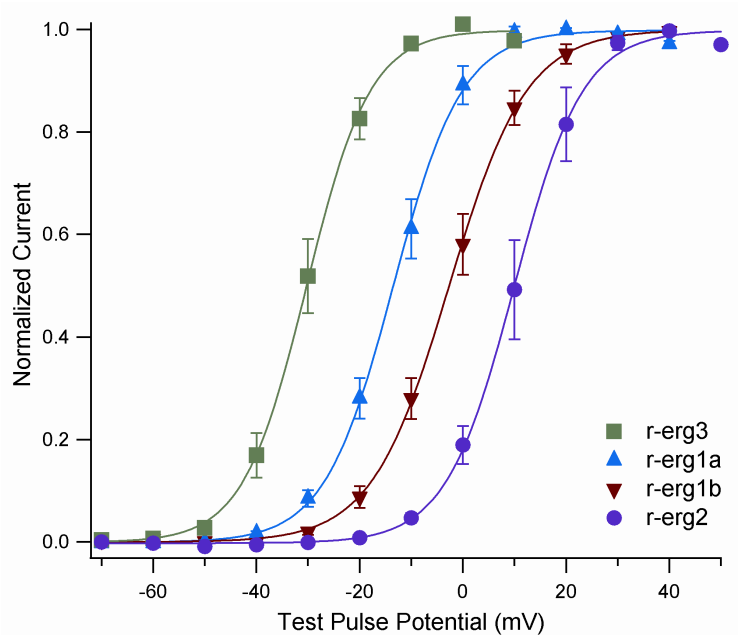

Figure 23. Voltage dependence of activation of four erg channel isoforms. Voltage dependence of activation of the erg current carried through homomeric channels, expressed in HEK293 cells. The $V_{1/2}$ values were -30.3 mV (r-erg3; n = 6), -13.5 mV (r-erg1a; n = 6), -2.7 mV (r-erg1b; n = 5) and 9.9 mV (r-erg2; n = 4).

The protocol for inactivation had a holding potential of -20 mV, which was followed by a step to 20 mV for 2 s in order to fully activate the erg currents; then the voltage was brought back to -20 mV for 100 ms and then to -100 mV for a time period depending on the recovery kinetics of each subunit. The main rule was to allow the erg currents to fully recover even though the beginning of deactivation could be noticed. Therefore, a 5 ms step at -100 mV was used for the "fast" subunits (r-erg1b and r-erg3), and a 10 ms step for the "slow" subunits (r-erg1a and r-erg2). After the step at -100 mV the test pulses lasting for 250 ms were run, starting from -60 mV and getting up to 100 mV with increments of 10 mV. During these steps the erg currents that had recovered from inactivation at -100 mV (but had not deactivated) inactivated with a voltage-dependent kinetic towards a steady-state. The last step of the protocol brought the cells back to the holding potential of -20 mV. The steady-state inactivation was calculated as the ratio between the steady-state current and the peak current (Figure 24B), representing the fraction of remaining current. The mean values of steady-state inactivation for each potential step were plotted against the voltage. An increasing amount of deactivation interfered with inactivation at more negative potentials, starting for example at potentials negative to -20 mV for r-erg3, visible as an apparent increase of steady-state inactivation. Since the remaining curve was incomplete, it could not be reliably fitted with a sigmoidal function in order to determine the half-maximal steady-state inactivation. When

presenting the voltage-dependence of activation and steady-state inactivation in one graph (Figure 24B) the voltage range is illustrated, in which the large r-erg3 “window” current could occur (between -45 and +30 mV). This voltage range corresponded to the membrane potentials at which steady-state outward current was possible, which thus could stably hyperpolarize the cell.

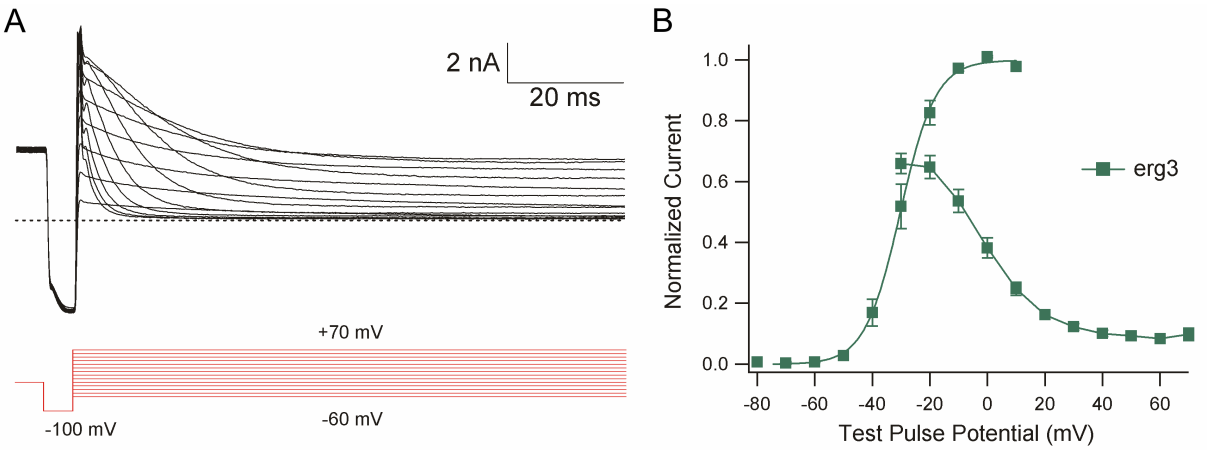

Figure 24. Voltage dependence of steady-state inactivation of r-erg3 currents. (**A**) Family of representative r-erg3 current traces are illustrated together with the equivalent voltage steps of the inactivation protocol (the 5 ms step to -100 mV, where current recovery from inactivation occurred, and the test pulses at which current inactivation was studied). (**B**) Voltage dependence of activation (taken from Figure 23) and inactivation (evaluated as the ratio between steady-state and peak currents; mean values from -30 to +70 mV, n = 12).

The same comparison of steady-state activation and inactivation was done for all erg channel isoforms (Figure 25). For r-erg2 currents, at potentials where steady-state activation started, the steady-state inactivation was already maximal, showing that no considerable “window” current was possible at any potential. For r-erg1a “window” current could occur between approximately -35 and +10 mV, whereas for r-erg1b it ranged between -25 and +40 mV.

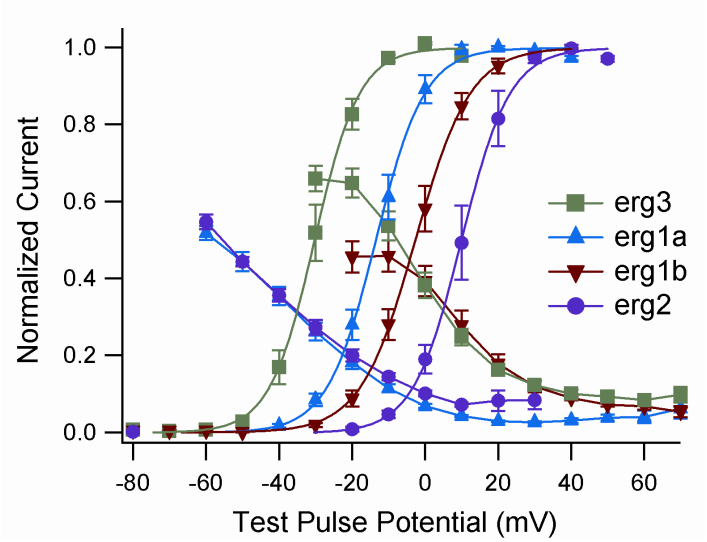

Figure 25. "Window" currents of four erg channel isoforms. The activation curves illustrated in Figure 23 are plotted together with the steady-state inactivation. The area below each corresponding activation and inactivation curve represents the possible "window" current for each isoform.

In order to determine which of the four erg homomeric channels expressed in HEK293 cells is most similar to the erg channels in Purkinje neurons, the activation curves measured in 40 mM K^+ ACSF were compared, since in native cells the erg currents were too small to evaluate in 5 mM K^+. When the activation curves of the homomeric channels in 5 mM K^+ were compared to the ones obtained in 40 mM K^+ it could be observed that the activation curves of all erg channel subunits were shifted to the left in the higher K^+ concentration solution (Figure 26A). The amount of the shift was variable though, with r-erg1a currents shifting most (-29 mV), and r-erg2 currents shifting least (-12 mV). The activation curve from Purkinje neurons had a $V_{1/2}$ of -44.11 ± 0.8 mV (n = 7), which was not significantly different to the $V_{1/2}$ of the r-erg3 carried current (-44.24 ± 1.8 mV, n = 6; p = 0.98, unpaired two-tailed t-test). The $V_{1/2}$ value for the current measured from r-erg1a expressing HEK293 cells was also not different ($V_{1/2}$ = -41.89 ± 3 mV, n = 3; p = 0.24) from $V_{1/2}$ of the erg current in PNs. The $V_{1/2}$ for the other two subunits were placed at more depolarized potentials (-25.44 ± 1.7 mV (n = 6) for r-erg1b and -1.98 ± 2 mV (n = 6) for r-erg2) and significantly different from r-erg3 and r-erg1a currents ($p < 0.001$, unpaired two-tailed t-test; Figure 26B).

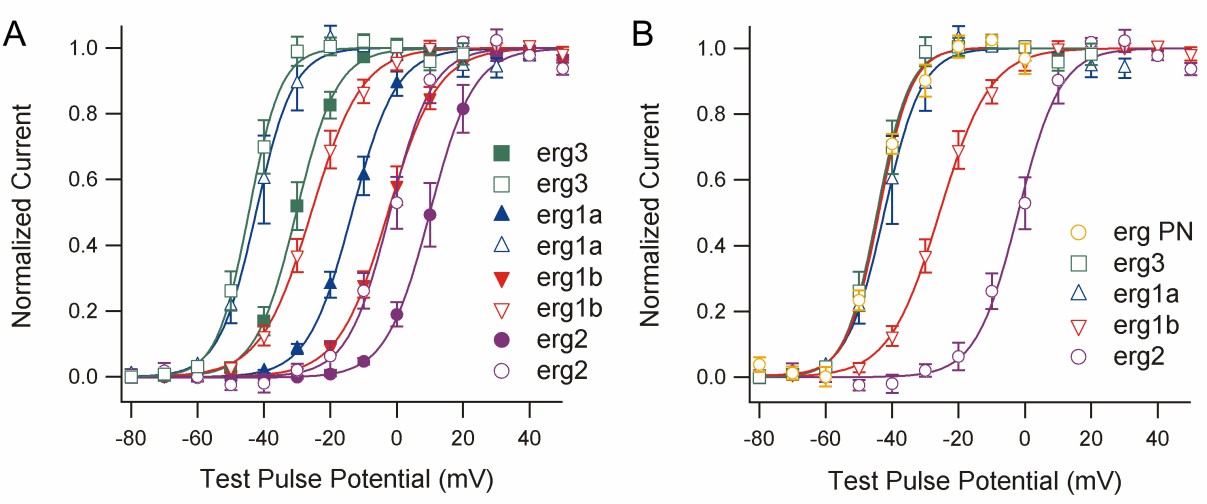

Figure 26. Voltage dependence of erg current activation in 40 mM K^+ for PNs and HEK293 cells. (**A**) Activation curves are shown for each isoform in 5 (●) and 40 (○) mM K^+. In 40 mM K^+ all curves were shifted to the left to different degrees, the larger shift belonging to r-erg1a whereas the smallest to r-erg2. (**B**) Activation curves in 40 mM K^+ from HEK293 cells are illustrated together with the activation curve for erg currents in PNs. Notice the close resemblance between the native current and the r-erg3 and r-erg1a currents ($V_{1/2}$ equals -44.11 (PN), -44.58 (r-erg3), -42.4 (r-erg1a), -25.75 (r-erg1b), -2.05 (r-erg2) mV.

In order to further compare and interpret the properties of the erg current in Purkinje neurons and of single isoforms expressed in HEK293 cells, the availability protocol was applied in the HEK293 cells; in this way the recovery from inactivation and deactivation time constants could be evaluated for the currents elicited during the different test pulses. Although these parameters were evaluated for all the potentials where erg currents were obvious, the values for the more hyperpolarized potentials were more reliable, since the currents were larger and could be better fitted with the exponential functions. Therefore, for the comparison of recovery from inactivation time constants three potentials were taken into consideration (-110, -100 and -90 mV). The most negative one (-120 mV) was also not very reliable since at that potential recovery from inactivation was very fast and it could combine with the occurring capacitive artifacts. At these three potentials, the recovery from inactivation time constant of erg currents from Purkinje neurons was closely resembled by r-erg1b and r-erg3 currents. And this resemblance was the strongest at -90 mV where the values for τ_{rec} from PN and HEK293 cells expressing r-erg1b and r-erg3 were almost identical (τ_{rec} equals 3.82 ± 0.62 ms (n = 6), 3.78 ± 1.01 ms (n = 5) and 3.43 ± 0.76 ms (n =4), respectively; $p > 0.7$, unpaired two-tailed t-test). For r-erg1a, τ_{rec} was at all these potentials approximately 1.5 larger than for PN (at -90 mV τ_{rec} = 5.33 ± 0.74 ms, but not significantly different; unpaired two-tailed t-test; Figure 27, Table 3).

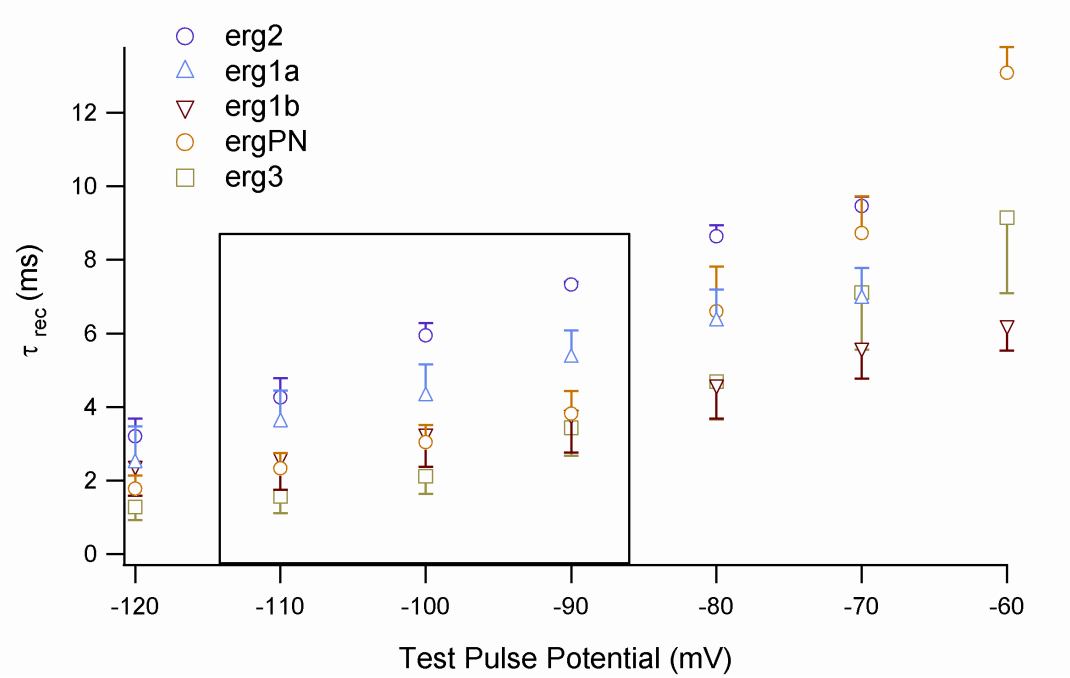

Figure 27. Recovery from inactivation time constants. The graph illustrates the comparison between recovery from inactivation time constants (τ_{rec}) of the native erg current in PNs (ergPN) and currents of four erg channel isoforms expressed in HEK-293 cells, measured in 40 mM K^+ ACSF. The box indicates potentials where the fitted values were more reliable, since at -120 mV subtraction artifacts can occur whereas at more depolarized potentials recovery from inactivation takes place to a smaller extent. The time constants for the three mentioned potentials are present in Table 3. Although τ_{rec} for the erg current in PNs approaches more the values for r-erg3 than for r-erg1a, it is not significantly different from either of them.

Table3. Recovery from inactivation time constants for homomeric and PN erg currents

	τ_{rec} (ms)			
erg current	-90 mV	-100 mV	-110 mV	n
r-erg1a	**5.33 ± 0.74**	**4.30 ± 0.86**	**3.59 ± 0.86**	3
r-erg1b	3.78 ± 1.01	3.27 ± 0.89	2.61 ± 0.86	5
r-erg2	7.33 ± 0.08	5.94 ± 0.33	4.26 ± 0.53	4
r-erg3	**3.43 ± 0.76**	**2.12 ± 0.47**	**1.57 ± 0.45**	4
erg PN	**3.82 ± 0.62**	**3.04 ± 0.47**	**2.34 ± 0.41**	6

So far, from the analysis of activation curves and τ_{rec}, the erg current in Purkinje neurons resembled to the r-erg3 current but also to the r-erg1a current. For the analysis of deactivation time constant, two exponentials were used for fitting the deactivation time course of the trace at the most negative potentials (-120, -110, -100 mV), since the slow component of the current becomes larger at these potentials. Although fitting with two exponentials at these

potentials gave better values for the fast components of deactivation (τ_{deacF}), the values for the slow component were not very reliable because the ratios between the slow and fast components were getting smaller as the potentials became more negative. Therefore, only the three most negative potentials were taken into consideration, where deactivation was fitted with two exponential functions and the fast component was relatively large. The values for τ_{deacF} showed a larger difference than τ_{rec} between the erg currents in PN and r-erg1a currents, the latter having a τ_{deacF} approximately 2-3 times larger than the PN erg currents (at -100 mV, 79.5 ± 30.9 ms (n = 3) and 22.77 ± 3.2 ms (n = 6), respectively; $p < 0.05$, unpaired two-tailed t-test). And again the τ_{deacF} for r-erg1b and r-erg3 currents were similar with PN erg currents (14.55 ± 1.53 ms (n = 5) and 16.87 ± 1.93 ms (n = 4), for r-erg1b and r-erg3 respectively; no significant difference between means; Figure 28, Table 4).

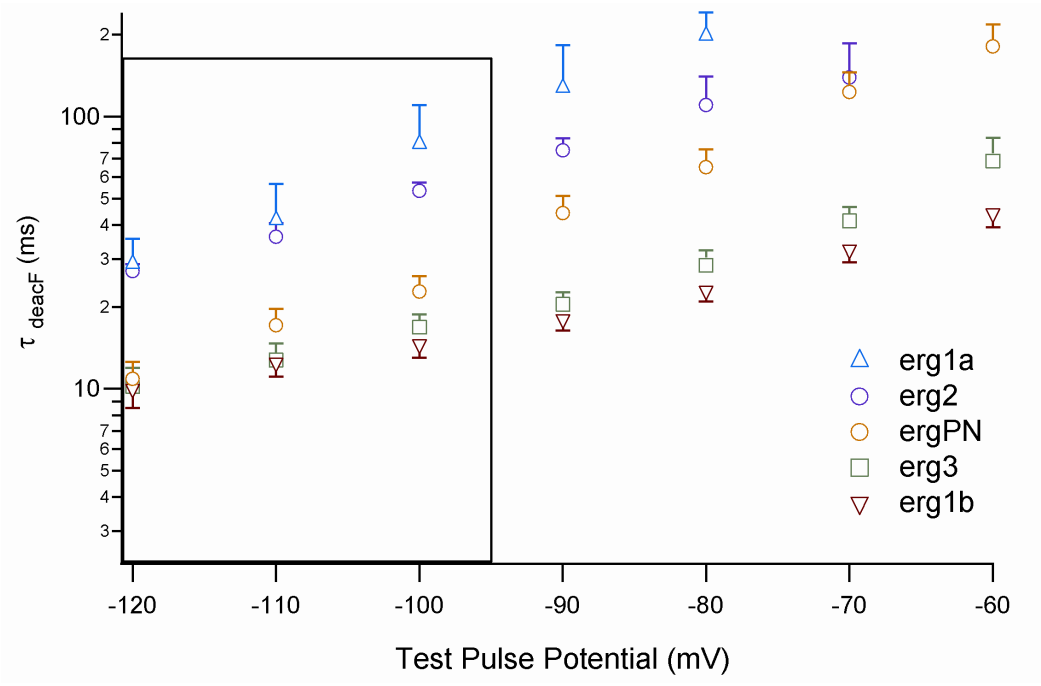

Figure 28. Deactivation time constant for the fast erg currents in PNs and HEK293 cells. For the fast erg currents the potentials at which the values are more reliable are the negative ones, since at strong hyperpolarizations the fast erg component is very large in absolute terms but also in comparison to the slow component. The mean values for -120, -110 and -100 mV can be found in Table 4. At -100 mV the mean values for r-erg1a are significantly different from the means of PN erg current (n = 3 and 6, respectively; $p < 0.05$, unpaired two-tailed t-test)

Table4. Deactivation time constants for fast homomeric and PN erg currents

	τ_{deacF} (ms)			
erg current	-100 mV	-110 mV	-120 mV	n
r-erg1a	**79.50 ± 30.86**	**41.64 ± 14.84**	**28.79 ± 6.77**	3
r-erg1b	14.55 ± 1.53	12.45 ± 1.34	9.98 ± 1.47	5
r-erg2	53.32 ± 4.00	36.15 ± 0.44	27.09 ± 1.66	4
r-erg3	**16.87 ± 1.93**	**12.77 ± 1.93**	**10.23 ± 1.70**	4
erg PN	**22.77 ± 3.20**	**17.11 ± 2.55**	**10.87 ± 1.66**	6

The measurements made in 5 mM K^+ concerning activation and inactivation were meant for understanding the resemblance in terms of kinetics of the Purkinje neuron erg current to any of the currents carried separately by each isoform. And although from those experiments it could be estimated how much current was available at each potential and what could be the involvement of these subunits in the physiology of a native cell, an additional approach was undertaken: the activation of overexpressed erg currents with templates taken from Purkinje neurons. The overexpressed currents are ideal for the study of small changes that can occur during spontaneous activity, or during different experimentally induced depolarizations. The reason for this are the large current amplitudes often in the range of nA. The templates obtained from traces showing differences between control and "+E-4031" conditions can be used to understand which of the four tested subunit types is most likely underlying the observed effects in PNs. Templates showing spontaneous firing were also used for the understanding of the small effects of erg current blockage seen in around half of the cells.

Currents similar to the ones obtained from Purkinje neurons with the "ramp firing" template were also observed in HEK cells. They activated approximately where the ramp started to rise, increasing in amplitude as the ramp depolarized the cell close to -40 mV (Figure 29). Although all cells had currents of relatively high amplitudes, the erg currents activated to very different maximal amplitudes during the ramp template. A reason for this could be various current amplitudes, or current densities. For the r-erg1a subunit the average maximal current amplitude was 43.15 ± 12.7 pA (with a current density of 2.28 ± 0.9 pA/pF, n = 8; Figure 29B), whereas for r-erg1b the current amplitude reached 28 ± 7.9 pA (current density of 1.08 ± 0.3 pA/pF, n = 9; Figure 29C). The last two subunits were at the margins of the spectrum, with r-erg2 not being able to activate currents in 80% of the cells, and r-erg3 that

expressed large activating currents in every cell, during the ramp template. The current amplitudes and densities varied tremendously between r-erg2 and r-erg3 (12.16 ± 4.1 pA, 0.56 ± 0.2 pA/pF (n = 4; Figure 29D) and 340.91 ± 88.9 pA, 11.3 ± 2.2 pA/pF (n = 9; Figure 29E), respectively). For Purkinje neurons, in the same ACSF, the amplitude of the erg current activated by the ramp template was 30.4 ± 3.4 pA, while the current density measured 0.43 ± 0.06 pA/pF, n = 5.

Since the absolute amplitudes of each type of erg current were not relevant for comparison to PNs erg current due to big differences in channel expression, an approximation had to be made for the amount of current that could be activated with the ramp template from the maximal current of a cell (evaluated as the peak current at -100 mV of the availability protocol). Therefore, for each of the four erg channel subunits the ramp current versus total current ratio was calculated. By far the highest ratio was found for the r-erg3 subunit of 0.15 ± 0.04 (n = 9) of the erg total current; and in sharp contrast all the other three ranged between 0.018 ± 0.005 (n = 5) for r-erg2 to 0.037 ± 0.008 (n = 9) for r-erg1b, with r-erg1a being in the middle with a ratio of 0.03 ± 0.01 (n = 8).

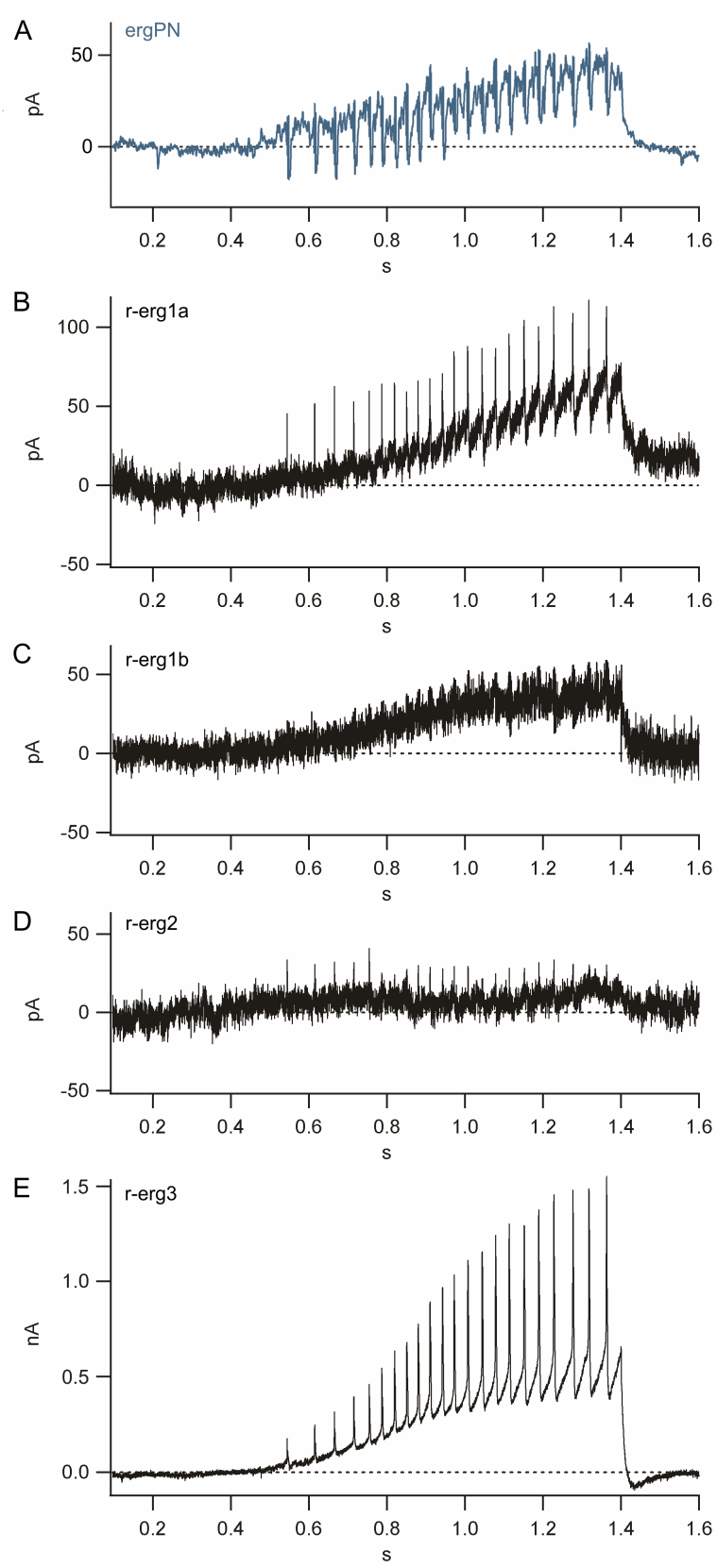

Figure 29. Erg currents activated with the "ramp firing" template in PNs and HEK293 cells. (**A**) PN erg current (blue trace) activated with the "ramp firing" template, in a 5 mM K^+, 1 mM Ca^{2+} ACSF, was compared with the homotetrameric erg currents. The dynamics of the r-erg1a (**B**) and r-erg1b (**C**) current activation during the ramp template appeared similar to PN erg current. R-erg2 (**D**) activated to a small extent, whereas r-erg3 (**E**) exhibited a large activation in all cells; the ratio of activated r-erg3 current with the ramp template versus total current (0.15 ± 0.04, n = 9) realistically approximated the possible current of a PN in 5 K^+ ACSF

In order to see how the erg current activates during spontaneous firing of Purkinje neurons, on the time course of depolarizations to threshold (from roughly -60 to -40 mV), a "spontaneous firing" template (2.3 Hz) recorded from Purkinje neurons was used (Figure 30A). In HEK293 cells expressing the r-erg1a subunit, an accumulation of current could be seen as the cell was depolarized to threshold, indicating that such a depolarization was enough to start activating the r-erg1a channels (Figure 30B). Such an effect could be seen only in cells that had currents big enough to activate to a level where they could be separated from noise. For the HEK293 cells expressing r-erg1b subunits (Figure 30C) the activation was almost absent, even in the cells with large currents. As for the r-erg2 subunit (Figure 30D) no difference could be seen between control and application of E-4031. The most striking difference could be seen in the HEK293 cells expressing r-erg3 channels (Figure 30E) that activated sharply and to a greater extent during the subthreshold depolarization. A difference could also be seen during the APs, a big reduction in the AP currents being noticed for r-erg3 after application of E-4031.

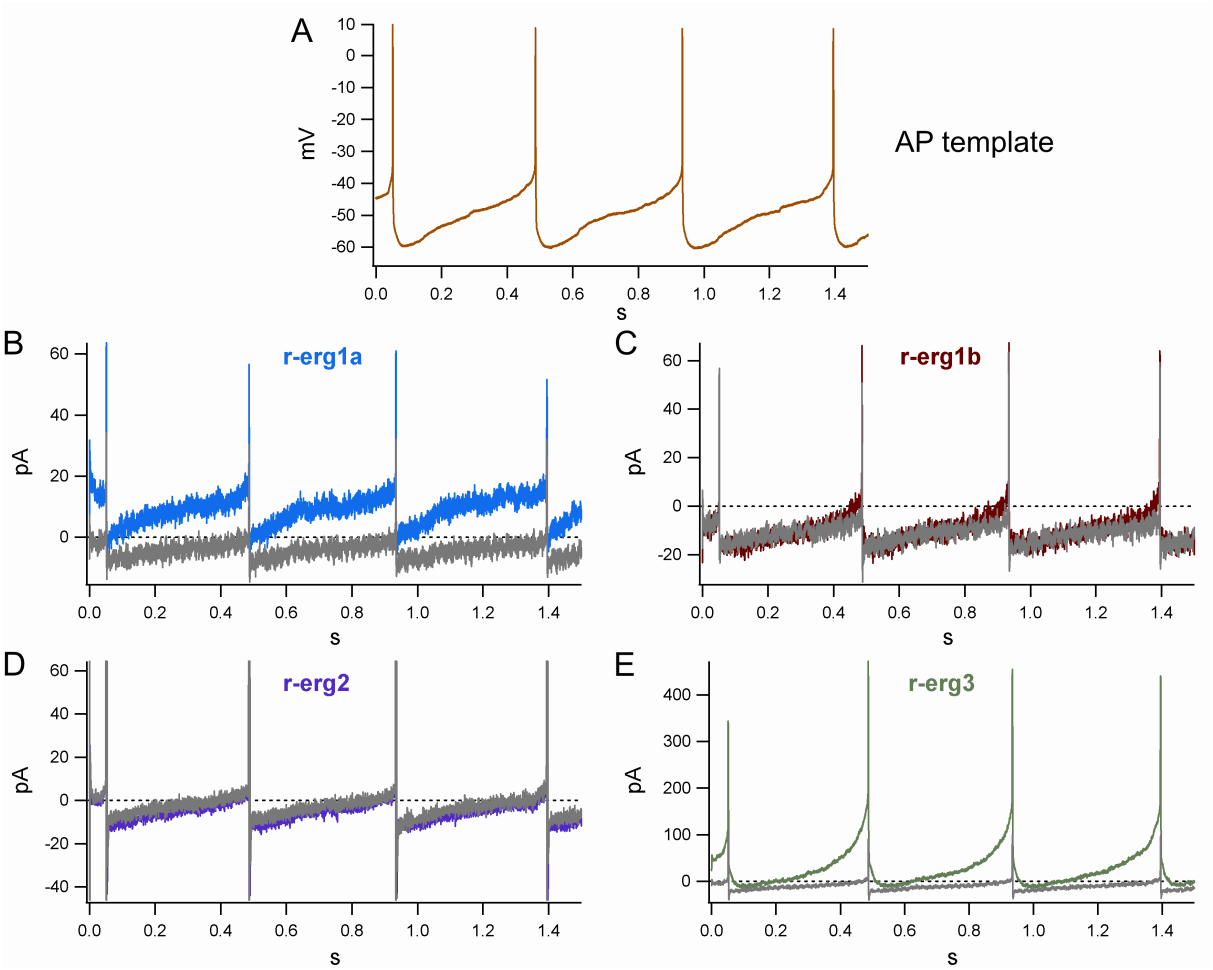

Figure 30. HEK293 cell erg currents in response to a "spontaneous firing" AP template. (**A**) AP template recorded from PNs. (**B**) The r-erg1a current activated on the depolarizing subthreshold slopes of the template. R-erg1b (**C**) and r-erg2 (**D**) currents showed no such activation. (**E**) The r-erg3 currents activated on the subthreshold slopes but also during each AP. [gray traces, after application of E-4031]

For testing if any accumulation of the erg current, during long lasting repetitive firing, takes place, one has to observe the currents elicited on events that are repeating for more than a few times. A protocol was designed in which the APs were artificially created maintaining the short duration typical to Purkinje neuron APs. The protocol fed artificial APs to the cell at a frequency of 1.7 Hz (Figure 31A). Each AP was composed of a depolarizing "subthreshold" ramp from -57 to -37 mV (which were approximate values close to the determined average membrane resting potential and average threshold values of PNs, respectively). The ramp lasted for 500 ms and was followed by a step to 10 mV of 1 ms. This short step was meant to approximate the half-width of Purkinje neuron APs which was approximately 2 ms. Following was a ramp of 2 ms from 10 mV back to -57 mV, a potential at which the cell was kept for 100 ms before the ramp to -37 of the next AP began. Even if the AP frequency in this protocol was actually lower than the one in the "spontaneous firing" template, because the number of APs was much larger, a different phenomenon could be seen apart from the activation that took place during the subthreshold ramp: accumulation. Accumulation depends on another property of the erg channel subunits, namely the deactivation kinetics. If during an AP some channels get activated and if until the next AP, the current does not totally deactivate, then the next AP will appear to activate more channels; this phenomenon occurs until a "saturation" level is reached, at which the amount of current that deactivates during one sweep equals the amount that activates during the next. For the subunits that showed almost no erg current activation when using the "spontaneous firing" template, the increased number of APs in the artificial AP protocol didn't make any difference (r-erg1b and r-erg2; Figure 31C and D, respectively). But for r-erg1a and r-erg3 that exhibited a consistent activation during the subthreshold ramp, the long train of APs illustrated a difference in the behavior of the two subunits. Although with the initial template the currents of both subunits seemed to activate pretty much to the same extent and only with different kinetics, when prolonging the number of APs the r-erg1a currents (Figure 31B) showed accumulation that was almost undetectable within the first three APs. The saturation level was reached shortly after the 10^{th} AP. In sharp contrast, the r-erg3 current didn't accumulate, since the r-erg3 subunits form channels that activate very fast, but also deactivate fast, so that the following APs must activate the same amount of current all over again (Figure 31E).

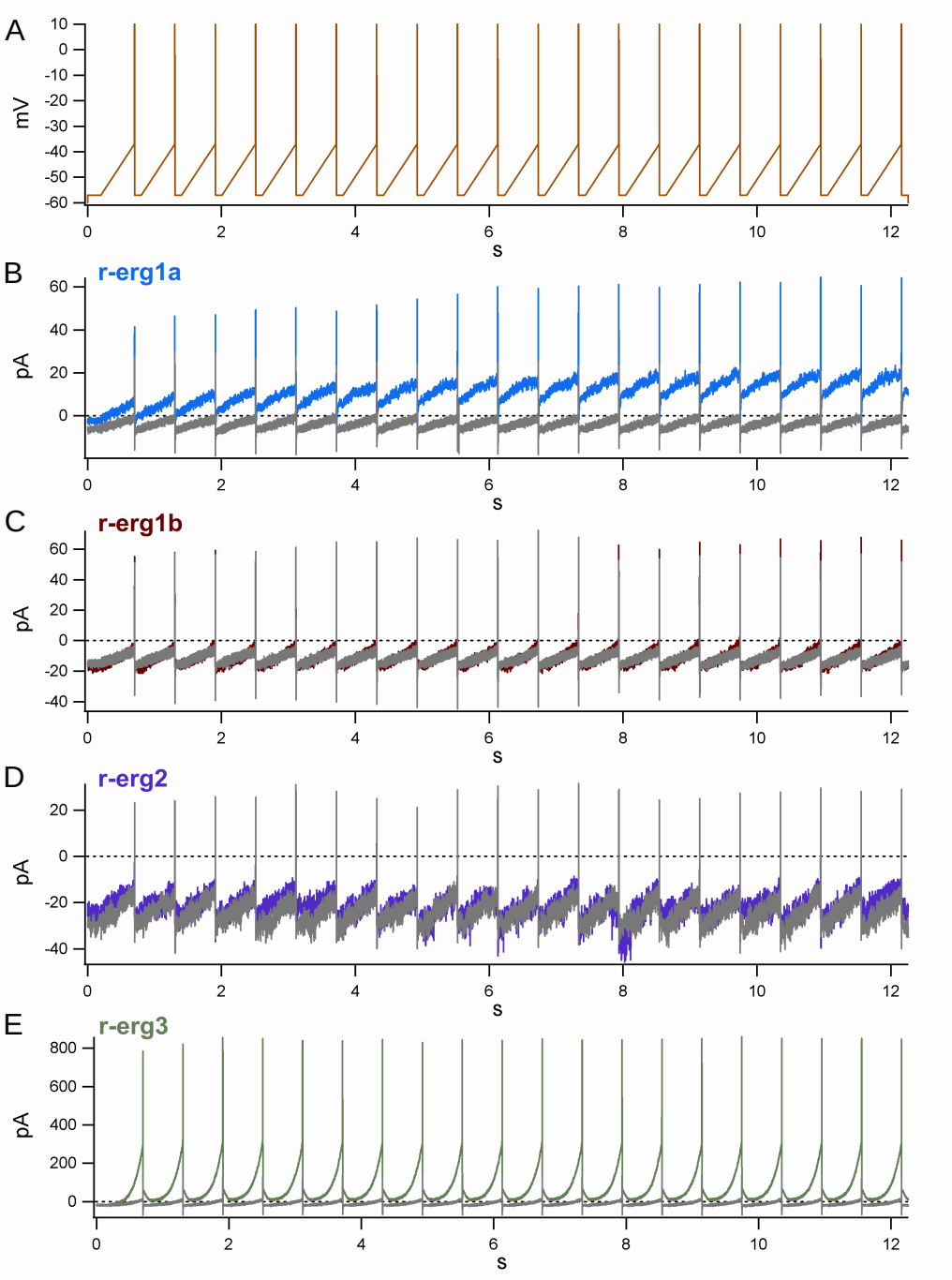

Figure 31. HEK293 cell erg currents in response to an artificially created AP trace. The artificial AP imitated the native APs from Purkinje neurons in terms of width, as the short pulses to +10 mV lasted for 1 ms in the constructed template whereas for Purkinje neurons the half width of an AP ranged around 2 ms. The r-erg1b and r-erg2 currents showed no activation; r-erg3 currents exhibited the same activation pattern as with the "spontaneous firing" template. But due to the long train of APs, r-erg1a current showed accumulation (which was not so obvious when only 3-4 APs are used in the template). The frequency in the AP protocol was 1.66 Hz. [gray traces, after application of E-4031]

Since the experiments, where most of the physiological effects of erg channel blockage were observed, involved current injections to a level were the cells could fire a high frequency train of APs, such a PN response was further considered as a template for further AP-clamp experiments. The template was obtained by injecting 100 pA of depolarizing current, which generated a sustained firing in almost all the cells (Figure 32 A). The approximate firing frequency in this template was 40 Hz, which was higher than the ones from previously described AP-clamp protocols. A different behavior was observed especially in the subunits known to have a fast deactivation (r-erg1b and r-erg3). If with the previous protocols only the currents carried through r-erg1a channels showed a prominent accumulation, this time, because of a stimulation at a higher firing frequency, such an accumulation could be seen also for the currents carried through homomeric r-erg1b (Figure 32C) and r-erg3 (Figure 32E) channels. The most striking effect was seen in the case of r-erg3 channels; due to a very fast activation time constant, the current accumulated much more than for the r-erg1a (Figure 32B) and r-erg1b. No activation seemed to occur for the r-erg2 subunits (Figure 32D).

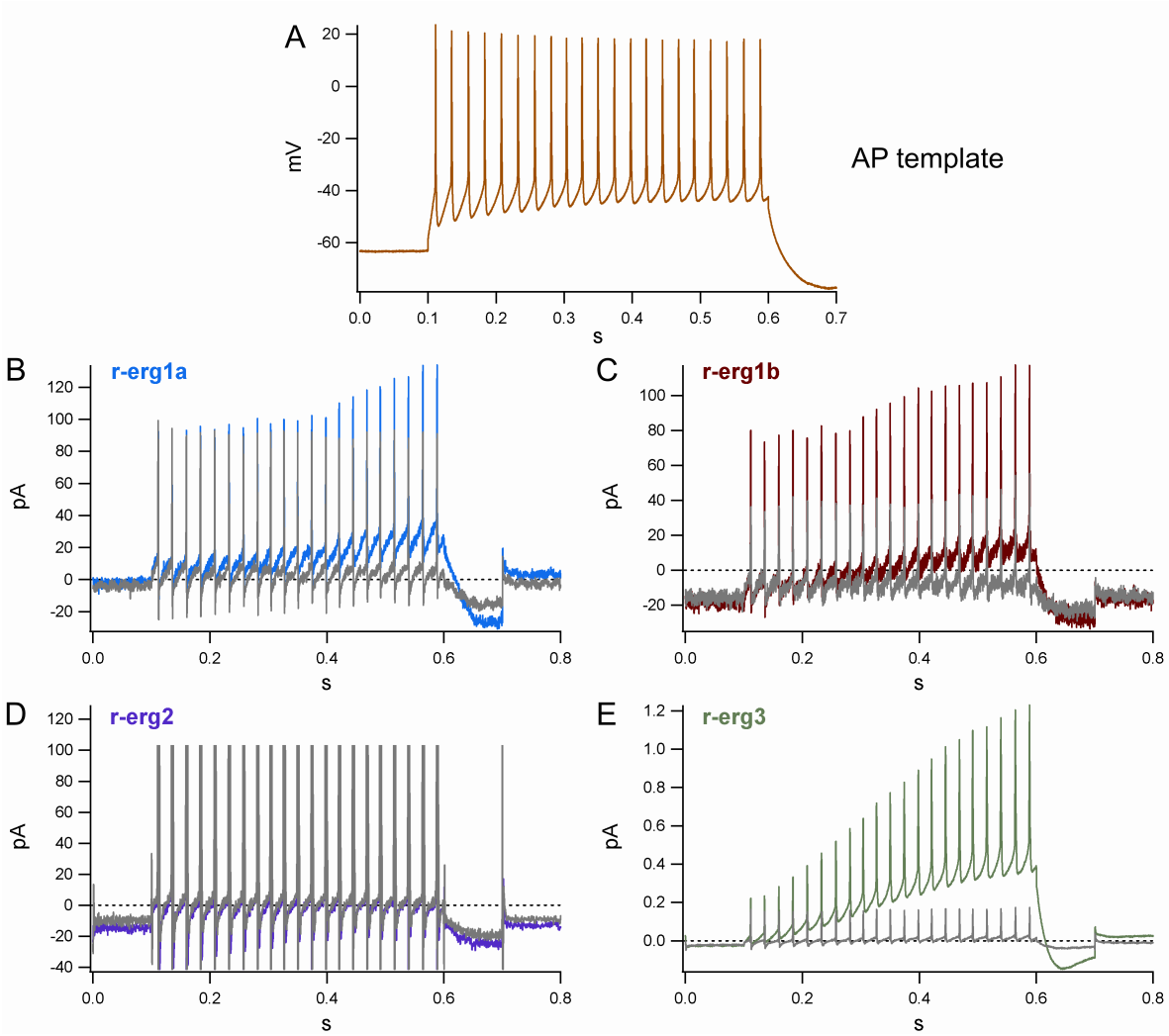

Figure 32. HEK293 cell erg currents in response to an "current injection firing" template. (**A**) HEK293 cells were stimulated with a template (40 Hz) from PNs obtained after a depolarization by injecting 100 pA. The erg channel isoforms expressed in HEK293 cells carried currents that were activated by the template in the case of r-erg1a (**B**), r-erg1b (**C**) and r-erg3 (**E**); (**D**) the r-erg2 currents exhibited no such activation. [gray traces, after application of E-4031]

3.6 Modulation of erg currents in Purkinje neurons by mGluR1

All the effects that have been so far observed were studied by application of a pharmacological substance (E-4031). In many cases, modulation of the biophysical properties of a certain type of ion channel is required, in order to change the responsiveness of a neuron. In the search for an intrinsic way to block/modulate the erg channels, the effect of mGluR1 activation on the properties of the erg current from PNs was evaluated. The mGluR1 receptors were activated by using DHPG (50 µM) which is an agonist of mGluRI receptors that include mGluR1 and mGluR5. The erg currents were elicited, with the same activation protocol that was used to study in the beginning the biophysical properties, before and after application of DHPG to the bath. After DHPG was applied a reduction of the peak tail current measured at -100 mV was observed (Figure 33A). When the erg current amplitudes, after application of DHPG were normalized, to the values before its application a reduction to 0.54 ± 0.02 (n = 4) of the initial current was observed. When the peak values for both conditions were normalized to themselves and plotted against the prepulse voltage, a shift to the right of the activation curve in the presence of DHPG (Figure 33B) was noted (in control conditions the $V_{1/2}$ = -40.81 ± 3.4 mV whereas after application of DHPG $V_{1/2}$ = -28.47 ± 4.52 mV; $p < 0.05$ paired two-tailed t-test, n = 4).

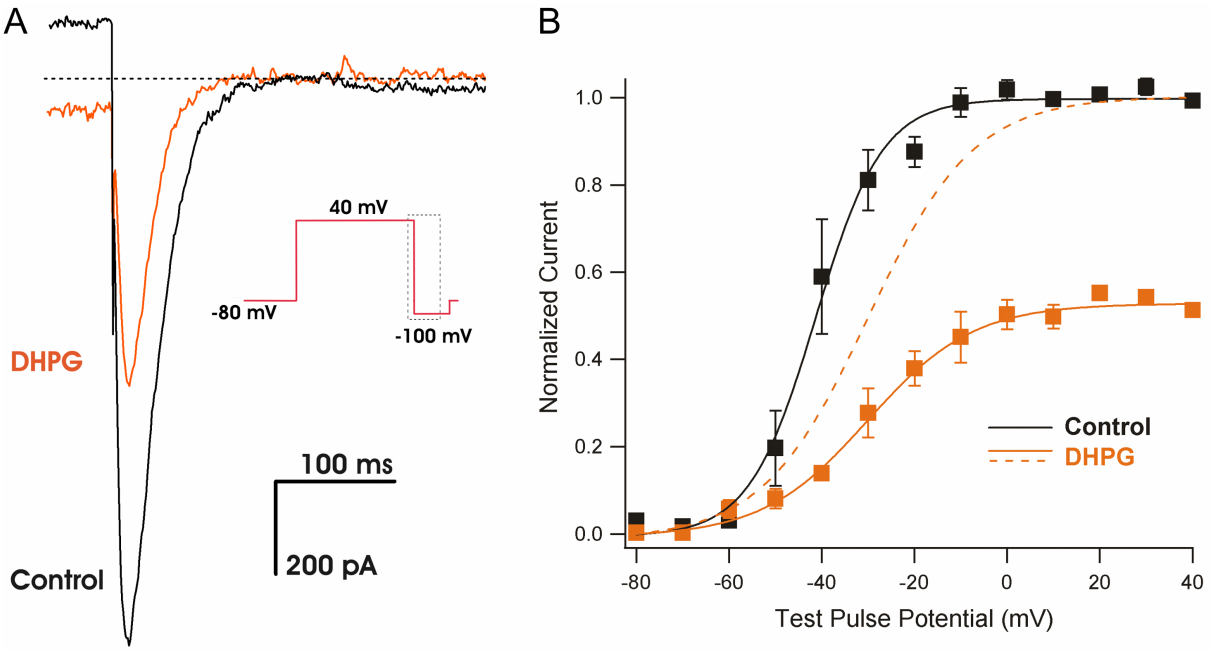

Figure 33. DHPG modulation of the erg current in PNs. (**A**) At -100 mV, after full activation of the erg current, DHPG blocked it by around 50%. (**B**) The voltage dependence of activation before (black) and after application of DHPG (50 µM; orange). When normalized to itself, the activation curve, in the presence of DHPG, showed a shift to the right of around 10 mV compared to control ($V_{1/2}$ shifted from -41.3 to -30.04 mV; $p < 0.05$ paired two-tailed t-test, n = 4) [P5-P10]

For a more dynamic view of the overall effect and for determining how the blockage of erg current contribute to the shape of the synaptic currents evoked by DHPG activation of mGluR1, the cells were clamped at -40 mV in order to have a good fraction of the erg channels activated. To have more stable recordings and without the influence of other kinds of synaptic transmissions, a Mg^{2+}-based 2.5 K^+ ACSF was used, including synaptic blockers for AMPA, NMDA and $GABA_A$ receptors. At -40 mV a net outward current was observed of an amplitude of up to 100 pA. When DHPG was applied to the bath a rapid decrease in the outward current could be seen and most of the time the net current became negative. After reaching the peak of the net outward current reduction, a less rapid increase to levels slightly above 0 mV could be observed. The response to DHPG could be separated into two components: a first component that generated a peak, transient reduction in the net outward current (I_{peak}); and a second component that evolved as a secondary increase in the net outward current ($I_{sustained}$; Figure 34A). Similar experiments were performed with cells clamped at -40 mV in which E-4031 was applied after the net outward current reached a steady level. Very soon after E-4031 was applied, the net outward current showed a fast reduction, proving that at -40 mV, in a 2.5 mM K^+ solution there are activated erg channels. Due to the already known property of erg channels to increase their conductance upon an

increase in the outward K^+ concentration, the same experiments with E-4031 were performed in a 5 mM K^+ Mg^{2+} based ACSF. The differences in the amplitudes of the current blocked by E-4031 were almost indistinguishable, because the increase in conductance was counterbalanced by the decrease in driving force in a higher concentration of K^+. Since activation of mGluR1s reduced the erg current by at least 50% depending on voltage (at -40 mV approximately 2/3 of the erg current is blocked) experiments were performed in which E-4031 was applied before or after application of DHPG, in order to see how the two components were affected. When E-4031 was applied subsequently to DHPG, after the synaptic response reached already the steady-state reduction of the net outward current, no further effect could be observed (Figure 34B); which meant that all the erg current available at that potential was already blocked after application of DHPG. The most interesting approach, to understand the contribution of the erg current to the observed synaptic current, was to apply first E-4031, and afterwards, DHPG. After application of E-4031 a reduction in the net outward current could be observed, and subsequent application of DHPG generated only a transient response (Figure 34C). These results proved that the steady-state component in the response to application of DHPG was due to the blockage of the erg channels, especially when looking at the values for current density. The mean current density for the current blocked by E-4031 was -0.62 ± 0.07 pA/pF (n = 13), whereas for the peak component (measured from the starting point of DHPG application, when both components were combined) the mean equaled -1.04 ± 0.2 pA/pF (n = 5) and for the steady-state component, -0.7 ± 0.15 pA/pF (Figure 34D). The two-tailed t-test showed that there were no significant differences between the current densities of the erg current blocked independently by E-4031 and the erg current blocked by activation of mGluR1.

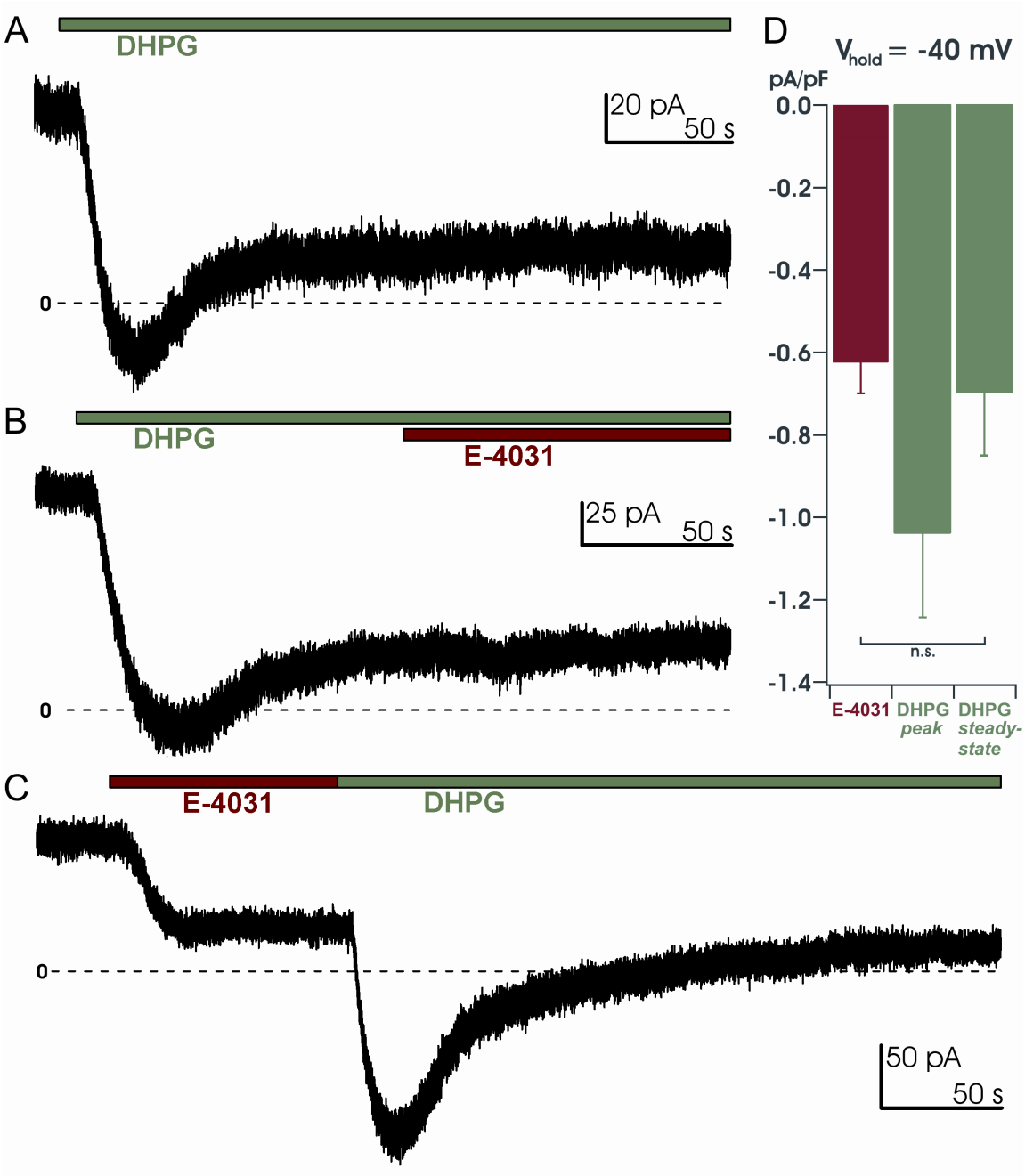

Figure 34. The erg current in PNs is part of DHPG-induced response. The recordings were done in the absence of Ca^{2+} in order to better isolate the erg component. (**A**) Typical response to DHPG (50 µM) application, composed of a transient and a sustained current component. (**B**) If E-4031 was applied after the transient component was gone, no change in the steady-state component could be observed. (**C**) If E-4031 was applied on a cell voltage-clamped at -40 mV the net outward current was reduced, and upon subsequent application of DHGP, only the transient component could be detected. (**D**) The mean amplitudes of the E-4031 sensitive current and of the sustained component were very similar (n.s.; unpaired two-tailed t test; n equals 13 and 5 respectively) [P5-P10]

Similar experiments were done in the current clamp mode in the absence of Ca^{2+} or in the presence of 2 mM Ca^{2+}. Without Ca^{2+} in the extracellular solution the neurons were unable to fire APs, but the depolarizations induced by the application of different drugs could be better evaluated. Therefore, if a Purkinje neuron was depolarized by current injection to -40 mV, and DHPG was subsequently applied, a transient followed by a sustained depolarization could be observed (Figure 35A). These depolarizations were the equivalent of the peak and sustained currents from the voltage clamp mode. If after clamping the neuron at around -40 mV, E-4031 was applied, the cell depolarized to a sustained level, and the subsequent application of DHPG produced only a transient depolarization (Figure 35B). In the presence of Ca^{2+}, the neuron was able to fire APs and the response to DHPG could be evaluated in terms of changes in the firing frequency. Therefore, upon DHPG application a transient and a sustained increase in firing frequency could be observed (Figure 35C).

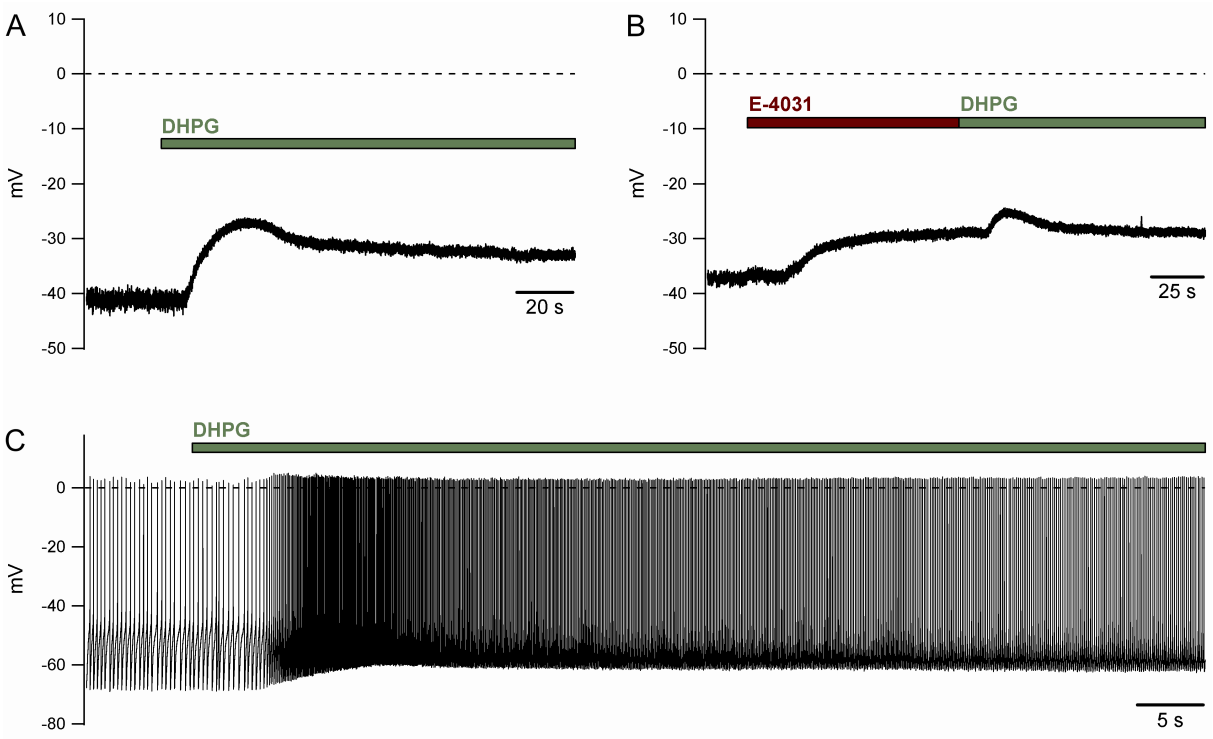

Figure 35. Current clamp responses to the application of DHPG and E-4031. (**A**) Current clamp trace equivalent to the voltage clamp recordings, showing a transient and a sustained depolarization in the presence of DHPG. (**B**) Only a transient depolarization could be elicited by application of DHPG if the erg currents had been previously blocked. (**C**) Typical firing response (in the presence of 2 mM Ca^{2+}) with a transient and sustained increase in firing frequency.

4. Discussion

The present study focuses mostly on the immature Purkinje neurons from the mouse, but comparisons between young and adult animals, in terms of PN behavior, are done either using new data or referring to data already existing in the literature (Sacco *et al.*, 2003; Hirdes *et al.*, 2005). A few studies have shown that the erg channels are well expressed in the Purkinje neurons of mouse and rat, all four major isoforms receiving the maximal expression score (Guasti *et al.*, 2005). Although initial studies have shown that the labeling of Purkinje neurons occurs mainly in the somatic region (Papa *et al.*, 2003; Guasti *et al.*, 2005), subsequent studies proved that the erg channels are expressed in dendrites too, the molecular layer being labeled throughout its entire thickness (Hagendorf *et al.*, 2009). The first goal was to characterize as completely as possible the biophysical properties of the erg currents in immature Purkinje neurons of wild type mice. In this way conclusions can be derived about the degree of homogeneity of isoform distribution in the population of PNs, concerning the possible functional predominance of one of the erg channel isoforms, or about the functional implications of a current with certain biophysical properties (by integrating them with membrane potential, firing pattern and synaptic activity). Although it has been shown that the intensity of erg channel labeling on PNs is more or less similar in the soma and proximal dendrites (Hagendorf *et al.*, 2009), a proof that all these channels are functional and the erg current density is also homogeneous, was needed.

The next goal was to observe the natural behavior of immature PNs, and how this behavior could be influenced by injecting different amounts of current into the neurons. The effect of erg channel blockage on these responses was evaluated. Experiments were also performed on young adults, where necessary; but in some cases, the results from immature PNs were compared to data from the PNs in adult mice already present in the literature (Sacco *et al.*, 2003).

In order to have a mechanistical understanding of the observations concerning excitability, feeding-back experiments were performed in which a response from a Purkinje neuron was used as a stimulus for another Purkinje neuron; in this way it has been possible not only to observe what happens to the firing of a neuron when the erg current is blocked, but also to visualize where and how this current interferes with the firing process.

When the erg current, responsible for the changes in the functionality of the cell, is isolated "in action", questions about its identity arise; and it is important to know which of the four main erg channel isoforms participates with the largest number of subunits to the constitution of the channels in native cells. In other words, to which of the erg currents carried by each subunit at a time, the erg current in PNs resembles the most. For answering this question experiments must be done in overexpression systems with each subunit separately, and also comparisons be made to the native currents.

And the last major step was to investigate if there was any intrinsic mechanism by which the erg currents could be blocked or modulated in any way. If the blockage of erg currents would occur only experimentally, by adding a specific blocker to the bath, then the observed functional effects would be only theoretical and would show how the cell excitability would have been if Nature hadn't "put" the erg channels in the cell. It was known already that the erg channels are influenced by the activation of some G protein-coupled receptors like the ones for TRH, GnRH or glutamate (Bauer, 1998; Hirdes *et al.*, 2010; Hirdes *et al.*, 2009, respectively).

4.1 The fast erg currents in Purkinje neurons are homogeneously distributed

An important fact that should be mentioned from the beginning is that more than 95% of the Purkinje neurons, investigated in the voltage clamp mode in 40 mM K^+ ACSF, had an erg current; and only some very small cells or cells with a higher degree of damage didn't express it. When the erg currents from Purkinje neurons were evaluated concerning the voltage dependence of activation, the $V_{1/2}$ values as well as the steepness indicated that the erg channels in this type of neurons most probably have a similar isoform constitution. As it can be observed in Figure 26 the activation curves for the four isoforms differ from each other in terms of $V_{1/2}$ by more than 15 mV, with the exception of r-erg1a and r-erg3 which are quite similar. If all the possible combinations of forming erg channels from the different subunits were taken into account, some would generate populations of erg channels quite different from each other. If this had been the case in Purkinje neurons, then the activation curves for some cells would have induced a great variability in the mean values. Moreover, the erg currents in Purkinje neurons have a very fast time course of activation (54 ms) compared to r-erg1a (215 ms; Hirdes *et al.*, 2005); and this would indicate that r-erg1a could have a

minimal contribution to the erg channels in PNs and r-erg3 could be the only present isoform with such a hyperpolarized $V_{1/2}$. Despite the great similarity of the activation curves among different Purkinje neurons, the current densities varied very much (-7.82 ± 1.04 pA/pF, n = 12) even between cells of mice of the same age or even belonging to the same mouse; therefore this cannot be accounted for by any differences in solutions or preparation procedure. The time course of activation was studied using the "envelope of tail protocol" in which the pulse at which the erg current is activated was chosen to be +20 mV so that comparison could be made with erg currents expressed in other neuronal types. τ_{act} (54 ms; Table 5) proved to be the fastest known so far for any native cell, but even faster that the isoform which was supposed to have the most rapid activation time course (r-erg3, 95 ms; Hirdes *et al.*, 2005). And again the mean values for different durations of the test pulse were very homogeneous proving once more the biophysical homogeneity of erg channels in Purkinje neurons.

The next biophysical property to evaluate was the availability curve that would give the amount of erg current, that doesn't undergo further deactivation, at different potentials of interest. Under physiological circumstances erg channels could be activated during a burst or a high frequency train of simple APs, and upon repolarization some current would still remain active, participating to the maintenance of a hyperpolarized membrane potential. As it can be observed from the availability curve in Figure 12, at potentials around threshold, like -50 or -40 mV, the erg current would be available at fractions of around 70% and 90% of the total current, respectively. The time courses of recovery from inactivation and deactivation that were obtained by fitting the currents elicited by repolarizing steps, showed that the erg currents in Purkinje neurons have again some of the fastest time constants when compared to other native cells (serotonergic neurons, Hirdes *et al.*, 2005; mitral/tufted neurons, Hirdes *et al.*, 2009).

Table 5. Approximate biophysical parameters in 40 mM K^+

Neuron type	***τ_{act} at 20 mV (ms)***				***τ_{deac} at -90 mV (ms)***				***$V_{1/2}$ activation (mV)***			
Serotonergic	123				83				-42			
Mitral/tufted	135				176				-51			
Purkinje	54				48				-44			
r-erg	**1a**	**1b**	**2**	**3**	**1a**	**1b**	**2**	**3**	**1a**	**1b**	**2**	**3**
CHO	215	106	821	95	400	20	200	50	-37	-40	-3	-64

So far, these time constants show that the erg currents in Purkinje neurons have fast kinetics resembling more the currents mediated by the r-erg3 isoform. The fact that the time course of activation in PNs is even smaller than the smallest among homomeric channels of the isoforms separately expressed (e.g. in CHO cells), suggest that additional factors could contribute to the modulation of erg channel properties, therefore a native channel could be more than a simple combination of the main four α subunits.

In order to evaluate if the erg channels, although present throughout the entire plasma membrane as immunohistochemistry studies have shown, are homogeneously distributed or really functional in all compartments, nucleated patch experiments have been performed. Since no difference was shown to exist between the erg current density in the somatic membrane as compared to the whole cell membrane, the current density in the somatic membrane must be similar to the current density in the dendrites. As for the latter compartment the existence of a gradient could be possible only if at one end the erg current density would be higher and at the opposite end would be lower than the somatic current density; so that the average for each compartment remains the same. But such a varying distribution hasn't been reported for an ion channel before. The homogeneous distribution comes as an argument against the possibility that slight variations in solutions or slice preparation procedure are responsible for the big variability of erg current density among Purkinje neurons.

4.2 Erg channels in Purkinje neurons decrease excitability and increase firing pattern regularity

For the functional involvement of the erg channels in PN excitability a first evaluation was performed in the on-cell mode, for the immature animals but also for the young adults. In the on-cell mode the only parameter that can be used, in the case of simple firing, is the interspike duration and implicitly the firing frequency. When a bursting behavior occurs, additional parameters occur, like burst duration, interburst interval and intraburst frequency. Purkinje neurons have been shown to present spontaneous activity although silent neurons are also quite frequent; the state of the cell can be influenced by many internal factors and especially in acute slices by the degree of recovery that each cell underwent. The PNs that were silent had a mean membrane potential of -56.6 ± 2.6 mV (n = 8) with values ranging from around

-45 to -65 mV. Therefore, the lack of spontaneous activity cannot be accounted for by a stronger hyperpolarization of the membrane. As for the spontaneously active neurons the resting membrane potential is obviously impossible to evaluate. For the on-cell recording evaluation, only the PNs that were spontaneously active were considered, so that the change in frequency upon blockage of the erg current could be evaluated. In immature PNs the firing frequency increased by approximately 2 Hz upon blockage of the erg channels. This finding suggests that at the membrane potential at which the cell was spontaneously active in the control solution some steady-state erg current was present, slightly hyperpolarizing the membrane and determining the neuron to fire APs at a lower frequency than in its absence. Other neuronal types have been shown to present a steady-state erg current at resting potentials or during spontaneous firing (ventral horn GABAergic interneurons, Furlan *et al.*, 2007; medial vestibular nucleus neurons, Pessia *et al.*, 2008 and mitral/tufted neurons Hirdes *et al.*, 2009). When this steady-state erg current was blocked, the neurons depolarized and the firing rate accelerated.

Another important fact is that only 40-50% of the spontaneously firing neurons reacted to the blockage of the erg current. Since the erg current was present in almost every PN, this relatively low percentage of reacting cells can only be explained by the large variability in current density among cells. In a Purkinje neuron that would have a small erg current, the change in firing frequency could be almost indistinguishable. Another explanation might be that the degree of membrane depolarization is different for responsive neurons than for the others. The level of depolarization cannot be approximated from the firing frequency, since different neurons could have different factors contributing to modulation of firing; therefore, two neurons with similar firing frequencies could have different baseline membrane potentials. And from the curves in Figure 26, if it is assumed that the erg currents in PNs are very similar to the r-erg3 currents, then in a 5 K^+ solution, at -40 mV, the fraction of current that can be activated reaches 20% of the total current. But as the potential goes to -50 mV, the fraction of available current drops to almost 0. And since the resting membrane potentials can vary across a range of around 10 mV, it is very possible that half of PNs have membrane potentials in the more hyperpolarized half of the range.

When the same 5 mM K^+ ACSF was used for bathing Purkinje neurons from P22-P42 mice another type of firing behavior was observed: bursting. The bursts were relatively short (around 200 ms) and quite regularly interspaced. It was already known that P/Q-type Ca^{2+}

channels are responsible for the termination of the bursts (Womack & Khodakhah, 2004); as the cell progressively depolarizes more Ca^{2+} channels are activated and the influx of Ca^{2+} would subsequently activate Ca^{2+}-activated K^{+} channels, mainly of the SK type. The SK channels hyperpolarize the membrane and terminate the burst. After erg current blockage the bursts became longer, in average by approximately 3.5 times, while some of the bursts increased many times more than the average duration of a burst in control conditions, whereas the interburst interval decreased. However, the intraburts frequency decreased two fold. A similar observation was made in the ventral horn GABAergic neurons from mouse spinal cord, in which the spontaneously occurring bursts were prolonged upon application of E-4031, although the intraburts firing frequency increased (Furlan *et al.*, 2007). In previous work it has been proposed that the dendritic Ca^{2+} spike is responsible for the process of burst initiation and termination. The depolarization due to the foot of the Ca^{2+} spike is the one that generate the initiation of the bursts, as soon as the threshold for the Na^{+} spikes is reached; while the depolarization progresses the burst increases in length and the firing frequency gradually increases. At some point the threshold for the initiation of the Ca^{2+} spike is reached, and as soon as the Ca^{2+} channels open and the influx on Ca^{2+} into the cell increases the SK channels are activated and by hyperpolarizing the membrane the bursts are terminated. As can be observed in Figure 21, during high frequency firing superimposed on a depolarization that brings the cell well above the normal resting potential, the erg current is activated; and its tendency is to repolarize the membrane. Although the amplitude of this current is not that big as to influence the whole process of stopping the burst, it could participate synergistically with other conductances to the process of tightly regulating burst duration or even the interbursts intervals. Although the SK channels have been shown to be very important for the hyperpolarization of the bursts, they are not the only factor involved, as the replacement of Ca^{2+} by Mg^{2+} in the external solution even promotes bursting behavior in PNs (Swensen & Bean, 2003). The complex spike, evoked in PNs by the stimulation of the climbing fibers, is composed of a first robust spike followed by a various number of spikelets, which have been shown (Davie *et al.*, 2008) to be generated in the axonal membrane. The frequency of spikelet firing is very high (more than 300 Hz; Hurlock *et al.*, 2008), therefore the complex spike constitutes a special type of burst in PNs. By erg channels blockage the duration of the complex spike can be increased by one additional spikelet in some PNs (Sacco *et al.*, 2003). The addition of a supplementary spikelet, after application of WAY-123,398, suggests that the build up of the erg current to the end of the complex spike would contribute to the termination of spikelet firing. A similar mechanism could be involved in the case of bursts.

One other possible mechanism for the increased duration of the bursts is not that the bursts are prolonged, but that the burst are more easily initiated. As an erg current conductance is present at membrane potentials above -50 mV, that conductance could be present, at least in some cases, when PNs are firing bursts; and when the erg currents are blocked the threshold for the initiation of the first spike in a burst is lowered, as Figure 17 demonstrates. Just like in the immature PNs, only half of the neurons from young adults have reacted to the erg current blockage, and the reason is most probably the same as for immature neurons. The mechanism of burst prolongation, supposedly happening because of a lower threshold for AP initiation, would differ from the mechanisms previously proposed that considered burst duration regulation either in terms of Na^+ current decline or in the availability of the hyperpolarizing conductances (SK channels) building up to the end of the burst (Swensen & Bean, 2003). It is clear, however, that the major factor responsible for burst prolongation is the increased delay to the activation of hyperpolarizing conductances, since the decrease in threshold could account for the addition of only a few spikes to the burst.

Although the on-cell experiments are not intrusive and disturbing for the cells, it is impossible to control the membrane voltage and manipulate the ion channels. Therefore, the next step was to use the whole-cell configuration for further investigations. In order to have a stable baseline from which the neurons could be stimulated, it has been necessary to inject hyperpolarizing current into the spontaneously active cells, to make them silent, but also into the silent cells if the membrane potential was too depolarized for the removal of Na^+ channels inactivation. From this baseline, the neurons were brought to different levels of depolarization and the firing pattern was analyzed. If a small amount of net depolarizing current from the baseline is injected into the cells, it might be insufficient for triggering any spike, as some cells showed. But after the blockage of the erg channels, the same amount of current was enough to trigger a simple spike (Figure 17). Since at this potential the effect is of the "on/off" kind, it was not possible to evaluate parameters such as firing frequency of delay until the first spike; but it could be deduced from such a behavior that the erg current blockage lowered the threshold for spike initiation. The same phenomenon was observed when larger amounts of depolarizing current (100 pA) were delivered to the neurons, generating a sustained firing. Upon blockage of erg currents the neuron was able to fire a few more APs, and the delay to firing initiation was decreased. Also the interspike duration between the first and the second AP decreased, which in terms of IFF translates into an

increase by more than 7 Hz. Just as the "on/off" response suggested, there is a lowering of the threshold upon blockage of the erg current, change that although very small (approximately 2 mV) is statistically highly significant. All these parameters show that when the erg current is present the excitability of Purkinje neurons is slightly reduced. Although the erg current has been identified and functionally studied in several neuronal types the mechanisms by which it increases excitability are not always the same. In the neurons of the medial nucleus of the trapezoid body (MNTB), blockage of the erg channels increased the firing frequency and reduced the threshold but there was no effect on the latency (Hardman & Forsythe, 2009). Whereas in the case of MVNn the threshold didn't modify after the erg channels were blocked although the firing frequency increased (Pessia *et al.*, 2008). One constant observation concerning the effects of erg channel blockage was that the shape of the APs remained unchanged, the amplitude, half-width, afterhyperpolarization (AHP) and afterdepolarization (ADP) being similar before and after application of erg channel specific blockers (Sacco *et al.*, 2003; Pessia *et al.*, 2008; Hardman & Forsythe, 2009).

An important feature of the firing pattern of immature PNs is the lack of accommodation. The first 2-3 APs show increasing interspikes, but afterwards the interspikes are quite constant, meaning that there is no conductance with the capacity to accumulate from one AP to the other or along the course of depolarization. And the main effect of erg channel blockage on the firing pattern is to shorten all interspikes allowing more APs to be generated during the 500 ms pulse. In the older animals, Sacco *et al.* (2003) have shown that at least half of Purkinje neurons exhibit accommodation, the 10^{th} interspike becoming much longer than the first. And upon erg channel blockage, the accommodation greatly decreased (Figure 36B). One explanation for the different firing pattern between immature and young adult animals could be that the erg channels have different sets of subunits in their composition. In the immature PNs fast deactivating subunits might predominate, as it was already suggested from the evaluation of activation curves and various time constants, whereas in the older PNs the slow deactivating subunits might be responsible for the accumulation of erg current to the end of the stimulating pulse. A developmental change in erg channel expression has already been shown to take place in spinal ventral interneurons (Furlan *et al.*, 2005); at 7 DIV, 77% of the interneurons presented an E-4031-sensitive current, whereas at 14 DIV only a minority (23%) displayed the erg current. Instead of downregulating all erg channel subunits, a more subtle switch between the predominant subunits can occur in PNs. In immature PNs, the plot of average IFFs, before and after application of E-4031, showed only a steep decrease in the

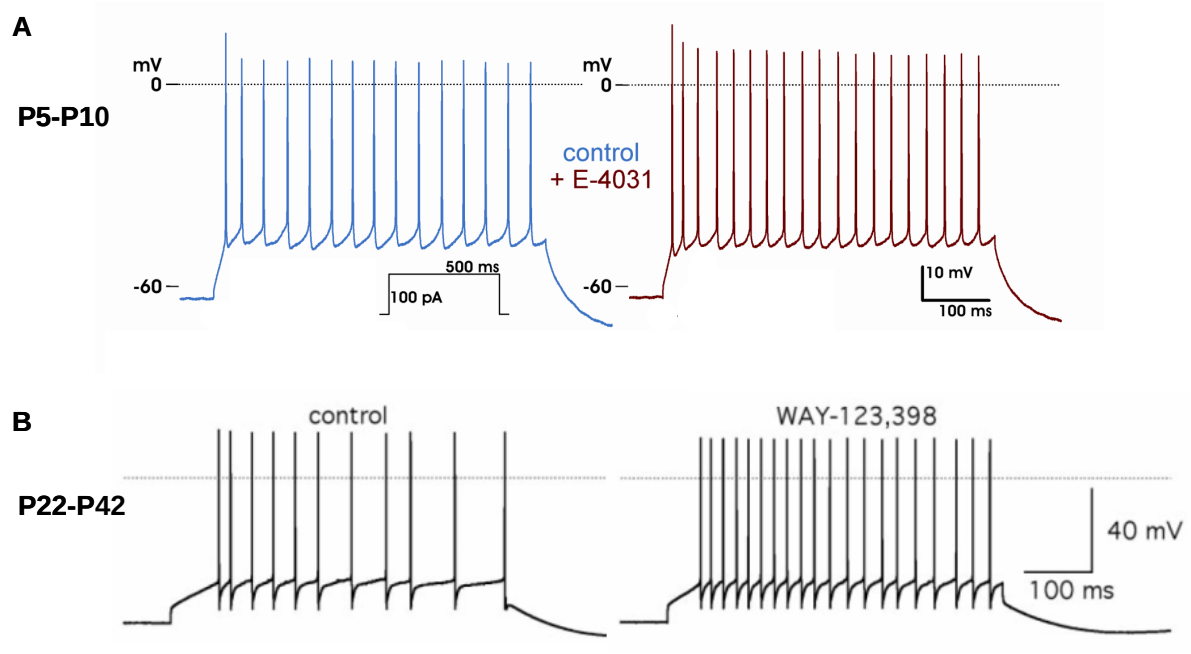

Figure 36. Comparison between the firing pattern of P5-P10 and P22-P42 mice. (**A**) Typical set of traces recorded before (blue) and after (red) application of E-4031 from immature PNs; no accommodation can be distinguished. (**B**) typical set of traces before and after application of WAY-123,398 (specific erg channel blocker), showing that cell firing accommodates in the presence of the erg current [modified from Sacco *et al.*, 2003]

beginning, for the first 2-3 APs, but afterwards the average values were almost constant; although there was a very slight decrease in IFF even for the last APs, there was no difference between control and "+E-4031" conditions in terms of accommodation (Figure 19).

By looking at the mean IFF values it can be implied that the erg channels have no role in setting the duration of the interspike intervals. But by looking at the IFFs of individual cells it can be observed that after the blockage of the erg channels, in 25% of PNs, the interspike duration varies quite a lot from one AP to the next. The explanation could be that fast deactivating erg currents would totally deactivate on the course of an interspike, not accumulating from one AP to another, but participating to the establishment of more regular durations between APs. A similar increase in discharge irregularity, after blockage of the erg channels, has been shown by Pessia *et al.* (2008) for the MVNn, together with an increase in firing frequency. Since the firing frequency depends on the membrane potential, on which the erg current activation also relies, it could be that the erg current activation attenuates the spontaneous membrane potential oscillations responsible for the irregular firing. In the middle of the interspike the net inward current is very small and the participating conductances have an absolute magnitude many times larger (Swensen & Bean, 2003); therefore, small changes in any of them could have great effects on the timing of spikes. In mutant mice, for the P/Q-

type Ca^{2+} channels, it has been shown that the precision of intrinsic pacemaking was significantly reduced (Walter *et al.*, 2006). Many other channels could contribute to the precise pacemaking of PNs, since this is thought to be an important background signal to DCN neurons on which motor coordination-related information would be relayed (Eccles, 1973).

The influence of erg channel blockage on the excitability of immature PNs was evaluated also at stronger depolarizations that would induce an even higher firing frequency. At high firing frequencies the effect of erg channel blockage becomes indistinguishable, because the capability of the neuron to increase its firing frequency becomes more and more difficult the higher the frequency is; this could be compared to a saturation effect. It seems that at membrane potentials around threshold and as long as the cell is not very much depolarized and has a relatively low firing frequency, the erg channel blockage induces an increase in excitability since the erg channels are conducting current at these potentials. As the depolarizations get stronger and the firing frequencies become too high, there is no obvious effect when the erg channels are blocked.

But what happens when the neuron is brought to membrane potentials where failure could occur because of a high degree of Na^+ channel inactivation? This question was addressed by using a longer depolarizing protocol, containing a 1 s spanning ramp that depolarized the cells by injecting up to 200 pA of current, and a plateau of 200 ms during which 200 pA of current was injected. Because of the longer and stronger depolarization the PNs were more prone to firing failure. However, failure did not occur in control conditions. But as soon as the erg channels were blocked, the APs failed to occur to the end of the stimulation protocol. This would indicate that during the depolarization a conductance with the tendency of hyperpolarizing the cell would activate, and therefore less Na^+ channels would undergo inactivation. A similar phenomenon was observed in basal vomeronasal neurons (Hagendorf *et al.*, 2009) where blockage of the erg channels decreased the firing frequency upon injecting low amounts of depolarizing current, whereas at higher amounts almost total failure occurred.

Taken together, the results concerning the involvement of the erg current in neuronal excitability make it obvious that there is an interplay between the erg channels and other types of ion channels participating to the regulation of neuronal firing. At threshold potentials the activated erg conductance dampens excitability, whereas at more depolarized potentials,

during high frequency firing, it can also prevent firing failure by allowing the Na^+ channels to recover from inactivation.

In order to understand exactly how the erg current, responsible for the above mentioned effects, activates, when the activation starts and to which extent this process happens, the control response to the ramp protocol was used as a template for stimulation. The currents recorded with this template in the presence of E-4031 were subtracted from the control traces, this way revealing the erg current component. For an optimal isolation of the erg current, a solution without Ca^{2+} was used (Figure 21); but since further comparisons with HEK293 cells expressing erg currents were to be made, the template was applied on PNs bathed also in solutions containing 1 mM Ca^{2+} and 2 mM Ca^{2+}. The current densities of the activated erg currents were similar among these three conditions, but it seemed that when 2 mM Ca^{2+} are present the current starts to activate after a longer delay than in the other two situations. This could be explained by the fact that in the presence of Ca^{2+} the activation curve of the erg current is shifted to more positive potentials (Johnson *et al.*, 2001); and so, in 2 mM Ca^{2+} the current activated when depolarization reached a more positive potential.

4.3 The erg current in Purkinje neurons resembles r-erg3 current

To better understand the properties of the erg current in Purkinje neurons, it was needed to functionally assign the native erg current to one of the currents mediated by single isoforms. The implications of erg current blockage in the physiology of the entire neuron would be different depending on the isoform that is the most responsible for constituting its erg channels. As it was shown already, that transfection of hippocampal neurons, which would otherwise have an accommodating firing pattern, with the DNA for an isoform that mediates fast currents (*KCNH2*-3.1), would greatly modify the firing pattern to a non-accommodating one (Huffaker *et al.*, 2009). Therefore it was necessary to overexpress each of the isoforms into HEK293 cells and evaluate the activation curves and the current elicited with different templates taken from PNs. The first step in this enquiry was to measure the voltage dependence of activation in 5 mM K^+ Ringer that would approach the naturally occurring ion concentrations. The activation curves had $V_{1/2}$ values differing by more than 10 mV from each other (Figure 23). This could be helpful when comparisons are made with activation curves from native cells. For a more realistic view of the available activated current,

inactivation had to be also evaluated. By intersecting the activation and inactivation plots, the "window current" can be appreciated. There is always an interplay between activation and inactivation and the "window current" would give the real current at more depolarized potentials. The "window currents" were estimated for each of the four subunits. As can be observed in Figure 25 the most abundant current at -40 mV, where the PNs were brought by the depolarizing protocols, is the r-erg3 current; very little r-erg1a current is present at this potential, whereas for r-erg1b and r-erg2 the currents activate at around -30 and -10 mV, respectively. Since all the other biophysical parameters in PNs were obtained in 40 mM K^+ ACSF, the exact same solution was used for recording the activation curves of erg currents carried by different isoforms. In different K^+ concentrations, the activation curves have different $V_{1/2}$ values, and the degree of shift varies from one isoform to another. In 40 mM K^+ the activation curves were shifted to more negative potentials when compared to the $V_{1/2}$ in 5 mM K^+. The biggest shift took place for the r-erg1a isoform, reaching almost 30 mV, whereas for the r-erg2 the shift was only of approximately 12 mV (Figure 26). Because of the great shift of the activation curve for the r-erg1a subunit (compared to r-erg3 that had a shift of only around 14 mV), the activation curves of r-erg1a and r-erg3 isoforms were brought very close to each other (separated by only a little more than 2 mV) and insignificantly different from the activation curve of PN erg current. For further discrimination between the four erg channel isoforms, and especially between r-erg3 and r-erg1a, the time courses of recovery from inactivation and deactivation were considered. Since recovery from inactivation is more prominent at negative potentials, three potentials were taken into consideration for further comparison (-90, -100 and -110 mV). The τ_{rec} for r-erg1a was always bigger and more apart than for r-erg3 and PNs, which seemed to have more similar values especially at -90 mV (Table 3). However, τ_{rec} for r-erg1a didn't prove to be significantly different from the values for r-erg3 or PN erg currents. A more contrasting comparison was in the case of fast erg current deactivation time constant. The slow component of the erg current is usually small at depolarized potentials and becomes larger at more negative potentials, where actually the ratio between the fast and the slow component increases very much. Because of these considerations the values for the slow component were not considered, although the deactivating part of the hook-like erg current was fitted with two exponentials in order to obtain a better isolated fast component. The most three negative potentials were considered (-120, -110, -100 mV), where fitting deactivation with two exponential functions was also possible in PNs. At these three potentials the τ_{deacF} for PNs and r-erg3 where very close to each other, especially at -120 mV, whereas the values for r-erg1a proved to be in

average three times higher than those for PNs (Table 4), and significantly different from them. As already mentioned, one other important parameter, the time course of activation, can be compared from the data published by Hirdes *et al*. (2005). In terms of activation time constant the difference between r-erg1a and r-erg3 is more than two fold, r-erg 3 having the smallest τ_{act} among the four major isoforms. However, the erg currents in PNs, although certainly a mixture of all four major isoforms, have the fastest τ_{act}, which leads to the idea that additional factors influencing the biophysical parameters are also present. In any case, it has been shown that one could know what to expect from overexpressing one isoform more than others, as the biophysical properties of the heteromultimeric channels approach the values of the predominant subunit (Huffaker *et al.*, 2009). No real average can be done between properties, but since there are no qualitatively new properties, approximations can be made concerning the most probable subunit composition.

Apart from the comparisons made concerning the biophysical properties of the erg current, which show in all cases a close resemblance of Purkinje neuron erg current to the r-erg3 current, it is also important to see how similar the heterologous erg currents, activated by different templates from PNs, are to the native current. Figure 29 shows that with the "ramp firing" template all isoforms except r-erg2 carry a prominent current that can be activated during the depolarization. Very similar to what has been observed in PNs are the r-erg1a and r-erg1b isoforms in terms of average current amplitudes (in the range of 30-40 pA); the starting points of erg current activation are similar, and also the kinetics of the rising slope. In the case of r-erg3, it seems that the kinetics are more robust and the channel activation occurs also during each AP. It could very well be that the current activation appears to be robust because of the large amplitude of the current. Generally the HEK cells expressing r-erg3 subunits have more current being activated by this kind of template, an average of approximately 350 pA, possibly because the activation of the current takes place faster than for the other subunits.

For each of the four erg channel subunits the ramp current versus total current ratio was calculated, which was in the range of 2-4% for r-erg1a, r-erg1b and r-erg2, and by far larger for r-erg3 (15%). Only the ratio of the r-erg3 isoform, when used with the average PN erg current amplitude activated by the ramp template, can give a peak current at -100 mV of realistic amplitude in a 5 K^+ ACSF (values close to the amplitudes measured in an 8 K^+ ACSF averaging -169.86 ± 18.5 pA, n = 7). The ratios for the other three types of subunits would

give values well beyond the mean peak amplitude at -100 mV in 40 K^+ (-712.08 ± 97.2 pA, n = 12), much larger than what would normally occur in a 5 K^+ ACSF.

Understanding how the erg currents could be involved in regulating spontaneous firing and generally low frequency firing is just as important. For this purpose a "spontaneous firing" template from PNs was used on HEK cells expressing different erg isoforms. With such a template no distinguishable activation or accumulation was observed for r-erg1b and r-erg2, but both r-erg1a and r-erg3 currents could be activated (Figure 30). The activation occurred mainly on the depolarizing slope leading to threshold and after each AP the current was deactivated and on the next slope it was activated again. If the firing frequency was too low it could take more than 3-4 APs until current accumulation became obvious. Therefore, with an artificially created AP template (1.66 Hz), but consisting of a long train of APs, accumulation could be distinguished in the case of r-erg1a. R-erg3 because of its fast kinetics didn't accumulate. Of course, depending on the frequency used for stimulation, r-erg3 could also be determined to accumulate, just like it happened in the case of "ramp firing" clamp. This fact could explain why in immature PNs accommodation of firing doesn't take place as it happened in the case of P22-P42 animals. To test this, one of the response traces elicited upon injection of 100 pA of depolarizing current was used as a template for HEK cell stimulation. In this case, because of the high frequency firing and the large amplitude of r-erg3 currents, accumulation was detected (Figure 32). However the amplitude of the maximal current influences accumulation; if the maximal current has a large amplitude and a fast activation, then a big fraction of the current can be activated during the depolarizing foot of an AP; and if deactivation is not fast enough during repolarization to deactivate the entire current, then additional current will be subsequently activated on top.

The data from HEK293 cells have shown that the erg currents in Pukinje neurons are most probably mediated to a great extent by the erg3 isoform because of the high similarity in terms of activation $V_{1/2}$, recovery from inactivation and fast deactivation time constants, also concerning the current that can be activated in a 5 K^+ solution by the "ramp firing" template, and by the lack of current accumulation at low firing frequencies.

4.4 The erg current in Purkinje neurons is modulated by mGluR1

Among the metabotropic receptors in Purkinje neurons, mGluR1 receptors have been shown to be involved in a series of important plasticity processes, like the PF-induced LTD (Hartell, 1994), LTP of inhibitory synapses (Sugiyama *et al.*, 2008) and regulation of CF connectivity during development (Kano *et al.*, 1998). Therefore the influence of their activation on the erg current was tested using a specific agonist, namely DHPG. It has been previously shown that DHPG application induces at most potentials a transient and a sustained inward current component (Yamakawa & Hirano, 1999). A controversy exists around the mechanism that generates such an inward wave. Everyone agrees that there are multiple partners involved, possibly in a voltage-dependent manner, some mediating one component across a range of potentials while others taking over at other potentials. So far the TRPC3 channels have been involved in the generation of the transient component, the PNs of double KO mice lacking such a component when DHPG was applied (Hartmann *et al.*, 2008). It has been also suggested that the Na^+/Ca^{2+} transporter might be involved as well, the outward transport of Ca^{2+} in exchange for Na^+ producing a net inward current (Knopfel *et al.*, 2000).

In the present study it has been shown that the erg channels can be modulated by activating the mGluR1 receptors. Application of DHPG reduced the maximal current by approximately 50% and shifted the activation curve to the right by around 10 mV. By these two mechanisms the erg current at the more negative potentials could be abolished by more than 70% and in this way the impact of mGluR1 activation on the excitability of PNs could be even greater.

Since the main goal was to study the involvement of the erg current in the DHPG generated inward wave, the neurons were clamped at -40 mV in order to activate a sufficient amount of erg current. Ca^{2+} was omitted for a better isolation of the erg component. At this potential, application of DHPG induces the same sequence of components, first a transient/peak component and subsequently a sustained component. If after application of DHPG, when the cell response has reached the sustained phase, E-4031 is applied to the bath, no further change occurs, as if the DHGP has either blocked or made unavailable almost all the erg channels. If E-4031 is applied on the neurons in the beginning, the blockage of an outward current occurs, which would represent the steady-state erg current available at -40 mV. Subsequent application of DHPG would only induce the generation of the transient component (Figure 34). This would indicate that the sustained component in the response to DHPG was

actually due to the modulation of the available erg current. “Symmetrical” experiments were done in the current-clamp mode, also in the absence of Ca^{2+} in order to avoid firing. And again, DHPG induced a transient and sustained depolarization, whereas the initial application of E-4031 depolarized the cell and subsequent application of DHPG generated only a transient depolarization (Figure 35). When 2 mM Ca^{2+} was present in the external solution the effects of E-4031 and/or DHPG were evaluated in terms of firing frequency. When DHPG was applied to the cell, a transient and a sustained increase in firing frequency could be observed, but something was different when E-4031 was applied in advance. Generally it is more difficult to control the membrane potential of a firing neuron and if the injected depolarizing current is too large the cell would stop firing; therefore, the cells didn’t respond consistently to application of E-4031. In any case, all the erg current that would have been present in the beginning, would have been blocked by the application of E-4031, and the subsequent application of DHPG should have induced only a transient increase in frequency. But that was not the case; application of DHPG still induced a sustained increase in firing. And this fact can be explained by the existence of an additional contributor to the generation of the sustained component in the presence of Ca^{2+}. Since the Na^{+}/Ca^{2+} transporter is activated whenever there is an influx of Ca^{2+} into the cell, it could be the one responsible for depolarizing the cell in a sustained manner while Ca^{2+} is pumped out of the cell. The mGluR1 receptor requires the activation of G proteins of the $G\alpha_q$ type, as indicated by the total absence of the slow EPSC in $G\alpha_q$–deficient mice (Hartmann *et al.*, 2004). It is not know however, what is the pathway from the activated mGluR1 or other GPCRs to the erg channels in order to determine their biophysical changes.

5. Summary

Erg currents were studied in Purkinje neurons of immature (P5-P10) and young adult (P22-P42) mice. In immature PNs, the erg current is the fastest native erg current known so far. The activation time constant of PN erg current proved to be faster than that of the currents carried through heterologously expressed homotetrameric erg3 channels (known to have the most rapid time course of activation among the four erg channel isoforms; Hirdes *et al.*, 2005). Recovery from inactivation and deactivation time constants were similar to the fast-deactivating erg1b and erg3 currents.

Using an electrophysiological approach it was found that the erg channels were functionally present in all compartments of Purkinje neurons to a similar degree. This supports what was previously shown in immunohistochemical studies (Hagendorf *et al.*, 2009).

Spontaneously active Purkinje neurons of immature mice, responded to the application of E-4031 (erg channel specific blocker), in the on-cell mode, with an increase in firing frequency (4 out of 10 cells). The P22-P42 mouse Purkinje neurons, which exhibited a bursting behavior, responded to the application of E-4031, with a prolongation in burst duration (which varied considerably) and a decrease in interburst duration; the overall firing frequency didn't change.

When the immature PNs were depolarized with a square pulse (100 pA), a sustained train of APs was elicited, which showed little accommodation (in comparison to the P22-P42 mouse PNs; Sacco *et al.*, 2003). Application of E-4031, decreased the firing threshold by 2 mV, decreased the latency to firing initiation, and shortened the interspike duration (the instantaneous firing frequency for the first 11 APs was significantly increased). The regularity of the interbursts decreased in 25% of PNs, after application of E-4031 in comparison to control. When the immature PNs were depolarized for a longer period with a ramp protocol (0 - 200 pA, 1 s), the cells exhibited failure in AP firing in the absence of the erg current. In the absence of the hyperpolarizing conductance of the erg current, the membrane resistance increased, the cells were depolarized to a greater extend, and more Na^+ channels became inactivated. The AP-clamp (clamping the cells at time-variant voltages characteristic for an

AP) experiments showed that during the AP firing generated by a ramp pulse, the erg current activated as depolarization progressed.

Experiments were made in HEK293 cells expressing one of the fours erg channel subunits: r-erg1a, r-erg1b, r-erg2 and r-erg3. The biophysical properties of the four erg currents revealed that the current carried through homotetrameric r-erg3 channels was similar to PN erg current in terms of voltage dependence of activation, recovery from inactivation and deactivation time constants, and accumulation properties during sustained low frequency firing (the r-erg3 current didn't accumulate supporting the lack of accommodation seen in immature PNs). From this it can be concluded that the majority of subunits participating to erg channel constitution in PNs are of the erg3 type.

Application of mGluR1 agonist (DHPG), reduced the maximal erg tail current by 50% and shifted the activation curve to more depolarized potentials by approximately 10 mV. The amplitude of steady-state erg current at -40 mV was similar to the amplitude of the sustained component of the DHPG-evoked current. When the erg channels were previously blocked by application of E-4031, only the transient component appeared upon application of DHPG, suggesting that the sustained component at -40 mV was mediated by the erg channels.

Zusammenfassung

Für die Untersuchung von erg (ether-à-go-go-related gene)-Strömen wurden Purkinje-Neuronen von sehr jungen, unreifen Mäusen (P5-P10) und juvenilen Mäusen (P22-P42) verwendet. Bei dem erg-Strom in unreifen Purkinje-Neuronen handelt es sich um die schnellste Aktivierung von nativen Erg-Kanälen, die bisher beobachtet wurde. Sie war schneller als die Aktivierung von erg3-Kanälen, die als Homotetramer in einem heterologen Expressionssystem gemessen wurden (Hirdes *et al.*, 2005). Die Zeitkonstanten, die für Erholung aus der Inaktivierung und für die Deaktivierung gemessen wurden, waren vergleichbar mit den Zeitkonstanten der schnell deaktivierenden erg1b- und erg3-Kanäle.

Mithilfe elektrophysiologischer Methoden wurde beobachtet, dass die erg-Kanäle im Soma und im Dendriten von Purkinje-Neuronen gleichmäßig vorhanden waren. Dies bestätigt immunhistochemische Untersuchungen von Hagendorf *et al.* (2009).

Unreife Purkinje-Neuronen zeigten in der *On cell*-Konfiguration Spontanaktivität und reagierten nach der Zugabe des spezifischen erg-Inhibiors E-4031 mit einer erhöhten Feuerfrequenz (4 von 10 Zellen). Purkinje-Neuronen aus juvenilen Mäusen zeigten ein *Burst*-Verhalten und antworteten nach Zugabe von E-4031 mit einer verlängerten *Burst*-Dauer, die einer erheblichen Schwankung unterworfen war, und einer Abnahme der *Burst*-freien Perioden. Die Feuerfrequenz insgesamt änderte sich nicht.

Durch Depolarisierung der unreifen Purkinje-Neuronen mit einem Rechteck-Puls (100 pA) wurde eine gleichmäßige Folge repetitive Entladungen von Aktionspotentialen beobachtet, die im Vergleich zu Neuronen aus juvenilen Mäusen (Sacco *et al.*, 2003) eine nur geringe Akkomodation zeigten. Die Applikation von E-4031 erniedrigte das Schwellenpotential um 2 mV, verkürzte die Latenzzeit bis zum Feuerbeginn und verkürzte die Dauer zwischen den Feuerereignissen (die instantane Feuerfrequenz für die ersten elf Aktionspotentiale war signifikant erhöht). Die Regelmäßigkeit der *Burst*-freien Perioden variierte nach Zugabe von E-4031 im Vergleich zur Kontrolle in 25% der Purkinje-Neuronen. Wenn die unreifen Purkinje-Neuronen in einem Rampenprotokoll (0-200 pA) für eine längere

Zeit depolarisiert wurden, folgten nach Blockade der erg-Kanäle keine Aktionspotentiale. In der Aktionspotential-Klemme (Veränderung der Membranspannung zur Simulierung von Aktionspotentialen) zeigte sich, dass während der Aktionspotentiale, die durch ein Rampenprotokoll herbeigeführt wurden, erg-Kanäle aktiviert wurden.

Es wurden Experimente in HEK293-Zellen durchgeführt, die jeweils eine der vier erg-Kanal-Untereinheiten exprimierten: r-erg1a, r-erg1b, r-erg2 und r-erg3. Beim Vergleich der biophysikalischen Eigenschaften der vier Untereinheiten zeigte sich, dass der Strom, der in Purkinje-Neuronen gemessen wurde, mit den Eigenschaften von r-erg3-Strömen in Bezug auf Spannungsabhängigkeit der Aktivierung, Geschwindigkeit der Erholung aus der Inaktivierung, Deaktivierungskinetik und Akkumulationsverhalten nach anhaltender, niedrig frequenter Feuerrate vergleichbar war. Daraus folgt, dass die erg3-Untereinheit vermutlich die vorherrschende Untereinheit der vier Isoformen in Purkinje-Neuronen darstellt.

Die Applikation des mGluR1-Agonisten DHPG reduzierte den maximalen erg-*Tail*strom um 50% und verschob die Spannungsabhängigkeit der Aktivierung um durchschnittlich 10 mV zu depolasisierenden Potentialen. Die Amplitude des *Steady state* erg-Stroms bei -40 mV war vergleichbar mit der Amplitude der anhaltenden Komponente, die nach Zugabe von DHPG hervorgerufen wurde. Wenn die erg-Ströme zuvor durch E-4031 geblockt wurden, konnte nach Zugabe von DHPG nur eine transiente Komponente beobachtet werden, was den Schluss nahe legt, dass die anhaltende Komponente durch erg-Kanäle verursacht wurde.

6. References

Akbarali HI, Thatte H, He XD, Giles WR & Goyal RK. (1999). Role of HERG-like K(+) currents in opossum esophageal circular smooth muscle. *Am J Physiol* **277,** C1284-1290.

Angelo K, London M, Christensen SR & Hausser M. (2007). Local and global effects of I(h) distribution in dendrites of mammalian neurons. *J Neurosci* **27,** 8643-8653.

Apps R & Garwicz M. (2005). Anatomical and physiological foundations of cerebellar information processing. *Nat Rev Neurosci* **6,** 297-311.

Arcangeli A, Becchetti A, Mannini A, Mugnai G, De Filippi P, Tarone G, Del Bene MR, Barletta E, Wanke E & Olivotto M. (1993). Integrin-mediated neurite outgrowth in neuroblastoma cells depends on the activation of potassium channels. *J Cell Biol* **122,** 1131-1143.

Arcangeli A, Bianchi L, Becchetti A, Faravelli L, Coronnello M, Mini E, Olivotto M & Wanke E. (1995). A novel inward-rectifying K+ current with a cell-cycle dependence governs the resting potential of mammalian neuroblastoma cells. *J Physiol* **489 (Pt 2),** 455-471.

Arcangeli A, Rosati B, Cherubini A, Crociani O, Fontana L, Ziller C, Wanke E & Olivotto M. (1997). HERG- and IRK-like inward rectifier currents are sequentially expressed during neuronal development of neural crest cells and their derivatives. *Eur J Neurosci* **9,** 2596-2604.

Aydar E & Palmer C. (2006). Expression and functional characterization of the human ether-a-go-go-related gene (HERG) K+ channel cardiac splice variant in Xenopus laevis oocytes. *J Membr Biol* **211,** 115-126.

Bauer CK. (1998). The erg inwardly rectifying K+ current and its modulation by thyrotrophin-releasing hormone in giant clonal rat anterior pituitary cells. *J Physiol* **510 (Pt 1),** 63-70.

Bauer CK, Meyerhof W & Schwarz JR. (1990). An inward-rectifying K+ current in clonal rat pituitary cells and its modulation by thyrotrophin-releasing hormone. *J Physiol* **429,** 169-189.

Benarroch EE. (2009). Potassium channels: brief overview and implications in epilepsy. *Neurology* **72,** 664-669.

Berger T, Larkum ME & Luscher HR. (2001). High I(h) channel density in the distal apical dendrite of layer V pyramidal cells increases bidirectional attenuation of EPSPs. *J Neurophysiol* **85,** 855-868.

Callewaert G, Eilers J & Konnerth A. (1996). Axonal calcium entry during fast 'sodium' action potentials in rat cerebellar Purkinje neurones. *J Physiol* **495 (Pt 3),** 641-647.

Canepari M, Auger C & Ogden D. (2004). Ca2+ ion permeability and single-channel properties of the metabotropic slow EPSC of rat Purkinje neurons. *J Neurosci* **24,** 3563-3573.

Catterall WA. (2000). Structure and regulation of voltage-gated Ca2+ channels. *Annu Rev Cell Dev Biol* **16,** 521-555.

Chiesa N, Rosati B, Arcangeli A, Olivotto M & Wanke E. (1997). A novel role for HERG K+ channels: spike-frequency adaptation. *J Physiol* **501 (Pt 2),** 313-318.

Corrette BJ, Bauer CK & Schwarz JR. (1995). Electrophysiology of anterior pituitary cells. In *The ELECTROPHYSIOLOGY of NEUROENDOCRINE CELLS*, ed. Scherubl H & Hescheler J, pp. 101-143. CRC Press Inc.

Corrette BJ, Bauer CK & Schwarz JR. (1996). An inactivating inward-rectifying K current present in prolactin cells from the pituitary of lactating rats. *J Membr Biol* **150,** 185-195.

Curran ME, Splawski I, Timothy KW, Vincent GM, Green ED & Keating MT. (1995). A molecular basis for cardiac arrhythmia: HERG mutations cause long QT syndrome. *Cell* **80,** 795-803.

Davie JT, Clark BA & Hausser M. (2008). The origin of the complex spike in cerebellar Purkinje cells. *J Neurosci* **28,** 7599-7609.

Dzubay JA & Otis TS. (2002). Climbing fiber activation of metabotropic glutamate receptors on cerebellar purkinje neurons. *Neuron* **36,** 1159-1167.

Eccles JC. (1973). The cerebellum as a computer: patterns in space and time. *J Physiol* **229,** 1-32.

Edgerton JR & Reinhart PH. (2003). Distinct contributions of small and large conductance Ca2+-activated K+ channels to rat Purkinje neuron function. *J Physiol* **548,** 53-69.

Einarsen K, Calloe K, Grunnet M, Olesen SP & Schmitt N. (2009). Functional properties of human neuronal Kv11 channels. *Pflugers Arch* **458,** 689-700.

Furlan F, Guasti L, Avossa D, Becchetti A, Cilia E, Ballerini L & Arcangeli A. (2005). Interneurons transiently express the ERG K+ channels during development of mouse spinal networks in vitro. *Neuroscience* **135,** 1179-1192.

Furlan F, Taccola G, Grandolfo M, Guasti L, Arcangeli A, Nistri A & Ballerini L. (2007). ERG conductance expression modulates the excitability of ventral horn GABAergic interneurons that control rhythmic oscillations in the developing mouse spinal cord. *J Neurosci* **27,** 919-928.

Guasti L, Cilia E, Crociani O, Hofmann G, Polvani S, Becchetti A, Wanke E, Tempia F & Arcangeli A. (2005). Expression pattern of the ether-a-go-go-related (ERG) family proteins in the adult mouse central nervous system: evidence for coassembly of different subunits. *J Comp Neurol* **491,** 157-174.

Guasti L, Crociani O, Redaelli E, Pillozzi S, Polvani S, Masselli M, Mello T, Galli A, Amedei A, Wymore RS, Wanke E & Arcangeli A. (2008). Identification of a posttranslational mechanism for the regulation of hERG1 K+ channel expression and hERG1 current density in tumor cells. *Mol Cell Biol* **28,** 5043-5060.

Hagendorf S, Fluegge D, Engelhardt C & Spehr M. (2009). Homeostatic control of sensory output in basal vomeronasal neurons: activity-dependent expression of ether-a-go-go-related gene potassium channels. *J Neurosci* **29,** 206-221.

Hancox JC, Levi AJ & Witchel HJ. (1998). Time course and voltage dependence of expressed HERG current compared with native "rapid" delayed rectifier K current during the cardiac ventricular action potential. *Pflugers Arch* **436,** 843-853.

Hardman RM & Forsythe ID. (2009). Ether-a-go-go-related gene K+ channels contribute to threshold excitability of mouse auditory brainstem neurons. *J Physiol* **587,** 2487-2497.

Harmar AJ, Hills RA, Rosser EM, Jones M, Buneman OP, Dunbar DR, Greenhill SD, Hale VA, Sharman JL, Bonner TI, Catterall WA, Davenport AP, Delagrange P, Dollery CT, Foord SM, Gutman GA, Laudet V, Neubig RR, Ohlstein EH, Olsen RW, Peters J, Pin JP, Ruffolo RR, Searls DB, Wright MW & Spedding M. (2009). IUPHAR-DB: the IUPHAR database of G protein-coupled receptors and ion channels. *Nucleic Acids Res* **37,** D680-685.

Hartell NA. (1994). Induction of cerebellar long-term depression requires activation of glutamate metabotropic receptors. *Neuroreport* **5,** 913-916.

Hartmann J, Blum R, Kovalchuk Y, Adelsberger H, Kuner R, Durand GM, Miyata M, Kano M, Offermanns S & Konnerth A. (2004). Distinct roles of Galpha(q) and Galpha11 for Purkinje cell signaling and motor behavior. *J Neurosci* **24,** 5119-5130.

Hartmann J, Dragicevic E, Adelsberger H, Henning HA, Sumser M, Abramowitz J, Blum R, Dietrich A, Freichel M, Flockerzi V, Birnbaumer L & Konnerth A. (2008). TRPC3 channels are required for synaptic transmission and motor coordination. *Neuron* **59,** 392-398.

Hausser M, Major G & Stuart GJ. (2001). Differential shunting of EPSPs by action potentials. *Science* **291,** 138-141.

Hildebrand ME, Isope P, Miyazaki T, Nakaya T, Garcia E, Feltz A, Schneider T, Hescheler J, Kano M, Sakimura K, Watanabe M, Dieudonne S & Snutch TP. (2009). Functional coupling between mGluR1 and Cav3.1 T-type calcium channels contributes to parallel fiber-induced fast calcium signaling within Purkinje cell dendritic spines. *J Neurosci* **29,** 9668-9682.

Hille B. (2001). Ion Channels of Excitable Membranes. 3rd edn. Sinaeur Associates, Inc., Sunderland.

Hirdes W, Dinu C, Bauer CK, Boehm U & Schwarz JR. (2010). Gonadotropin-releasing hormone inhibits ether-a-go-go-related gene K+ currents in mouse gonadotropes. *Endocrinology* **151,** 1079-1088.

Hirdes W, Napp N, Wulfsen I, Schweizer M, Schwarz JR & Bauer CK. (2009). Erg K+ currents modulate excitability in mouse mitral/tufted neurons. *Pflugers Arch* **459,** 55-70.

Hirdes W, Schweizer M, Schuricht KS, Guddat SS, Wulfsen I, Bauer CK & Schwarz JR. (2005). Fast erg K+ currents in rat embryonic serotonergic neurones. *J Physiol* **564,** 33-49.

Huffaker SJ, Chen J, Nicodemus KK, Sambataro F, Yang F, Mattay V, Lipska BK, Hyde TM, Song J, Rujescu D, Giegling I, Mayilyan K, Proust MJ, Soghoyan A, Caforio G, Callicott JH, Bertolino A, Meyer-Lindenberg A, Chang J, Ji Y, Egan MF, Goldberg TE, Kleinman JE, Lu B & Weinberger DR. (2009). A primate-specific, brain isoform of KCNH2 affects cortical physiology, cognition, neuronal repolarization and risk of schizophrenia. *Nat Med* **15,** 509-518.

Hurlock EC, McMahon A & Joho RH. (2008). Purkinje-cell-restricted restoration of Kv3.3 function restores complex spikes and rescues motor coordination in Kcnc3 mutants. *J Neurosci* **28,** 4640-4648.

Jackson AC & Bean BP. (2007). State-dependent enhancement of subthreshold A-type potassium current by 4-aminopyridine in tuberomammillary nucleus neurons. *J Neurosci* **27,** 10785-10796.

Johnson JN, Hofman N, Haglund CM, Cascino GD, Wilde AA & Ackerman MJ. (2009). Identification of a possible pathogenic link between congenital long QT syndrome and epilepsy. *Neurology* **72,** 224-231.

Johnson JP, Jr., Balser JR & Bennett PB. (2001). A novel extracellular calcium sensing mechanism in voltage-gated potassium ion channels. *J Neurosci* **21,** 4143-4153.

Kano M, Hashimoto K, Watanabe M, Kurihara H, Offermanns S, Jiang H, Wu Y, Jun K, Shin HS, Inoue Y, Simon MI & Wu D. (1998). Phospholipase cbeta4 is specifically involved in climbing fiber synapse elimination in the developing cerebellum. *Proc Natl Acad Sci U S A* **95,** 15724-15729.

Khaliq ZM & Raman IM. (2005). Axonal propagation of simple and complex spikes in cerebellar Purkinje neurons. *J Neurosci* **25,** 454-463.

Knopfel T, Anchisi D, Alojado ME, Tempia F & Strata P. (2000). Elevation of intradendritic sodium concentration mediated by synaptic activation of metabotropic glutamate receptors in cerebellar Purkinje cells. *Eur J Neurosci* **12,** 2199-2204.

Konnerth A, Dreessen J & Augustine GJ. (1992). Brief dendritic calcium signals initiate long-lasting synaptic depression in cerebellar Purkinje cells. *Proc Natl Acad Sci U S A* **89,** 7051-7055.

Larsen AP. (2010). Role of ERG1 isoforms in modulation of ERG1 channel trafficking and function. *Pflugers Arch* **460,** 803-812.

Llano I, Marty A, Armstrong CM & Konnerth A. (1991). Synaptic- and agonist-induced excitatory currents of Purkinje cells in rat cerebellar slices. *J Physiol* **434,** 183-213.

London B, Trudeau MC, Newton KP, Beyer AK, Copeland NG, Gilbert DJ, Jenkins NA, Satler CA & Robertson GA. (1997). Two isoforms of the mouse ether-a-go-go-related gene coassemble to form channels with properties similar to the rapidly activating component of the cardiac delayed rectifier K+ current. *Circ Res* **81,** 870-878.

Martina M, Yao GL & Bean BP. (2003). Properties and functional role of voltage-dependent potassium channels in dendrites of rat cerebellar Purkinje neurons. *J Neurosci* **23,** 5698-5707.

Mintz IM, Adams ME & Bean BP. (1992). P-type calcium channels in rat central and peripheral neurons. *Neuron* **9,** 85-95.

Molleman A. (2003). *Patch clamping: an introductory guide to patch clamp electrophysiology*. John Wiley & Sons Ltd., Chichester.

Monsivais P, Clark BA, Roth A & Hausser M. (2005). Determinants of action potential propagation in cerebellar Purkinje cell axons. *J Neurosci* **25,** 464-472.

Mori Y, Wakamori M, Oda S, Fletcher CF, Sekiguchi N, Mori E, Copeland NG, Jenkins NA, Matsushita K, Matsuyama Z & Imoto K. (2000). Reduced voltage sensitivity of activation of P/Q-type Ca2+ channels is associated with the ataxic mouse mutation rolling Nagoya (tg(rol)). *J Neurosci* **20,** 5654-5662.

Ohya S, Asakura K, Muraki K, Watanabe M & Imaizumi Y. (2002). Molecular and functional characterization of ERG, KCNQ, and KCNE subtypes in rat stomach smooth muscle. *Am J Physiol Gastrointest Liver Physiol* **282,** G277-287.

Overholt JL, Ficker E, Yang T, Shams H, Bright GR & Prabhakar NR. (2000). HERG-Like potassium current regulates the resting membrane potential in glomus cells of the rabbit carotid body. *J Neurophysiol* **83,** 1150-1157.

Ovsepian SV & Friel DD. (2008). The leaner P/Q-type calcium channel mutation renders cerebellar Purkinje neurons hyper-excitable and eliminates Ca2+-Na+ spike bursts. *Eur J Neurosci* **27,** 93-103.

Papa M, Boscia F, Canitano A, Castaldo P, Sellitti S, Annunziato L & Taglialatela M. (2003). Expression pattern of the ether-a-gogo-related (ERG) K+ channel-encoding genes ERG1, ERG2, and ERG3 in the adult rat central nervous system. *J Comp Neurol* **466,** 119-135.

Parr E, Pozo MJ, Horowitz B, Nelson MT & Mawe GM. (2003). ERG K+ channels modulate the electrical and contractile activities of gallbladder smooth muscle. *Am J Physiol Gastrointest Liver Physiol* **284,** G392-398.

Pellequer JL, Brudler R & Getzoff ED. (1999). Biological sensors: More than one way to sense oxygen. *Curr Biol* **9,** R416-418.

Pessia M, Servettini I, Panichi R, Guasti L, Grassi S, Arcangeli A, Wanke E & Pettorossi VE. (2008). ERG voltage-gated K+ channels regulate excitability and discharge dynamics of the medial vestibular nucleus neurones. *J Physiol* **586,** 4877-4890.

Pouille F, Cavelier P, Desplantez T, Beekenkamp H, Craig PJ, Beattie RE, Volsen SG & Bossu JL. (2000). Dendro-somatic distribution of calcium-mediated electrogenesis in purkinje cells from rat cerebellar slice cultures. *J Physiol* **527 Pt 2,** 265-282.

Raman IM & Bean BP. (1997). Resurgent sodium current and action potential formation in dissociated cerebellar Purkinje neurons. *J Neurosci* **17,** 4517-4526.

Raman IM & Bean BP. (1999). Ionic currents underlying spontaneous action potentials in isolated cerebellar Purkinje neurons. *J Neurosci* **19,** 1663-1674.

Rancz EA & Hausser M. (2006). Dendritic calcium spikes are tunable triggers of cannabinoid release and short-term synaptic plasticity in cerebellar Purkinje neurons. *J Neurosci* **26,** 5428-5437.

Rossi S, Mataluni G, De Bartolo P, Prosperetti C, Foti F, De Chiara V, Musella A, Mandolesi L, Bernardi G, Centonze D & Petrosini L. (2008). Cerebellar control of cortico-striatal LTD. *Restor Neurol Neurosci* **26,** 475-480.

Sacco T, Bruno A, Wanke E & Tempia F. (2003). Functional roles of an ERG current isolated in cerebellar Purkinje neurons. *J Neurophysiol* **90,** 1817-1828.

Saganich MJ, Machado E & Rudy B. (2001). Differential expression of genes encoding subthreshold-operating voltage-gated K+ channels in brain. *J Neurosci* **21,** 4609-4624.

Sanguinetti MC, Jiang C, Curran ME & Keating MT. (1995). A mechanistic link between an inherited and an acquired cardiac arrhythmia: HERG encodes the IKr potassium channel. *Cell* **81,** 299-307.

Sanguinetti MC & Jurkiewicz NK. (1990). Two components of cardiac delayed rectifier K+ current. Differential sensitivity to block by class III antiarrhythmic agents. *J Gen Physiol* **96,** 195-215.

Schafer R, Wulfsen I, Behrens S, Weinsberg F, Bauer CK & Schwarz JR. (1999). The erg-like potassium current in rat lactotrophs. *J Physiol* **518 (Pt 2),** 401-416.

Schledermann W, Wulfsen I, Schwarz JR & Bauer CK. (2001). Modulation of rat erg1, erg2, erg3 and HERG K+ currents by thyrotropin-releasing hormone in anterior pituitary cells via the native signal cascade. *J Physiol* **532,** 143-163.

Schmahmann JD. (1997). *The Cerebellum and Cognition*. Academic Press, San Diego.

Schwarz JR & Bauer CK. (1999). The ether-a-go-go-Related Gene K(+) Current: Functions of a Strange Inward Rectifier. *News Physiol Sci* **14,** 135-142.

Schwarz JR & Bauer CK. (2004). Functions of erg K+ channels in excitable cells. *J Cell Mol Med* **8,** 22-30.

Shi W, Wymore RS, Wang HS, Pan Z, Cohen IS, McKinnon D & Dixon JE. (1997). Identification of two nervous system-specific members of the erg potassium channel gene family. *J Neurosci* **17,** 9423-9432.

Shibasaki T. (1987). Conductance and kinetics of delayed rectifier potassium channels in nodal cells of the rabbit heart. *J Physiol* **387,** 227-250.

Shoeb F, Malykhina AP & Akbarali HI. (2003). Cloning and functional characterization of the smooth muscle ether-a-go-go-related gene K+ channel. Potential role of a conserved amino acid substitution in the S4 region. *J Biol Chem* **278,** 2503-2514.

Stuart G & Hausser M. (1994). Initiation and spread of sodium action potentials in cerebellar Purkinje cells. *Neuron* **13,** 703-712.

Sturm P, Wimmers S, Schwarz JR & Bauer CK. (2005). Extracellular potassium effects are conserved within the rat erg K+ channel family. *J Physiol* **564,** 329-345.

Sugiyama Y, Kawaguchi SY & Hirano T. (2008). mGluR1-mediated facilitation of long-term potentiation at inhibitory synapses on a cerebellar Purkinje neuron. *Eur J Neurosci* **27,** 884-896.

Sultan F & Glickstein M. (2007). The cerebellum: Comparative and animal studies. *Cerebellum* **6,** 168-176.

Swensen AM & Bean BP. (2003). Ionic mechanisms of burst firing in dissociated Purkinje neurons. *J Neurosci* **23,** 9650-9663.

Taglialatela M, Castaldo P, Iossa S, Pannaccione A, Fresi A, Ficker E & Annunziato L. (1997). Regulation of the human ether-a-gogo related gene (HERG) K+ channels by reactive oxygen species. *Proc Natl Acad Sci U S A* **94,** 11698-11703.

Tempia F, Miniaci MC, Anchisi D & Strata P. (1998). Postsynaptic current mediated by metabotropic glutamate receptors in cerebellar Purkinje cells. *J Neurophysiol* **80,** 520-528.

Titus SA, Warmke JW & Ganetzky B. (1997). The Drosophila erg K+ channel polypeptide is encoded by the seizure locus. *J Neurosci* **17,** 875-881.

Trudeau MC, Warmke JW, Ganetzky B & Robertson GA. (1995). HERG, a human inward rectifier in the voltage-gated potassium channel family. *Science* **269,** 92-95.

Vandenberg JI, Varghese A, Lu Y, Bursill JA, Mahaut-Smith MP & Huang CL. (2006). Temperature dependence of human ether-a-go-go-related gene K+ currents. *Am J Physiol Cell Physiol* **291,** C165-175.

Walter JT, Alvina K, Womack MD, Chevez C & Khodakhah K. (2006). Decreases in the precision of Purkinje cell pacemaking cause cerebellar dysfunction and ataxia. *Nat Neurosci* **9,** 389-397.

Warmke J, Drysdale R & Ganetzky B. (1991). A distinct potassium channel polypeptide encoded by the Drosophila eag locus. *Science* **252,** 1560-1562.

Warmke JW & Ganetzky B. (1994). A family of potassium channel genes related to eag in Drosophila and mammals. *Proc Natl Acad Sci U S A* **91,** 3438-3442.

Wimmers S, Bauer CK & Schwarz JR. (2002). Biophysical properties of heteromultimeric erg K+ channels. *Pflugers Arch* **445,** 423-430.

Womack M & Khodakhah K. (2002). Active contribution of dendrites to the tonic and trimodal patterns of activity in cerebellar Purkinje neurons. *J Neurosci* **22,** 10603-10612.

Womack MD & Khodakhah K. (2004). Dendritic control of spontaneous bursting in cerebellar Purkinje cells. *J Neurosci* **24,** 3511-3521.

Wulff H, Castle NA & Pardo LA. (2009). Voltage-gated potassium channels as therapeutic targets. *Nat Rev Drug Discov* **8,** 982-1001.

Yamakawa Y & Hirano T. (1999). Contribution of mGluR1 to the basal activity of a mouse cerebellar Purkinje neuron. *Neurosci Lett* **277,** 103-106.

Zagha E, Lang EJ & Rudy B. (2008). Kv3.3 channels at the Purkinje cell soma are necessary for generation of the classical complex spike waveform. *J Neurosci* **28,** 1291-1300.

Zaza A, Micheletti M, Brioschi A & Rocchetti M. (1997). Ionic currents during sustained pacemaker activity in rabbit sino-atrial myocytes. *J Physiol* **505 (Pt 3),** 677-688.

7. Appendix

7.1 Abbreviations

° C - grad Celsius
% - percent
ACSF - artificial cerebrospinal fluid
ADP - afterdepolarization
AHP - afterhyperpolarization
AMPA - α-amino-3-hydroxyl-5-methyl-4-isoxazole-propionate
AP - action potential
AP-5 - (2R)-amino-5-phosphonovaleric acid
BK - big-conductance calcium dependent potassium channel
C57BL/6 - C57 black 6
Ca^{2+} - calcium
$CaCl_2$ - calcium chloride
$[Ca^{2+}]_i$ - intracellular calcium concentration
Ca_v - voltage-gated calcium channel
C_{cell} - cell capacitance
cDNA - complementary deoxyribonucleic acid
CF - climbing fiber
CHO - Chinese hamster ovary cell
C_m - membrane capacitance
CNBD - cyclic nucleotide binding domain
$C_{nc\ pt}$ - nucleated patch capacitance
CNQX - 6-cyano-7-nitroquinoxaline-2,3-dione
$C_{pipette}$ - pipette capacitance
C-terminus - carboxy terminal end
DCN - deep cerebellar nucleus
Δt - time increase
DHPG - dihydroxyphenylglycine
DIV - days *in vitro*
DNA - deoxyribonucleic acid
EAG - *ether-à-go-go* gene
eag - *ether-à-go-go* potassium channel
EGTA - ethylene glycol tetraacetic acid
elk - *ether-à-go-go* like potassium channel
EPSC - excitatory postsynaptic current
EPSP - excitatory postsynaptic potential
erg - *ether-à-go-go* related gene potassium channel
ergPN - Purkinje neuron erg current
et al. - et alii
FBS - fetal bovine serum
GABA - gamma aminobutyric acid
$GABA_AR$ - A-type GABA receptor
$GABA_BR$ - B-type GABA receptor

Glu - glutamate
GnRH - gonadotropin releasing hormone
GPCRs - G protein coupled receptors
H_2O - water
HEK293 - human embryonic kidney 293 cell line
HERG - human erg1 gene
hK_v11.1 - human erg1 channel
Hz - Hertz
I - ionic current
I_{ERG} - erg current k - slope factor
IFF - instantaneous firing frequency
iGluR - ionotropic glutamate receptor
I_h – hyperpolarization-activated cation current
I_{Kr} - rapidly activatinv potassium current
I_{Ks} - slowly activating potassium current
I_{peak} - peak current
$I_{sustained}$ - sustained current
K^+ - potassium
K_{2P} - 2-pore potassium channel
$[K^+]_i$ - intracellular potassium concentration
$[K^+]_o$ - outside/extracellular potassium concentration
KOH - potassium hydroxide
K_{Ca} - calcium-activated potassium channel
KCl - potassium chloride
Kcnh2 - mouse erg1 gene
KCNH2 - human erg1 gene
KCNH2-3.1 – primate-specific erg1a-3.1 isoform
Kcnh6 - mouse erg2 gene
Kcnh7 - mouse erg3 gene
kHz - kilohertz
K_{ir} - inwardly rectifing potassium channel
KO - knock-out
K_v - voltage gated potassium channel
K_v1 - *Shaker*-related potassium channels
Kv3 - *Shaw* potassium channel
K_v10 - eag channel subfamily
K_v11 - erg channel subfamily
Kv11.1 - erg1 potassium channel
Kv11.2 - erg2 potassium channel
Kv11.3 - erg3 potassium channel
K_v12 - elk channel subfamily
LB - lysogeny broth
LH - luteinizing hormone
LQT - long QT syndrome
LQT2 - KCNH2 associated LQT syndrome
LTD - long term depression
LTP - long term potentiation
M1-M4 - transmembrane domains 1-4
Mg^{2+} - magnesium
MgATP - magnesium adenosine-5'-triphosphate
$MgCl_2$ - magnesium chloride

mGluR - metabotropic glutamate receptor
MNTB - medial nucleus of the trapezoid body
µM - micromolar
mM - milimolar
MΩ - megaohm
mRNA - messenger ribonucleic acid
ms - milisecond
mV - milivolt
MVNn - medial vestibular nucleus neuron
n - number
nA - nanoampere
Na^+ - sodium
Na_2ATP - sodium adenosine-5'-triphosphate
Na_3GTP sodium guanosine-5'-triphosphate
NaCl - sodium chloride
NaH_2PO_4 - sodium dihydrogen phosphate
$NaHCO_3$ - sodium bicarbonate
$[Na^+]_i$ intracellular sodium concentration
NMDA - N-methyl-D-aspartic acid
NR-ISH - nonradioactive in situ hybridization
n.s. - not significant
N-terminus - amino terminal end
O_2 - oxygen
ORF - open reading frame
p - *probability*
P - postnatal
pA - picoampere
PAS - Per-Arnt-Sim domain
pF - picofarad
PF - parallel fiber
PLL - Poly-L-*Lysine*
PTX - pertussis toxin
r - rat
R_{access} - access resistance
r-erg - rat erg channel
R_f - feedback resistance
R_{leak} - leak resistance
R_m - membrane resistance
RNase - ribonuclease
RP - rebound potentiation
R_{patch} - patch resistance
$R_{pipette}$ - pipette resistance
s - second
S1-S6 - transmembrane domains 1-6
SK - small-conductance calcium dependent potassium channel
SOC - Super Optimal broth with Catabolite repression
τ_{rec} - recovery from inactivation time constant
τ_{deac} - deactivation time constant
τ_{deacF} - deactivation time constant of the fast current component
τ_{deacS} - deactivation time constant of the slow current component
TBOA - threo-b-Benzyloxyaspartic acid

TRH - thyrotropin releasing hormone
Tris-HCl - tris(hydroxymethyl)aminomethane, hydrochloride
TRPC3 - C3-type transient receptor potential channel
TTX - tetrodotoxin
$V_{1/2}$ - potential at which the current is 50% of the maximum
V_c - voltage command
V_m - membrane voltage

7.2 Table of drug concentrations

Drug	**Action**	**Concentration (µM)**
E-4031	erg channel blocker	1/5
AP-5	NMDAR antagonist	50
CNQX	AMPA/Kainate receptor antagonist	10
Bicuculline	$GABA_AR$ antagonist	20
(S)-3,5-DHPG	mGluRI agonist	50

8. Acknowledgements

First, I would like to thank Prof. Dr. Jürgen R. Schwarz for inviting me to ZMNH, in the spring of 2007, for a four month period during which I could complete my Master program training as ERASMUS student. It had been a great opportunity for developing the skills and knowledge in electrophysiology that I had just started to discover in Bucharest.

Most of all I am grateful for being proposed to continue my work in ZMNH as PhD student. The last three years have been very demanding but at the same time exciting with each new experiment that Prof. Schwarz and I imagined. My presence in ZMNH was made possible also by Prof. Dr. Olaf Pongs, the director of the Institute for Neural Signal Transduction, whom I would like to thank as well.

Dr. Wiebke Hirdes, although not my direct supervisor, proved to be a great mentor and colleague, from whom I had a lot to learn. I cannot mention all the moments when we discussed different scientific topics trying to find explanations, and explanations… My colleagues Crenguta, Axel, Phanindra, Lijuan, Sönke, Vitya, Joanna, Christian, Oliver, Devesh, Soumya, Alexander, Gregor, Niklas, Frederik, Yu have always been close to reach when small issues occurred in the lab or just in the everyday life, and I would like to thank them for that.

It is said that the atmosphere in the lab is important for one's work, and truly it was. We were almost all the time in contact with each other, discussing, advising, helping; and the feed-back that I continuously received soon became indispensable.

I would also like to thank my colleagues from the Center who attended my progress reports and gave me their suggestions, and all the others who don't seem to be "there" but make things work in the entire ZMNH.

I will never forget the places where I've got my first contact to neuroscience, which are the labs of the Department of Biophysics and Animal Physiology (University of Bucharest) under the supervision of Prof. Dr. Maria-Luisa Flonta and Conf. Dr. Violeta Ristoiu.

Not less thankful I am when I think of Prof. Dr. Veronica Lazar who carried me on the steps of writing my first thesis and graduating the Faculty of Biology, or of Prof. Ion Pestritu without whom I wouldn't have been writing this thesis in English.

I have to mention the persons whom I maybe should have started with: my parents. They have been always supporting and understanding the young emerging scientist in me.

And of course, I thank Nature for creating these intriguing biological systems for the study of which a lifetime is by far insufficient.